Hindawi
International Journal of Energy Research
Volume 2023, Article ID 6680001, 52 pages
https://doi.org/10.1155/2023/6680001

Review Article

Recent Progress of Potassium Metal Anodes: How to Regulate the Growth of Dendrite

Seunghwi Baek,[1] Taeksoo Jung,[1] Sunghyun Jie,[1] Myeongjin Kim,[2] and Byeongyong Lee[1]

[1]*School of Mechanical Engineering, Pusan National University, Republic of Korea*
[2]*Department of Hydrogen & Renewable Energy, Kyungpook National University, Republic of Korea*

Correspondence should be addressed to Myeongjin Kim; myeongjinkim@knu.ac.kr and Byeongyong Lee; blee1015@pusan.ac.kr

Received 14 August 2023; Revised 4 October 2023; Accepted 21 November 2023; Published 14 December 2023

Academic Editor: Hongtao Sun

Potassium- (K-) based batteries with K metal anodes have been regarded as a substitute for lithium- (Li-) and sodium- (Na-) based batteries. In this review, motivations for K metal anodes with various advantages over Li and Na metals are presented at the beginning. Nevertheless, the practical applications of K metal anodes are still impeded by various challenges originating from their highly reactive nature. Then, major challenges of K metal are introduced in comparison with those of Li and Na metals, including unstable SEI, dendrite growth, low melting point, and gas generation. These issues become more severe in K metal due to its different physical and chemical properties compared with Li and Na metals. Consequently, this leads to varying electrochemical behaviors. In particular, the mechanism of K dendrite growths is different from that of Li and Na. Subsequently, approaches with an emphasis on the suppression of dendrites are described, falling into two categories: direct and indirect engineering on electrodes. Direct engineering is K metallic electrode designs by utilizing a host framework, alloy electrode, and interface modification. Notably, the most crucial aspect considered in direct engineering is the potassiophilicity of the host and interface, which contributes to the uniform deposition of K. The section on indirect engineering addresses the suppression of dendrite growth through separators and liquid/solid electrolytes. Finally, future perspectives and research directions toward the suppression of K dendrites are provided.

1. Introduction

Lithium-ion batteries (LIBs) are one of the most successful energy storage systems due to their energy storage mechanism being based on intercalation chemistry, where ions are inserted and diffused into active materials [1]. This reversible electrochemical reaction enables LIBs to work as energy suppliers for long periods without sudden performance fall-off. Additionally, LIBs have a high energy density, making them capable of storing considerable amounts of energy in a small package ranging from portable electronic devices to electric vehicles [2]. These features have revolutionized many aspects of our daily lives by enabling the development of new technologies such as drones and wearable electronics. Despite their commercial success and impact on our lives, LIBs have a limitation in energy density that may not be sufficient to meet the ever-increasing demand for high-energy-density storage systems [3]. In this regard, Li metal anodes have gained significant attention as a substitute for graphite due to their high theoretical gravimetric capacity of 3861 mAh g^{-1} and lowest redox potential [4]. Li metal, however, has limited availability, buried unevenly in the earth's crust with an amount of approx. 0.0017 wt%, possibly leading to a fluctuation and rise in price in the near future [5]. Additionally, the scarcity of the Li precursor could raise concerns for Li industries [6], and exposure to chemicals utilized in Li mining and associated industries could also pose health risks to workers and local communities, particularly in countries with poor health and safety regulations [7].

To address the issues, researchers have been searching for alternative energy storage systems beyond LIBs as well as Li metal anodes. Among the candidates for next-generation batteries, sodium- (Na-) and potassium- (K-)

Table 1: Comparison of various properties of alkali metals.

Properties	Parameter	K	Na	Li
Element	Atomic number	19	11	3
	Ionic radius (Å)	1.38	1.02	0.76
Physical	Density ($g\,cm^{-3}$)	0.86	0.97	0.53
	Lattice parameter (nm)	0.533	0.429	0.351
	Melting point (°C)	63.4	97.7	180.5
	Shear modulus (GPa)	1.3	3.3	4.2
	Brinell hardness (MPa)	0.363	0.69	5
Electrochemical	Redox potential (V vs. SHE)	-2.93	-2.71	-3.04
	Redox potential in PC solvent	-2.88	-2.56	-2.79
	Gravimetric capacity ($mAh\,g^{-1}$)	687	1166	3860
	Volumetric capacity ($mAh\,cm^{-3}$)	589	1131	2062
Conductivity	Stokes radius (Å)	3.6	4.6	4.8
	Ionic conductivity in 1 M PC ($mS\,cm^{-1}$)	~10	~7.8	~7
	Desolvation energy in DEC ($kJ\,mol^{-1}$)	105.1	147.9	205.6
	Desolvation energy in EC ($kJ\,mol^{-1}$)	114.6	152.8	208.9
Economic	Abundance in earth's crust (wt%)	~2.09	~2.4	~0.0017
	Cost of metal ($\$\,ton^{-1}$)[a]	23000	2200	414000
	Cost of carbonate ($\$\,kg^{-1}$)[b]	215	178	706
	Cost of hydroxide ($\$\,kg^{-1}$)[b]	87.6	84.7	3140

Real-time cost from Shanghai Metals Market[a] and Merck[b]. Properties extracted from refs. [23, 26, 38].

based batteries have recently gained enormous attention owing to their numerous advantages [8, 9]. The working mechanism of Na-ion batteries (SIBs) and K-ion batteries (PIBs) is most closely similar to that of LIBs based on the rocking chair principle, endowing the greatest potential to achieve practical application [10, 11]. Moreover, both Na and K are more abundant natural resources, with natural reservoirs approximately 1400 and 1200 times greater, respectively, than that of Li (~2.4, ~2.09, and ~0.0017 wt% of Na, K, and Li, respectively) [12]. The worldwide availability of Na and K resources makes SIBs and PIBs more economically attractive, whereas Li resources are geographically concentrated in South America [13]. The prices of metals, carbonates, and hydroxides of Na and K are much cheaper compared to those of the corresponding Li compounds (the real-time cost is provided in Table 1). Apart from material availability, it is worth mentioning that Na and K metals do not undergo an alloying reaction at a low potential with aluminum (Al) unlike Li metal [14, 15]. This allows the use of inexpensive Al foils as current collectors for both the anode and cathode in SIB and PIB systems, making them more desirable for low-cost energy storage systems.

In terms of mass production, PIBs seem to possess a major advantage over SIBs. In 2015, researchers demonstrated that graphite can be employed as an anode active material for PIBs with a similar storage mechanism to LIBs (i.e., intercalation) [16]. However, graphite has not been regarded as a suitable electrode for SIBs due to the thermodynamic instability of Na ion-graphite intercalation compounds [17]. This finding would bring various benefits for the commercialization of PIBs by employing similar manufacturing processes to those used for LIBs.

Though the graphite electrode has exhibited the feasibility for PIBs, graphite can only store K ions with a theoretical capacity of $279\,mAh\,g^{-1}$, which is far below the capacity to host Li ions ($372\,mAh\,g^{-1}$) [18]. Given the insufficient gravimetric capacity of graphite, researchers have explored various candidate materials for anodes that offer higher capacity [19, 20]. Among the numerous active materials explored for anodes, K metal is considered the most ideal candidate for PIBs as the K metal has a higher specific capacity ($687\,mAh\,g^{-1}$) compared to other anode materials reported recently [16, 21].

The K metal electrode also has various advantages over both Li and Na metal electrodes. (i) The K metal exhibits a lower standard redox potential (-2.93 V vs. standard hydrogen electrode (SHE)) compared to Na (-2.71 V vs. SHE) and is even comparable to the redox potential of Li (-3.04 V vs. SHE) [22]. Interestingly, the K metal has a lower redox potential in propylene carbonate (PC) solvent than Na and Li [23]. Komaba et al. showed that the standard potential of K^+/K is located at -0.15 V vs. that of Li^+/Li in ethylene carbonate/diethyl carbonate (EC/DEC) electrolytes, indicating the possibility of a higher working voltage and power operation in a nonaqueous system [24]. (ii) K ions exhibit the smallest Stokes radius among alkali metal ions (K^+ (3.6 Å) < Na^+ (4.6 Å) < Li^+ (4.8 Å)) owing to its weaker Lewis acidity [23]. The small Stokes radius of the K ion may lead to higher mobility of the K ion compared to Li and Na ions, which can contribute to a higher transference

number and ionic conductivity of K ions than of Li and Na ions [22]. Indeed, the K ion exhibits a higher ionic conductivity ($10\,mS\,cm^{-1}$ in 1 M PC) in PC solvents compared to Li and Na ions [23]. (iii) In a view of the solvation structure, Na and K ions possess disordered and flexible structures compared to Li ions, resulting in the lower desolvation energy of Na and K ions than of Li ions [25]. In particular, K ions require the lowest desolvation energy compared to Na and Li ions, enabling faster K ion diffusion and thus an enhanced rate performance [26]. It is worthwhile to mention that a low-concentration K ion electrolyte could be achieved due to its low desolvation energy, which can contribute to additional cost saving [27, 28]. (iv) Cathode materials for PMBs (i.e., PTCDA, Prussian blue, and their analogs), which show best performances, are cobalt-free (state-of-the-art cathode materials are described in Table 2) [11]. Cobalt, which is considered the most crucial component of the cathode, is also a less abundant element and is distributed unevenly in the earth's crust, raising concerns over its supply availability [29]. Furthermore, the extraction process of cobalt raw materials is highly associated with toxicity and ethical issues [29, 30]. These technoeconomic issues would provide rationales for K-based batteries rather than Li-based batteries. (v) K metal anodes facilitate high-energy-density batteries based on conversion chemistry with potassium-free cathodes, such as potassium-oxygen (K-O_2: $K + O_2 \leftrightarrow KO_2$) and potassium-sulfur batteries (K-S: $3S + 2K \leftrightarrow K_2S_3$) [31, 32]. Studies have shown that potassium superoxide (KO_2) is thermodynamically and kinetically stable, resulting in a higher round-trip energy efficiency compared to Li- and Na-O_2 batteries [33]. Ren and Wu showed that K-O_2 batteries could potentially offer a high theoretical specific energy density of up to $935\,Wh\,kg^{-1}$ and a low discharge/charge potential gap of less than 50 mV without the presence of catalysts [34]. Zhao et al. suggested that K-S batteries could achieve a gravimetric energy density of $1023\,Wh\,kg^{-1}$ (2.1 V as the average voltage used for calculation) [35]. In this regard, the K metal batteries, combined with the K-free cathodes, could deliver much higher energy densities than commercial LIBs (graphite-$LiCoO_2$, graphite-$LiNi_{0.33}Co_{0.33}Mn_{0.33}O_2$, graphite-$LiFePO_4$, and so on), making them more appealing for large-scale and low-cost energy storage systems [36].

Although the K metal anodes present numerous advantages, they face several challenges that are not only similar to those of Li and Na metals but often more severe. More seriously, it is often limited to transferring the legacy of LIBs (or lithium-metal batteries (LMBs)) to PMBs. For instance, due to its large ionic radius which leads to losing its valence electron easily, the K metal possesses a higher reactivity compared to Li and Na [34, 37]. Hence, the K metal must be treated much more carefully and stored in mineral oil, unlike commercial Li metal which is available in regulated forms such as foils and wires. That is, to employ the K metal, battery manufacturers would need facilities to remove mineral oils and form a sheet metal in a rigorously controlled environment.

The lattice parameter of the K metal is larger than that of Li (0.533 nm vs. 0.351 nm), causing significant dimensional changes during the plating/stripping process [38]. Of course, the severe volume fluctuation can more seriously pulverize the liquid/solid interphase during the continuous plating/stripping of K, potentially putting K metal electrodes in a worse state than Li metal electrodes [39]. It is known that continuous damage and reconstruction of the interface, coupled with nonuniform ion flux, can promote dendrite formation [40, 41]. Considering K has much poorer mechanical properties than Li and Na, K dendrites are expected to be weaker than those of Li and Na. Consequently, it is likely for K metal anodes to exhibit a short lifetime of cells compared to Li metal anodes [42, 43]. The challenges associated with K metal anodes are often compared to those of Li metal anode issues, but they have distinct properties and electrochemical behavior. Therefore, it is crucial to figure out the underlying differences between the K metal anode and other alkali metal anodes and identify which knowledge learned from LMBs can be implanted into PMBs.

Although a couple of review articles about K metal electrodes have already been reported [5, 44], only a few reviews have been published with a comparison to other alkali metals. Also, recent research trends are rapidly changing with the reports of advanced techniques. Thus, the comprehensive review articles, including recent reports, could provide valuable insights for the uptake of next-generation batteries. In this review, we first discuss the specific challenges of K metal anodes in comparison to other alkali metal anodes (Figure 1). Then, we review recent research and development regarding the K metal anode. We categorize various strategies for resolving the issues into two groups: direct and indirect engineering. Direct engineering refers to the inhibition of dendrite growth through K electrode design. On the other hand, the suppression of dendrite growth by electrolyte and separator engineering is discussed in the section of indirect strategy. At last, we provide perspectives and missing spots for research on K metal anodes, aiming for practical application of the low-cost and large-scale rechargeable PMBs. The contents of this review are tabulated below.

2. Challenges of Potassium Metal Anodes

2.1. Unstable Solid Electrolyte Interface. The spontaneous reaction occurring at the interface between the electrolyte and electrode forms a unique layer called a solid electrolyte interface (SEI) [45–47]. The SEI layer has two major characteristics: it is conductive to ions, but insulative to electrons. These remarkable properties contribute to enhancing the stability of battery operation [48]. A robust and stable SEI layer enabled the successful commercialization of LIBs with graphite and lithium transition metal oxide electrodes since the 1990s [49]. As the demand for high-energy-density storage systems grows, alkali metals considered as a next-generation anode material may replace graphite [41, 50–53]. However, metal anodes have safety issues, and the culprit of the issue is often identified as unstable SEI on alkali metal anodes. Unstable SEI can cause dendrite growth and finally lead to a fire. To address the safety issue,

Table 2: Summary of electrochemical performance of the state-of-the-art K metal batteries.

Cathode	Anode	Electrolyte	Voltage (V)	Current density ($mA\,g^{-1}$)	Initial capacity ($mAh\,g^{-1}$)	Capacity retention (cycles) (%)	Ref.
$K_4Fe(CN)_6$	CBC-K	3 M KFSI DME	2.0-3.8	20	53.8	500 (85)	[101]
$K_{0.7}Mn_{0.7}Ni_{0.3}O_2$	K@CC	0.8 M KPF_6 EC/DEC	2.0-3.9	1000	81	8000 (68.5)	[71]
PTCDA	K-OPCMs	3 M KFSI DME	1.5-3.5	2000	143	1500 (69.4)	[291]
$Se_{0.05}S_{0.95}$@pPAN	MSCNF-K	1 M KFSI EC/DEC	1.0-3.0	500	850	600 (60)	[106]
$K_2Ti_4O_9$	a-Ti_3C_2-K	0.8 M KPF_6 EC/DEC	0.0-3.0	200	97.5	1000 (77)	[292]
Prussian blue	KBi_{80}/NrGO	3 M KFSI DME	1.5-3.8	100	85.5	550 (95.6)	[293]
$K_{1.56}Mn[Fe(CN)_6]_{1.08}$/G	Sn@3D-K	Sat. $KClO_4$PC + FEC	2.5-4.6	156	108.2	150 (67.9)	[127]
PTCDI	K-CC@SnO_2	1 M KFSI EC/DEC	1.5-3.5	2000	110	10000 (70.9)	[128]
PPB	CNT-2@NaK	0.8 M KPF_6 EC/DEC	2.5-4.5	80	96.9	200 (86.5)	[158]
TiS_2	PPS-treated K	1 M KFSI DME	1.0-3.0	235	110	400 (90)	[183]
PB/G	K@NGM	Sat. $KClO_4$PC + FEC	2.5-4.5	100	90.5	200 (84)	[120]
AQDS	Co-CNF@K	1 M KFSI DME	1.4-3.0	125	65	700 (58)	[105]
$K_{0.5}V_2O_5$	CC@CuO@K	1 M KFSI EC/DEC	1.5-3.8	20	100	200 (67.8)	[122]
SPAN	K@DN-MXene/CNT	0.8 M KPF_6 EC/DEC	0.8-2.8	125	638	500 (67)	[72]
PTCDA	CoZn@HCT@K	1 M KFSI DME	1.5-3.5	100	122	200 (71)	[125]
PTCDA	SA-Co@HC	3 M KFSI EC/DEC	1.5-3.5	200	130	200 (84)	[126]
PB	K-NiCo@NOGC	0.8 M KPF_6 EC/DEC	1.5-3.8	50	100	500 (80)	[294]
PPB	rGCA-K	0.8 M KPF_6 EC/DEC	2.0-4.5	70	70	450 (79.1)	[295]
AQDS	PCNF@SnO_2-K	1 M KFSI DME	1.2-3.0	650	120	400 (75)	[130]
$K_{0.220}Fe[Fe(CN)_6]_{0.805}$	K-GIC	0.8 M KPF_6 EC/DEC	2.0-4.5	130	80	500 (78.4)	[144]
PB	K-ACF	0.8 M KPF_6 EC/DEC	2.5-4.5	200	91.7	200 (91.2)	[143]
$K_{0.220}Fe[Fe(CN)_6]_{0.805}$	CFC/KOL@NaK	0.8 M KPF_6 EC/DEC	2.0-4.5	114	75.3	150 (93)	[37]
$K_{0.220}Fe[Fe(CN)_6]_{0.805}$	KNA@C	0.8 M KPF_6 EC/DEC	2.0-4.5	1000	104.4	200 (91)	[151]
$FeFe(CN)_6$	KNA-3.5	0.4 M KFSI-$NaPF_6$ DME	2.4-3.8	36	100	65 (100)	[154]
PB	K/CNT	0.5 M KPF_6 EC/DEC	2.5-4.5	50	103.2	200 (88)	[177]
$K_xFeFe(CN)_6$	K-Hg	0.5 M KPF_6 EC/DEC	2.5-4.5	20	125	240 (80)	[93]
PTCDA	K@K_2Te	1 M KFSI EC/DEC	1.5-3.5	2000	125	1000 (76)	[94]
PTCDA	K_3OCl/K_3Bi@K	1 M KFSI EC/DEC	1.5-3.0	1000	130	1000 (84.6)	[296]
KMCFC@rGO	K	Buffered K-Cl-IL	2.0-4.5	100	90	820 (89)	[243]
KPB	K	4 M KFSI DEGDME	2.5-4.0	85	61.1	500 (99.7)	[225]
PB	K	2.3 M KFSI G2/TFETFE	2.5-4.3	50	120	2000 (83)	[236]
$KVTiPO_4$	K	0.8 M KHFDF EC/DMC	2.0-4.4	100	125	200 (83)	[208]

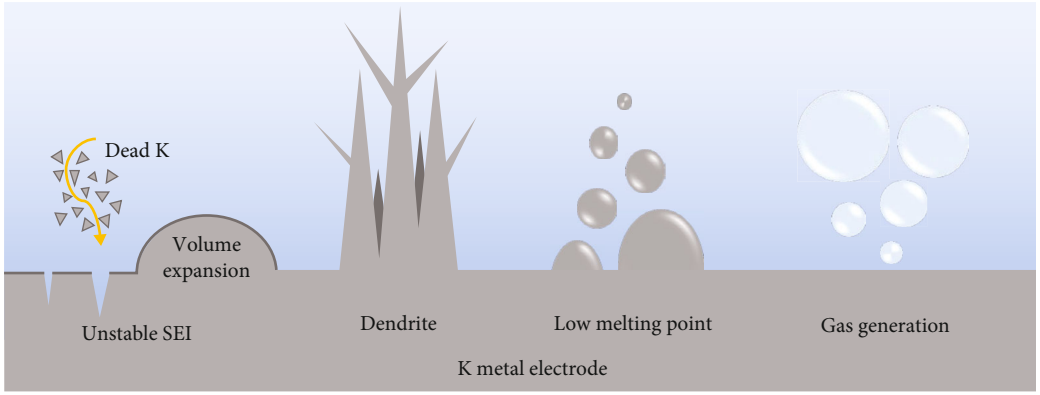

Figure 1: Schematic illustration of challenges of K metal anode.

researchers have designed stable SEI layers on alkali metals with high mechanical and chemical stability [54–56].

It is thought that the SEI layer naturally forms due to the difference between the Fermi level of the anode and the lowest unoccupied molecular orbital (LUMO) of the solvents [47]. When the anode has a higher potential energy than the E_{LUMO} of electrolytes, electrons transfer from an anode to electrolytes and induce spontaneous reduction reactions of electrolytes (Figure 2(a)). On the anode surface, decomposed electrolytes are stacked, showing an encrusted structure [39, 57]. Similar to Li- and Na-based SEI (Figure 2(b)), it is considered that K-based SEI also shows a mosaic model of the Li-SEI layer with the organic/inorganic products (e.g., ROCOOK, KF, ROK, K_2CO_3, and $KHCO_3$) (Figures 2(b)–2(e)) [58]. Although the SEI layers in PMBs showed a similar structure to those of LMBs and sodium metal batteries (SMBs), SEI layers from K-based electrolytes represented different characteristics (e.g., chemical composition, morphology, and mechanical stability) [59–61]. Hosaka et al. analyzed the chemical compositions of SEI layers on hard carbon electrodes with MFSA ("M" is either Li, Na, or K) [61]. The authors found that the outermost surface of SEI layers induced from KFSA (or NaFSA) was composed of a larger content of inorganic components than that of LiFSA (Figures 2(c)–2(e)). Also, the SEI layer induced from KFSA contained a smaller amount of sulfide species which were not observed for Li- and Na-based SEI layers. The inner SEI layer in the KFSA electrolyte system was highly concentrated with organic components. The authors argued that the different distributions of organic and inorganic components are rooted in the different solubilities and reduction stabilities of Li, Na, and K [62, 63]. The mechanical stability of SEI on alkali metals is known to vary depending on the chemical composition of the SEI and the properties of the metal [64, 65]. Researchers have used atomic force microscopy (AFM) to analyze Young's modulus and force curves (Figures 2(f)–2(h)) [66]. In the AFM test, the SEI layer on K and Na metals exhibited noticeable fractures in contrast to that of Li. Their results indicate that the SEI layer on the K metal is less mechanically stable than that on Li and Na. The authors also bent alkali metal foils up to 180° and only observed cracks from the K metal (Figures 2(i)–2(k)). As evidenced by the presence of bending and indentation tests, the SEI layer on the K metal is less flexible than that of Li and can be broken during cycling more readily.

Direct observation and analysis of the SEI layer on the K metal are challenging due to its low damage threshold and sensitivity to electron beams which are ascribed to weak atomic bonding energy and low melting point [67]. To overcome the difficulty, Zhang et al. investigated the SEI layer and dendrites on the K metal using cryotransmission electron microscopy (cryo-TEM) techniques (Figures 3(a) and 3(b)) [57]. The authors showed that K dendrites formed in a carbonate ester-based electrolyte have a relatively chaotic moss structure and an average diameter of 1.9 μm which may pierce the pores of glass fiber separators [68]. The authors also observed that the SEI layer on the K metal consists of amorphous inorganic components, including $KHCO_3$ and K_4CO_4 (Figures 3(c)–3(f)). Due to the chemical instability, K_4CO_4 could be decomposed into K_2CO_3 and K_2O [69]. Thus, the porous morphology of dendrites, continuous gas formation (discussed in the following section) from the SEI layer, and poor ionic conductivity of the SEI layer in potassium batteries could be attributed to the presence of the components.

With the different characteristics of K compared to Li and Na, it is inadequate to apply conventional methods to stabilize Li- and Na-SEI layers. In this regard, it would be required for K-SEI layers to control the components of the SEI layer and strengthen mechanical/chemical stabilities. To reinforce the poor stabilities of the K-SEI layer, artificial-SEI engineering, high concentration of electrolytes, electrochemical pretreatments, and electrolyte additives that would be applicable (discussed further in the section of electrolyte engineering) have been recommended as effective solutions for improving the mechanical and chemical stabilities of the K-SEI layer. Overall, the recent attentions given to the studies of the SEI layer on K metal highlights the need to better understand and control the components of the SEI layer to enhance the performance and safety of potassium-based batteries.

2.2. Dendrite Growth. Dendrite growth is a common phenomenon observed in all types of alkali metal anodes during

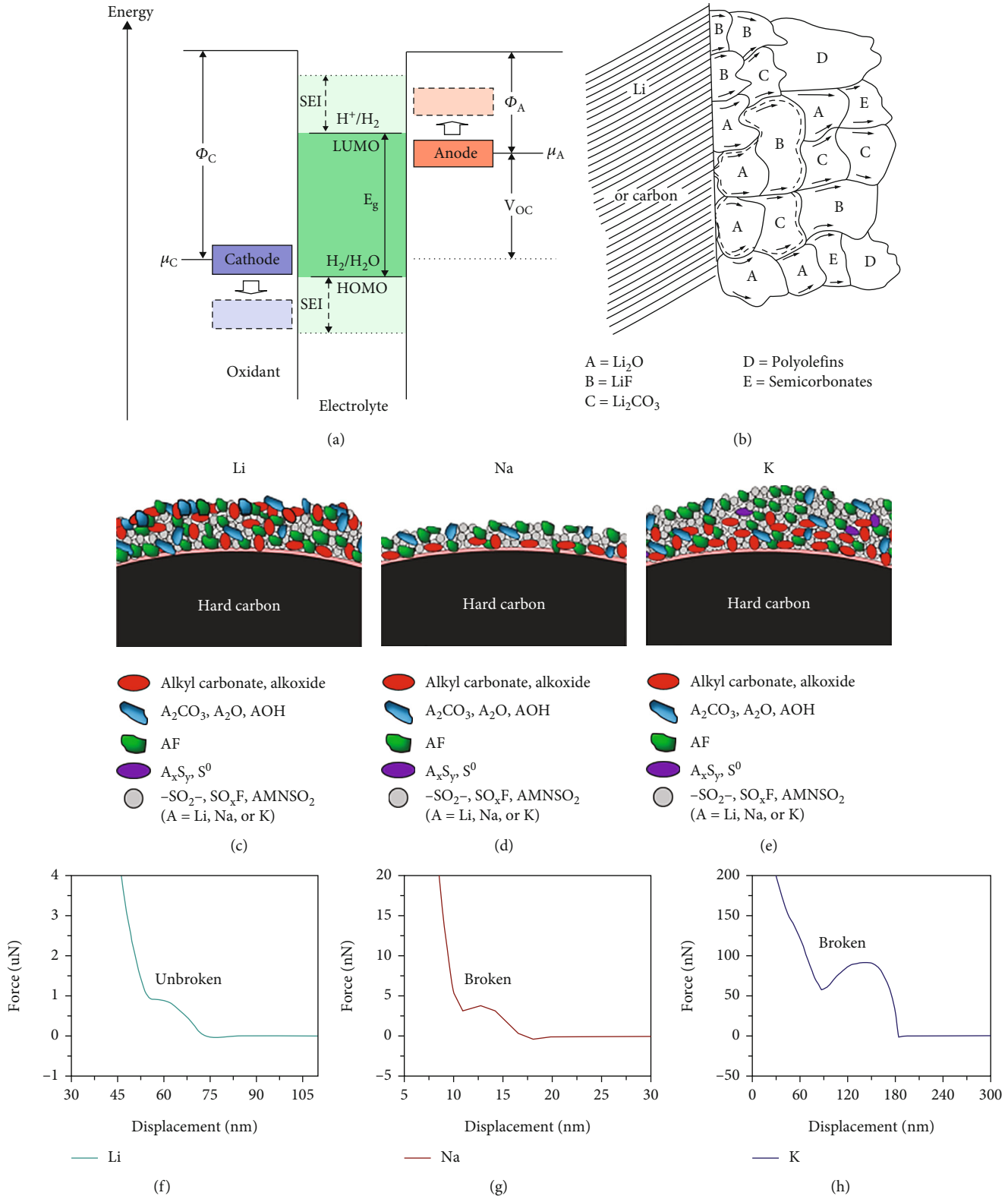

Figure 2: Continued.

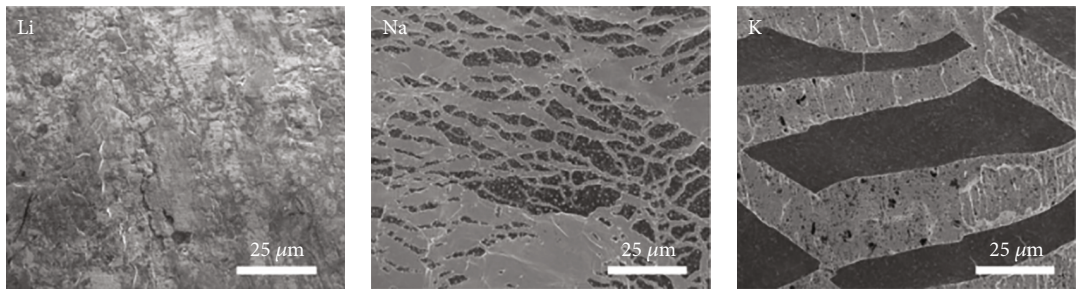

(i) (j) (k)

Figure 2: (a) Schematic of electrolyte energy diagram. (b) Conventional mosaic model of SEI layer on lithium or carbon electrode, reproduced with permission [47]. Copyright 2009, American Chemical Society. (c–e) Schematic illustration of the SEI compositions and thickness formed on hard carbon electrodes, reproduced with permission [61]. Copyright 2009, American Chemical Society. (f–h) Typical AFM force curves of Li, Na, and K covered with SEI. (i–k) Microscopic images of metal anodes' surface after bending test, reproduced with permission [66]. Copyright 2020, Elsevier.

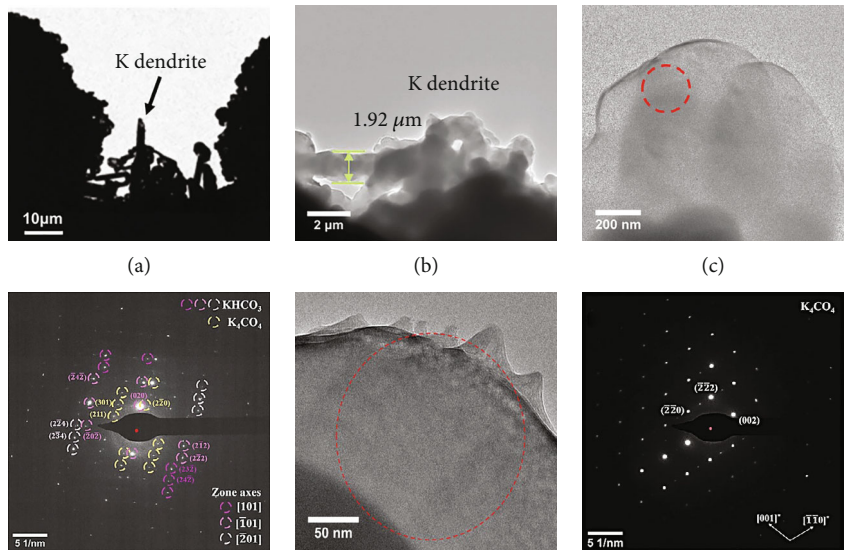

(a) (b) (c)

(d) (e) (f)

Figure 3: (a, b) Cryo-TEM images of K dendrites. (c) Large-scale cryo-TEM images of K dendrites with (d) selected-area electron diffraction (SAED). (e) Small-framed cryo-TEM images of K dendrites with (f) SAED, reproduced with permission [57]. Copyright 2021, Wiley.

electrochemical plating under various types of electrolytes and depths of discharge [70]. Due to the inherently fragile SEI and large volume fluctuation during the plating/deplating process of alkali metal electrodes, cracks can be generated in the SEI on the alkali metal surfaces. These cracks can result in a nonuniform ion flux, thereby causing uneven metal plating and dendrite growth [71]. Once dendrites form on the metal electrode surface, they can continuously grow towards a cathode with various sizes from micro- to nanometers [66]. Eventually, they might pierce separators and cause alkali metal batteries to undergo short circuits via the direct contact between the anode and cathode. This electrical shortening may lead to thermal runaway, potentially resulting in catastrophic explosions and fires. Although K dendrite growth is considered more severe than that of Li, the models describing the Li deposition behavior could be employed to explain K dendrite growth to a large extent. In the following section, the growth theory and behavior of metallic dendrites are summarized, and the comparison with Li and Na dendrites will be discussed.

2.2.1. Space-Charge Model. The space-charge model is the most widely adopted theory to describing the nucleation and protrusion of metallic dendrites [70, 72]. This model depends on a concentration gradient of cations in the electrolyte during electrodeposition. The concentration gradient in a cell with a short distance between electrodes can be defined as follows:

$$\frac{\partial C}{\partial x}(x) = \frac{J\mu_a}{eD(\mu_a + \mu_c)}, \tag{1}$$

where J is the effective current density, e is the electronic charge, D is the diffusion coefficient, and μ_a and μ_c are the

mobilities of anions and cations, respectively [73]. According to Equation (1), a high current density increases the ion concentration gradient, while depleting cations near the metallic electrode surfaces. This ruins the electrical neutrality at the deposited metal surface, resulting in the accumulation of a local space charge and thus formation of a branch-like metal deposition [70]. Dendrites would evolve at time τ, called as "Sand's time," which is defined as follows:

$$\tau = \pi D \left(\frac{C_0 e z_c}{2J}\right)^2 \left(\frac{\mu_a + \mu_c}{\mu_a}\right)^2, \quad (2)$$

where C_0 is the initial salt concentration and z_c is the charge number of cations [73]. Equation (2) proposes that the starting time of dendrite growth relies on J^{-2} and indicates that a high current density highly promotes the formation of dendrites. Therefore, it is expected that K dendrites would emerge at the diffusion limitation when a high current density is applied. Ma et al. observed that a needle-like K dendrite burst out of the K metal surface at Sand's time, demonstrating the feasibility of the space-charge model for K metal electrodes [74]. Based on Equation (2), various strategies to suppress dendrite growth have been proposed to delay Sand's time, including high concentration electrolytes (discussed in *(3) Highly Concentrated Electrolytes*) and 3D current collectors (*(1) 3D Host Structures Based on Sand's Time*) for the K metal anode.

2.2.2. Film-Growth Model. The classical theory of film growth would be applicable to the initial plating process of the K metal [38, 70]. The formation and growth of K dendrites can be explained by a thermodynamic parameter, surface energy [75]. This film-growth model proposes that the type of growth can be determined by a balance between the surface energy of the substrate, surface energy of the film, and energy of their interface [76]. Based on this, the three models are suggested during K plating: (i) 3D island-like growth (Volmer-Weber (V-W)), (ii) 2D layer-by-layer growth (Frank-van der Merwe (F-M)), and (iii) 2D layer followed by 3D island-like growth (Stranski-Krastanov (S-K)), which are established in the vacuum deposition theory [38]. The growth mode of film on a substrate can be described by the wetting angle θ of Young's equation, the balance point of surface tensions, defined as follows:

$$\gamma_{sf} + \gamma_{f-\mathrm{SEI}} \cos\theta = \gamma_{s-\mathrm{SEI}}, \quad (3)$$

where γ_{sf} is the surface tension of the substrate film, $\gamma_{f-\mathrm{SEI}}$ is the surface tension of the film-SEI layer, and $\gamma_{s-\mathrm{SEI}}$ is the surface tension of the substrate and SEI layer [77]. The balance of forces determines the thermodynamic shape of a film on a substrate. This is characterized by its wetting angle, expressed as follows:

$$\cos\theta = \frac{\gamma_{s-\mathrm{SEI}} - \gamma_{fs}}{\gamma_{f-\mathrm{SEI}}}. \quad (4)$$

Based on Equation (4), when the inequality $\gamma_{s-\mathrm{SEI}} - \gamma_{sf} < \gamma_{f-\mathrm{SEI}}$ increases, the wetting angle also increases, and thus, the film follows the V-W growth. As a result, the film no longer wets the substrate, exhibiting as an island-like growth on the substrate. However, if the inequality $\gamma_{s-\mathrm{SEI}} - \gamma_{sf} \geq \gamma_{f-\mathrm{SEI}}$ is satisfied, the wetting angle goes to zero, following the F-M growth with a planar 2D thin film on the substrate. It is worthwhile to mention that the S-K growth could be realized if there are changes to the surface tensions as a function of film thickness (i.e., accumulation of strain energy causes a rise in γ_{sf}) [75]. As a result, the film grows planar at the early stage; however, eventually, islands form on the substrate as the film thickens.

The K metal inherently exhibits poor wettability on bare Cu and Al foil current collectors, which leads to the V-W growth during the K deposition process [15, 75]. These island-like deposits would act as seed points to initiate the growth of K dendrites. Thus, to realize the F-M growth on Cu and Al current collectors, it is essential to control the competition between surface forces through (i) increasing the potassiophilicity of current collectors or (ii) increasing the surface energy of the substrate (discussed in Section 3.1.4).

2.2.3. K Dendrites Differ from Li and Na Dendrites. K dendrites appear to be weaker than Li and Na dendrites. As shown in Table 1, the K metal has the lowest shear modulus (1.3 GPa) and Brinell hardness (0.36 MPa) [38]. Furthermore, with its low melting point of 63.4°C and high surface diffusion constant, the K metal could flatten the uneven surface morphology attributed to nonuniform K deposition [78–80]. Accordingly, it may be rationale to assume that K dendrites can be blocked more easily, even though mechanical properties of K-SEI are a bit low. However, the opposite results were observed with K dendrites, with short lifetimes and internal short circuits being more severe in potassium metal batteries, regardless of the electrolyte used [42, 43]. The observed phenomenon can likely be attributed to two main factors: (i) the different ion behavior through the SEI layer (i.e., despite identical anion species and thus similar chemical composition of SEI) and (ii) different protrusion growth modes (i.e., the Li dendrite is mostly described by the root growth overcharging process while K depends on the surface growth mode; discussed further in the following paragraphs).

The behaviors of Li, Na, and K dendrites inherently differ from one another due to distinct chemical, electrochemical, and mechanical properties. The K metal, for example, acts as a super reducing agent for organic electrolytes, thereby leading to difficulties in constructing an efficient passivation layer on its surface [33]. Figure 4(a) displays the open circuit voltage (OCV) profiles of symmetric cells of Li||Li, Na||Na, and K||K with 1 M $LiPF_6$, 1 M $NaPF_6$, and 0.8 M KPF_6 in EC/DEC, respectively. The K||K cell exhibits a higher OCV than the others, averaging over 500 mV with a large fluctuation of greater than 100 mV. Moreover, a substantial polarization of at least 100 mV is observed in the K||K cell with voltage spikes up to 1 V, even

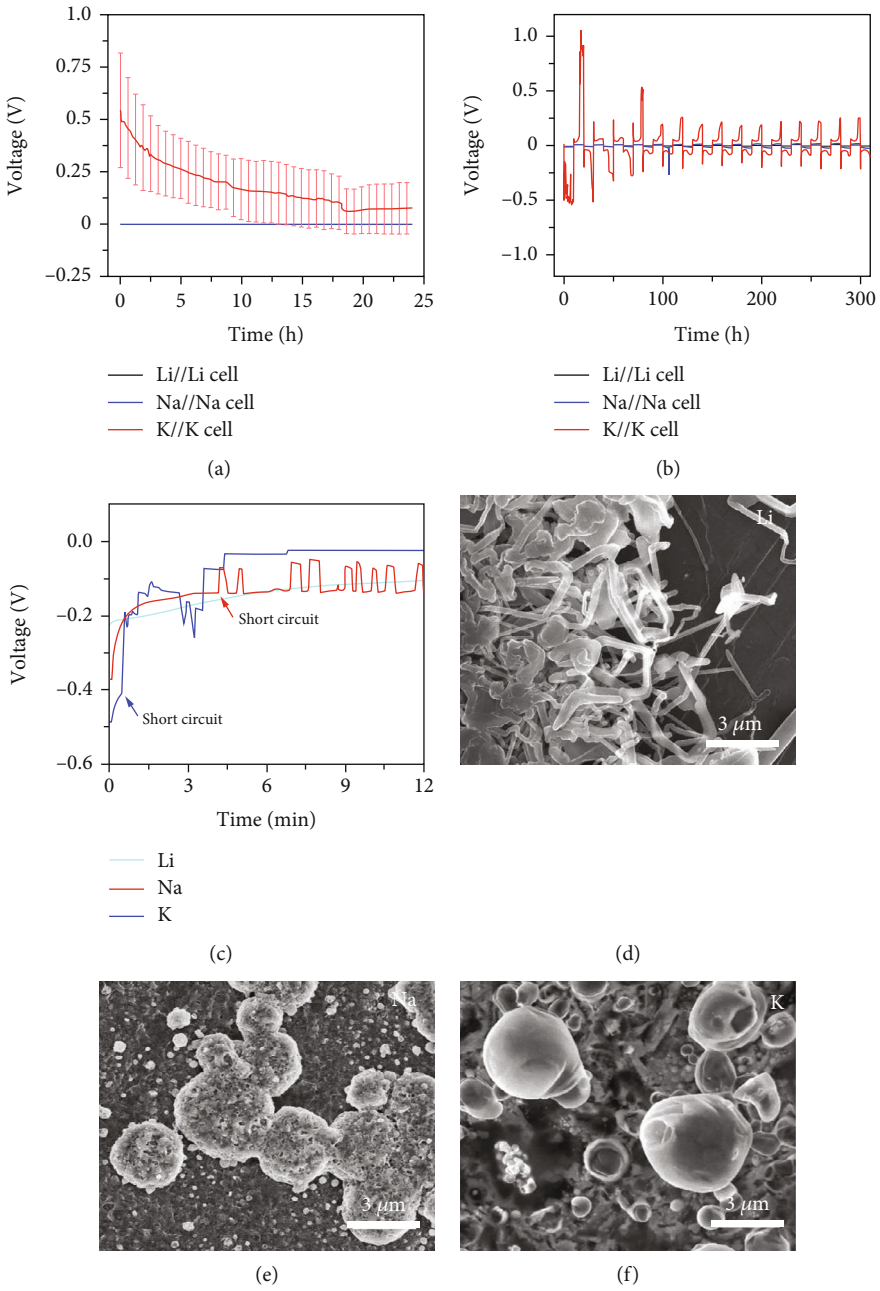

Figure 4: Continued.

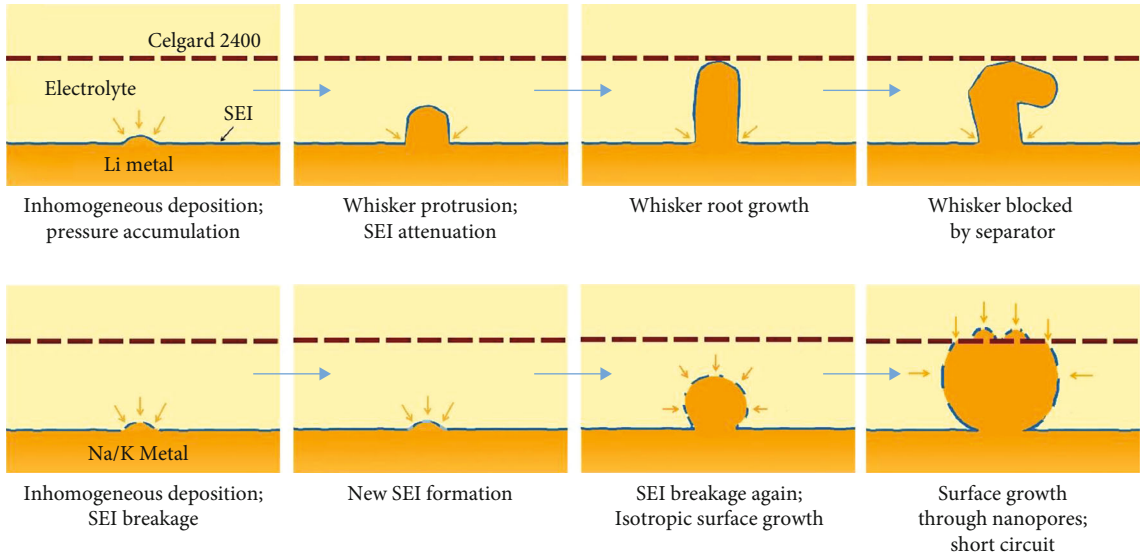

Figure 4: (a) Open circuit voltage profiles of symmetric cells of Li||Li, Na||Na, and K||K with 1.0 M $LiPF_6$-EC/DEC, 1.0 M $NaPF_6$-EC/DEC, and 0.8 M KPF_6-EC/DEC, respectively. (b) Voltage curves of the symmetric cells during the plating-stripping process, reproduced with permission [98]. Copyright 2019, American Chemical Society. (c) Voltage profiles of the symmetric cells using Celgard 2400 separator. (d–f) Li, Na, and K deposits on metal surfaces after 50 s deposition. (g) Schematic illustration of Li, Na, and K deposition mechanism, reproduced with permission [66]. Copyright 2020, Elsevier.

at a relatively low current density of 25 $\mu A\,cm^{-2}$. In contrast, the Li||Li and Na||Na cells represent relatively smaller overpotential profiles (Figure 4(b)). These results suggest that even with identical electrolyte compositions and current density, the K metal forms unstable SEI layers compared to Li and Na. Considering the unstable SEI layer on K metal anodes (discussed in Section 2.1), it appears that inhomogeneous plating of the K metal and acceleration of K dendrite growth may be highly associated with the different nature of K-based SEI to the others.

Metal deposition theory proposes three modes of protrusion growth: tip growth, root growth, and surface growth [66]. Tip growth is a general phenomenon in metal deposition from electrolytes, occurring when the Li deposition rate surpasses the limiting current density (J_{lim}) after Sand's time [73]. This is due to the limitation of long-range electrolyte diffusion. The root growth mechanism takes place at a current density below J_{lim}. During the electroplating process of the Li metal at rates below J_{lim}, deposition is inhomogeneous due to the nonuniformity of the interface between the Li metal and electrolyte. As Li is deposited, the pressure beneath the SEI increases, leading to tensile stress to SEI layers. When these stresses exceed the mechanical limit of the SEI, the Li metal protrudes from beneath the SEI, forming whiskers [74]. The surface growth mechanism can also occur below J_{lim} during Li deposition. Generally, the integrity of the SEI is a crucial factor in determining whether the deposition follows the root growth or surface growth mode [81]. During deposition, the formation of SEI competes with the deposition of Li, and the current density influences this competition. If the SEI layer forms faster than the Li deposition at a specific current density, the SEI becomes dense and robust, and the deposition will follow the root growth mode. Otherwise, the SEI becomes disconnected, causing deposits to grow on the exposed metal points and spread across the surface, forming granules [81]. Hu et al. investigated the morphologies of electrochemically deposited Li, Na, and K metals with the use of 0.5 M MPF_6("M" is either Li, Na, or K) in EC/DEC electrolytes at the current density of 1 $mA\,cm^{-2}$ [66]. Short circuits were observed at around 5 minutes for Na and 1 minute for K symmetric cells (Figure 4(c)). This claims that K deposits pass through the separator more readily due to a different deposition mode compared to Li. The different deposit morphologies of each alkali metal are illustrated in Figures 4(d)–4(f). Li deposits show whisker-shaped dendrites, indicative of root growth mode. However, the K metal (as well as Na metal) is deposited in a granular shape, suggesting that K follows the surface growth mode (Figure 4(g)). These differences may come from the unstable and fragile SEI on the K metal, which can also explain why a lot of research has employed glass fibers as separators for K metal electrodes [68, 72, 82]. That is, since the K metal is deposited in the surface growth mode, K deposits are likely to easily pierce the nanosized pores of the Celgard separator. Thus, a glass fiber which is thicker and has randomly distributed pores should be used as a separator for K metal electrodes [83]. Consequently, to control K dendrite growth, the strategies that have worked for Li dendrites should serve as benchmarks rather than direct solutions.

2.3. Low Melting Point of Potassium. Ensuring batteries operate at an appropriate temperature is key to obtaining high performance, as it helps prevent irreversible degradation of their active materials and electrolytes. The battery temperature can rise continuously during charging/

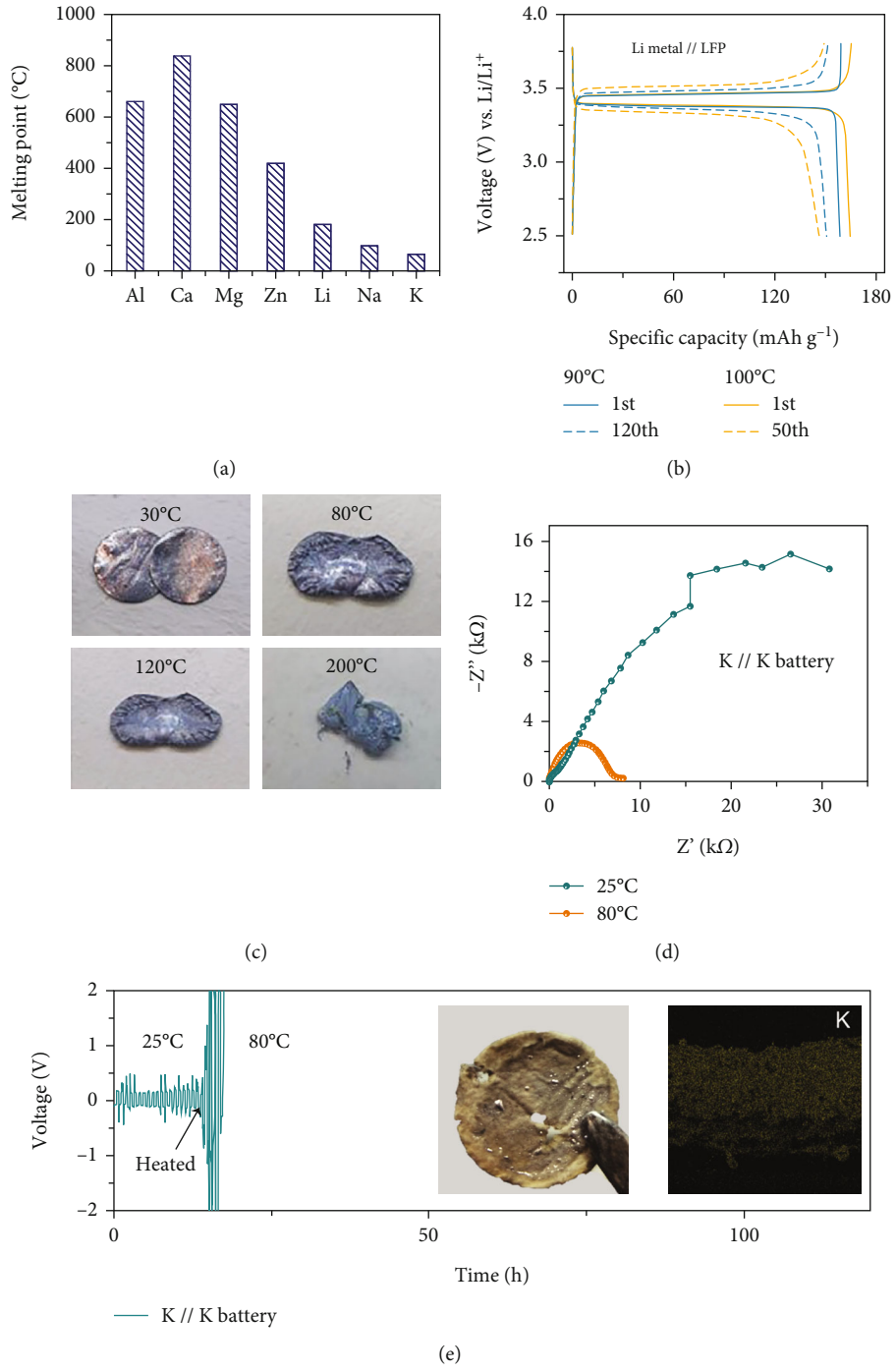

Figure 5: (a) Melting points of promising candidates of metal anode, reproduced with permission [67]. Copyright 2021, Wiley. (b) The voltage profiles of Li||LFP cells at 90°C and 100°C, reproduced with permission [84]. Copyright 2022, Wiley. (c) Digital photos of K metal at different temperatures at 30°C, 80°C, 120°C, and 200°C. (d) EIS measurement at different temperatures of K||K cells after 1st cycle. (e) The voltage profiles during galvanostatic cycling at 25°C and 80°C. Insets: digital image and SEM image of the separator from K||K cells at high temperature, reproduced with permission [67]. Copyright 2021, Wiley.

discharging cycles or when they are under harsh external conditions and ineffective thermal management. When the temperature exceeds the safety limit (60°C) [84], it can lead to thermal runaway or even explosions [85]. K, in particular, has a lower melting point of 63.4°C than Li (180.5°C) and Na (97.7°C) (Figure 5(a)), indicating that PMBs should be more thoroughly designed in view of temperature management. For instance, LMBs can cycle over 120 cycles at 90°C and more than 50 cycles even at 100°C, which are much higher than the meting point of the K metal (Figure 5(b)) [84].

Concerning the lower melting point of K compared to Li, the K metal anode can be transited into a molten state at such a high temperature. Molten K can exacerbate parasitic reactions with liquid electrolytes, dropping the electrochemical

performance of K metal anodes, flowing into the pores of separators, and coming into contact with the cathode side. Liu et al. investigated the effect of working temperature on K metal anodes. When the temperature increases over 80°C, it transitions to a liquid state and merges together, losing its metallic luster (Figure 5(c)) [67]. Electrochemical performance was also largely dropped at the elevated temperature. As shown in the Nyquist plots (Figure 5(d)), the K metal electrode cycled at 80°C exhibited a much larger impedance than that at 25°C. In addition to the increased impedance, the overpotential of the K||K symmetric cell at 80°C was higher and increased up to 5 V during cycling (Figure 5(e)) [67]. The authors observed that the separator of K||K symmetric cells changed its color and contained molten K metal, indicative of a serious safety risk (insets of Figure 5(e)). Therefore, PMBs may require more thorough thermal management systems than other systems. Moreover, designing host electrodes to prevent the leakage of molten potassium from the host matrix is a crucial step in ensuring the safe application of potassium metal batteries.

2.4. Gas Generation. Gas generation is a safety concern for all secondary batteries, including Li-based and Na-based batteries, even in Li-ion batteries which are commercially successful [86, 87]. Continuous gas generation increases the internal pressure within cells, causing them to swell and potentially explode. Coin cells, due to their small sizes and designs, may withstand increased pressure. However, large-size batteries such as pouch cells may experience significant volume change from continuously generated gas bubbles during charging/discharging processes, which can negatively impact the structure of cell stacks (or electrode contact) and deteriorate performance.

Researchers have sought to reveal the origin of gas evolution in LIBs. They have identified various sources for gas generation, such as SEI formation, film formation on cathode, electrolyte oxidation, oxygen release from metal oxides, and residual water reduction [88]. In LIBs, it is thought that ether-based electrolytes with Li metal release methane and ethane gas. In carbonate-based electrolyte systems, it tends to generate CO_2, CO, and C_2H_4 via carbonate solvent decomposition [89]. High-water-content electrolytes will form H_2 gas resulting in water reduction at the anode side (Figure 6(a)) [90]. Recent studies have investigated gas evolution in LMBs and SMBs [86, 87, 91]. Chen et al. found that the use of organic solvents such as propylene carbonate (PC) with Na ions can lead to more severe electrolyte decomposition and gas generation rates than the use of pure PC [86]. This is because sodium-ion-solvent complexes have lower unoccupied molecular orbital (LUMO) energy than pure PC solvents, making them more susceptible to reduction during SEI formation, thereby releasing gas bubbles (Figure 6(b)) [92].

Recently, researchers have observed gas evolution on K metal electrodes through in situ optical microscopy [73, 93–95]. Bai et al. observed gas bubbles forming during the K deposition process in both carbonate- and ether-electrolyte systems. These gas bubbles consequently occupied the whole cross-section of the glass capillary, resulting in perfect blockage of the ion diffusion pathway with enlarged and unstable voltage profiles [74]. To mitigate and prevent gas generation in metal batteries, it is required to build an effective insulating layer on the metal electrode. This interfacial engineering could be applied to metal electrodes by employing electrolyte additives [96]. In a recent study, the effect of fluoroethylene carbonate (FEC) on gas generation was reported (Figures 6(c)–6(h)) [97]. The authors observed that the as-fabricated cell without FEC shows varied sizes of bubbles, and the bubbles continuously evolved during the electroplating process. In contrast, bubbles were rarely observed with FEC and less evolved during the electroplating process (Figures 6(f)–6(h)). The authors claimed that an FEC-containing electrolyte produces a more insulative layer, preventing electron transfer from the K metal to the electrolyte and, as a result, inhibiting further decomposition of electrolytes and gas generation [97]. Compared to gas generation in LIBs or SIBs, gas generation on K metal anodes has drawn less attention so far. Considering the K metal is more highly reactive to organic electrolytes than Li and Na [98], the gas evolution issue should be on an imminent list to resolve.

3. Suppression of Dendrite Growth

3.1. Direct Engineering of an Electrode

3.1.1. Hosts for Potassium Metal

(1) 3D Host Structures Based on Sand's Time. Based on the space charge model and the equation, which is called Sand's time, the lower effective current density can help metal electrodes to delay the emergence of dendrite [74, 99]. Thus, the electrode design with larger surface areas would be a promising host framework for metal electrodes. Also, such a design with superior mechanical properties is benign with regard to accommodating volume expansion during cycling. In an effort to decrease the local current density of electrodes, 3D-host materials have attracted great attention in alkali metal anode engineering [100, 101]. Considering that the space of a cell is limited, porous (or interconnected materials) would be the most effective way to mitigate the dendritic issue of an alkali metal electrode [102, 103].

Among various host materials for alkali metals, carbonaceous materials can provide many advantages due to their high electrical conductivity, excellent mechanical strength, flexibility, lightweight, and tunability [104]. In particular, graphene, carbon nanotubes (CNTs), carbon fibers (CNF), and carbon cloths have been used to create sturdy host structures that offer a large surface area [67, 99, 102]. In many studies, freestanding K/CNT and K/CNF composite electrodes were prepared by immersing freestanding CNT films into molten K [71, 99, 101, 102, 105, 106]. Compared to bare K metal electrodes, those K/CNT and K/CNF composites showed a much longer lifetime over 200 h with a small overpotential of ~200 mV [99, 102]. Besides the 3D-structured carbon framework, 3D Cu foam or mesh might be utilized as host structures due to their attractive feature (e.g., high

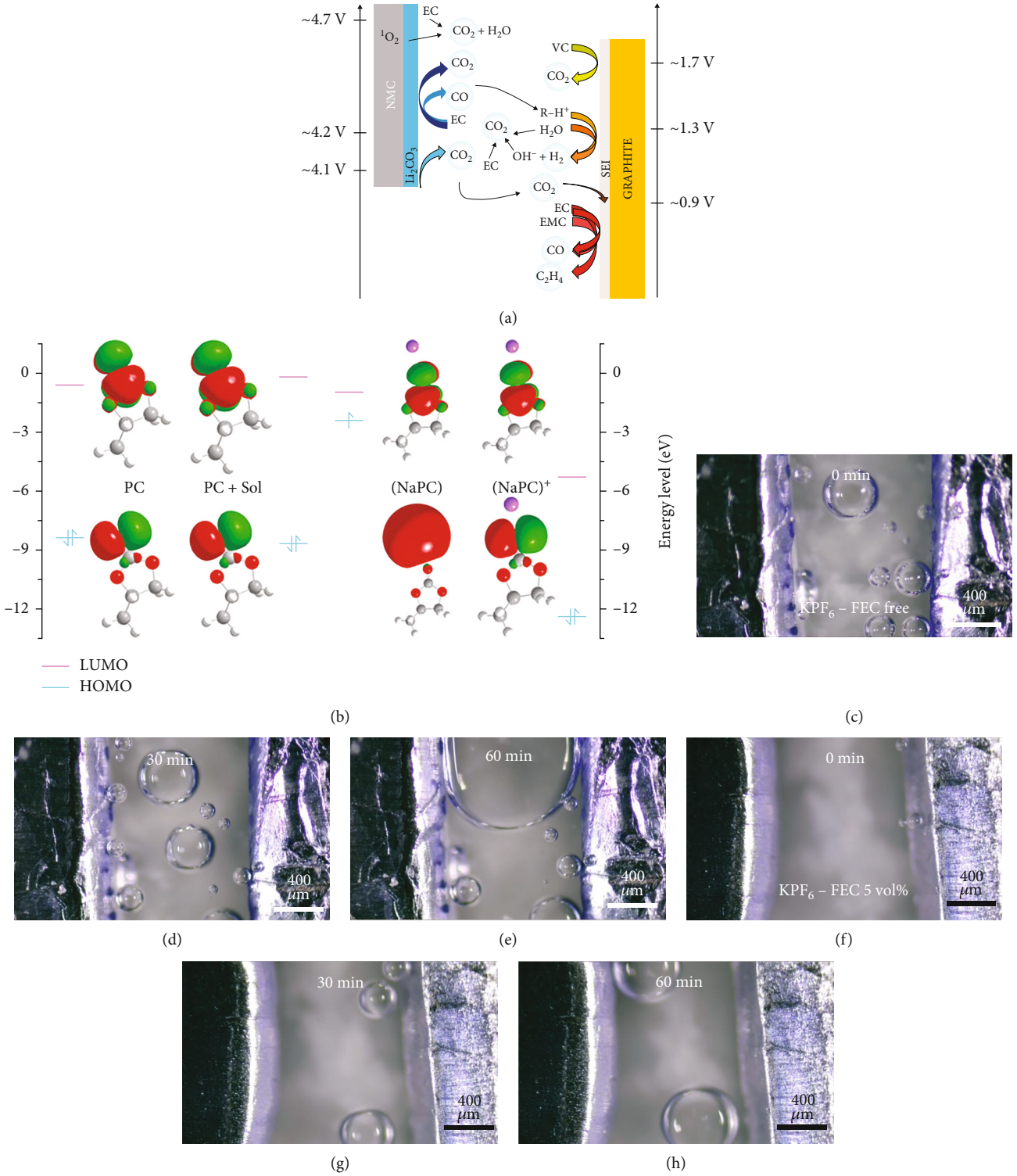

FIGURE 6: (a) Scheme of various routes of gas generation in Li-ion batteries, reproduced with permission [88]. Copyright 2021, Elsevier. (b) Molecular orbital theory analysis of single PC molecule (PC), PC molecules with solvent effects (PC + Sol), Na-atom-PC complex (NaPC), and Na-ion-PC complex ($NaPC^+$). Positive and negative regions of LUMO and HOMO are represented in red and green, respectively. H: white; Li: purple; C: gray; O: red, reproduced with permission [86]. Copyright 2018, Wiley. *Operando* snapshots of K symmetric cells filled with (c–e) KPF_6 and (f–h) KPF6-FEC electrolytes. (c, f) At the start point, (d, g) after electroplating for 30 min, and (e, h) 60 min, reproduced with permission [97]. Copyright 2023, Springer Nature.

electrical conductivity, superior mechanical properties, and high surface area) [75, 82, 100, 107, 108].

(2) Motivation of Potassiophilic 3D Host Structures. Although the strategy based on Sand's time has shown progress in LMBs [109], solely depending on the modification of the host architecture would be an insufficient solution to dendrite growth on K metal anodes. Indeed, some researchers have reported that pristine CNT electrodes often fail to suppress the K dendrites' growth [72, 110]. Therefore, on top of the scaffold design with a large surface area, another strategy is still needed. As a promising approach to address the K dendrite growth, "potassiophilicity" has recently drawn great attention. "Potassiophilicity" literally represents sites on an electrode that preferentially attract K ions, and the spots with K ions become affinitive sites for K ions [73]. With morphological and electrochemical advantages, a potassiophilic 3D host could regulate the internal electric field and homogenize the K depositions at the ion and electronic levels, eventually limiting K dendrite growth [95, 111]. The strategy for making a host structure preferentially attract certain ions has worked in LMBs and SMBs too. For example, Cui et al. designed a hollow carbon sphere with gold (Au) nanoparticles inside which could serve as a lithiophilic host. During the deposition process of Li, Li ions preferentially nucleated on the Au nanoparticle seeds inside hollow carbon spheres, and thus, Li could fill in the hollow carbon rather than plate on the outer surface of the hollow carbon [112]. In the line of similar thoughts, researchers have studied various methods (e.g., elemental doping, functional-group introduction, loading potassiophilic nanoparticles on an electrode, potassiophilic material coating, and fine structure tuning) to make a host framework potassiophilic.

(3) Potassiophilic 3D Hosts via Elemental Doping and Introduction of Functional Groups. Elemental doping and introduction of functional groups on a material have been widely adopted to modify material properties [113]. For instance, Zhang et al. utilized a nitrogen-doped graphene (NG) matrix as a framework for Li metal deposition [114]. The surface of NG is composed of lithiophilic functional groups, such as pyridinic, pyrrolic, and quaternary nitrogen groups. These functional groups exhibited higher binding energy to Li ions compared to bare graphene and Cu. Consequently, Li tends to preferentially deposit on the NG matrix, resulting in reduced nucleation overpotential [115]. In a similar way, it is found that elemental doping and the introduction of functional groups on host materials can help to enhance the electrochemical performance of K metal anodes [116, 117]. For example, oxygen groups (e.g., carboxyl, carbonyl, epoxy, and ketone) on graphene exhibited higher binding energy to K ions than those of pristine graphene and accordingly contribute to a low K nucleation barrier as well as uniform K deposition (Figure 7(a)) [101, 118]. Besides the oxygen species, researchers reported that the other heteroatoms can help to modify the binding energy of K ions to the doped sites (Figure 7(b)) [119]. The authors showed that B-, N-, and S-doping on certain sites of graphene, such as graphitic boron in the bulk phase (bgB-), graphitic boron on the edge (egB-), pyridinic nitrogen (pN), and sulfonyl groups (oS), increases the binding energy (Figure 7(b)). Xiong et al. reported that a K metal electrode using an N-doped graphene nanomesh (NGM) host can achieve a low overpotential of 12.4 mV for 1700 h (Figure 7(c)) [120]. Also, the NH-functional group can promote uniform K deposition, working as affinitive sites to K ions and showing the aligned electric field distribution (Figure 7(d)). Meanwhile, it is worth mentioning that the NH-functional groups contribute to an increase in wettability (wettability is further discussed in Section 3.1.3) (Figure 7(e)). Indeed, the pristine carbon cloth tends to rarely absorb molten K while the carbon cloth with the NH-group can absorb molten K fast within a few seconds [71].

(4) Potassiophilic 3D Hosts via Particle Loading and Coating. In addition to elemental doping or introducing functional groups on a host, potassiophilic nanoparticle loading or potassiophilic material coating on a host framework has emerged as an effective strategy to mitigate dendritic growth [72, 105, 121]. The potassiophilic materials are evenly distributed on a 3D host, leading to a uniform K nucleation. Although this approach shares similarities with functional group doping in terms of suppressing dendrite growth, it differs in that particles are directly incorporated into the host material, making the host potassiophilic [110]. For example, Liu et al. decorated the 3D-Cu current collector with reduced graphene oxide (rGO) sheets to enhance potassiophilicity of the current collector [75].

To enhance the potassiophilicity of various hosts, materials that exhibit lithiophilicity and sodiophilicity have been explored. For example, transition metals have been frequently selected as doping elements for improving the potassiophilicity of carbon frameworks [73, 95, 121, 122]. In particular, cobalt (Co) nanoparticles are one of the general dopants for improving the lithio- and sodiophilicity of carbon substrates [123, 124]. As Co worked for Li and Na metal hosts, Co nanoparticles loaded on carbon materials also showed enhanced potassiophilicity [105, 125]. Zhang et al. embedded Co nanoparticles into the carbon matrix via calcination after immersing the wood in cobalt chloride solutions (Figure 8(a)) [126]. After carbonization, the N-doped carbon matrix with vertically aligned channels was obtained (SA-Co@HC), which controls the K deposition spatially (Figures 8(b)–8(d)). When the K is stripped from the composite electrode, the microchannels guide the vertical K ion transport through them. During the plating of K, the vertical channels provide numerous K nucleation sites within their walls. As a result, the channels become filled with K again (Figure 8(e)). Under the synergetic effects of structure and potassiophilicity of SA-Co@HC, their symmetric cell achieved excellent cycling stability over 2500 h even in carbonate-based electrolytes (Figure 8(f)) [126].

Another facile approach to increase the potassiophilicity of a host is coating potassiophilic materials on the surface of the host directly. For example, Sun et al. coated Sn on a carbonized framework [127]. Due to the presence of Sn, the

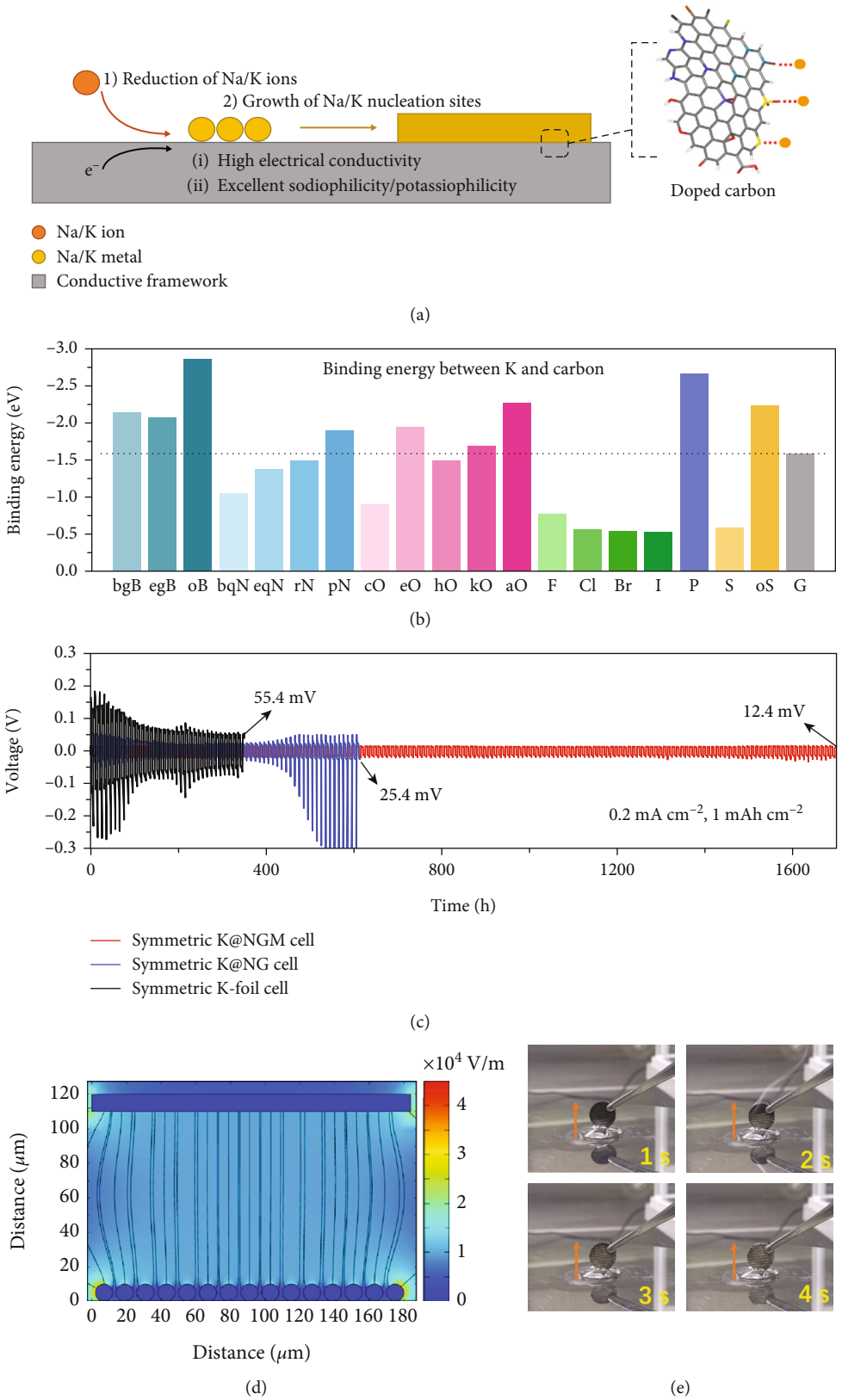

Figure 7: (a) Schematic of deposition mechanism of Na/K ions on doped carbon substrates. (b) The summary of binding energy between K and carbon, reproduced with permission [119]. Copyright 2020, Elsevier. (c) Overpotential profiles of K||K, K@NG||K@NG, and K@NGM||K@NGM cells, reproduced with permission [120]. Copyright 2022, Elsevier. (d) Electric field distribution of NH_3-treated carbon cloth electrode after cycling. (e) Infiltration process of molten K into freestanding NH_3-treated carbon cloth, reproduced with permission [71]. Copyright 2022, American Chemical Society.

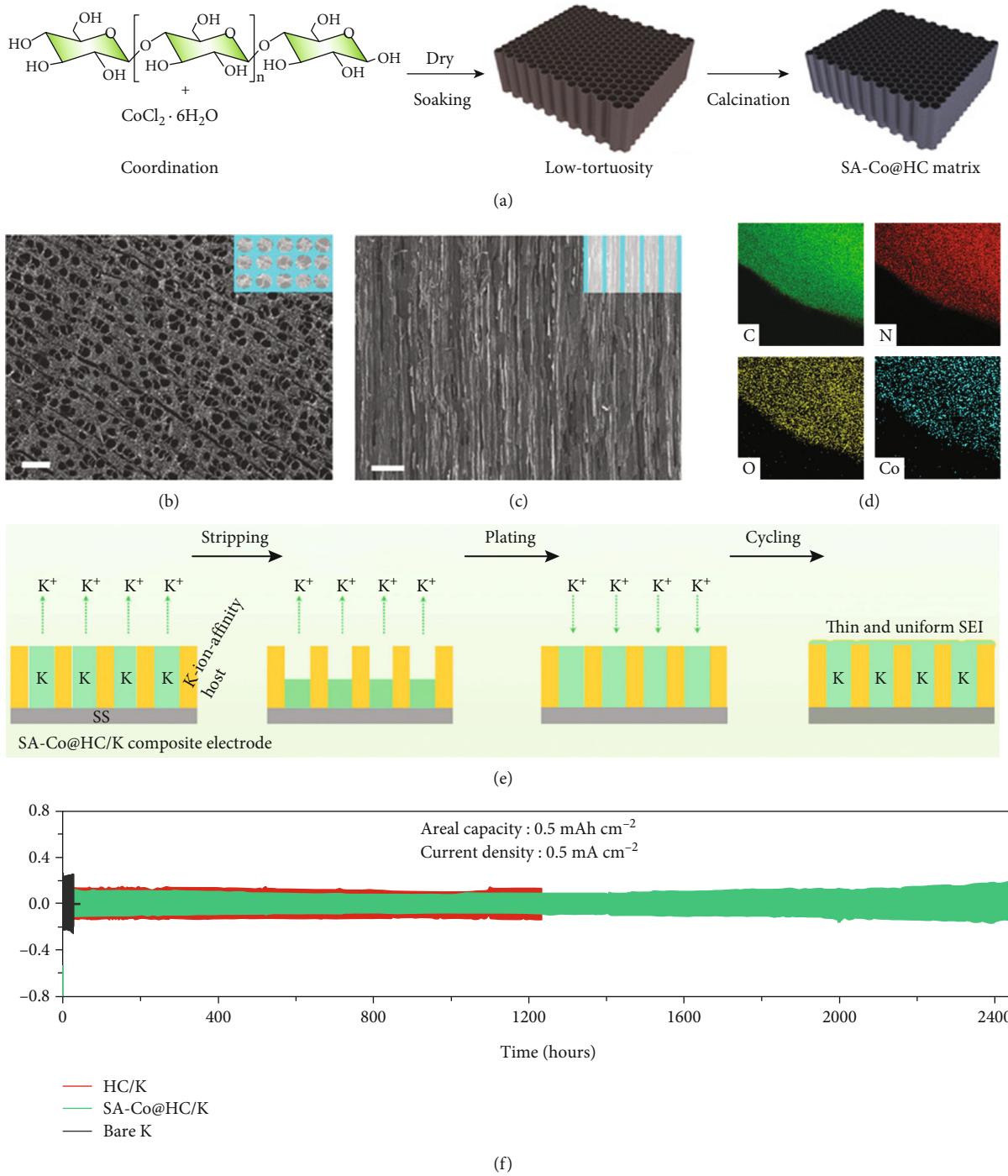

Figure 8: (a) Schematic of the synthesis process of SA-Co@HC. (b) Top-view SEM image of SA-Co@HC matrix. (c) Cross-section SEM image of SA-Co@HC matrix. (d) TEM EDX elemental mappings of SA-Co@HC. (e) Schematic illustration of stripping/plating process of SA-Co@HC/K composite electrode. (f) Cycling performance of various symmetric HC/K, SA-Co@HC/K, and K cells at 0.5 mA cm^{-2} with 0.5 mAh cm^{-2}, reproduced with permission [126]. Copyright 2022, Wiley.

K_4Sn_{23} alloy formed in the SEI layer, thus facilitating K plating/deplating and effectively reducing voltage hysteresis. Motivated by the role of Sn coating, various Sn-based coating techniques for K metal hosts have been further investigated [128, 129]. Zhao et al. designed a SnO_2-coated porous carbon nanofiber (PCNF@SnO_2) which exhibits a higher binding energy to the K ion compared to that of pristine carbon [130]. With potassiophilic SnO_2 surface, PCNF@SnO_2 enables a fast intake of molten K into the scaffolds and guides homogeneous K plating, thereby exhibiting stable cycling for 1700 h at a current density of 1 mA cm^{-2} [130]. Besides the carbon host, researchers wrapped Cu foam with noble metals. For instance, Cu_3Pt-Cu and Pd-Cu successfully worked for PMBs, showing stable stripping

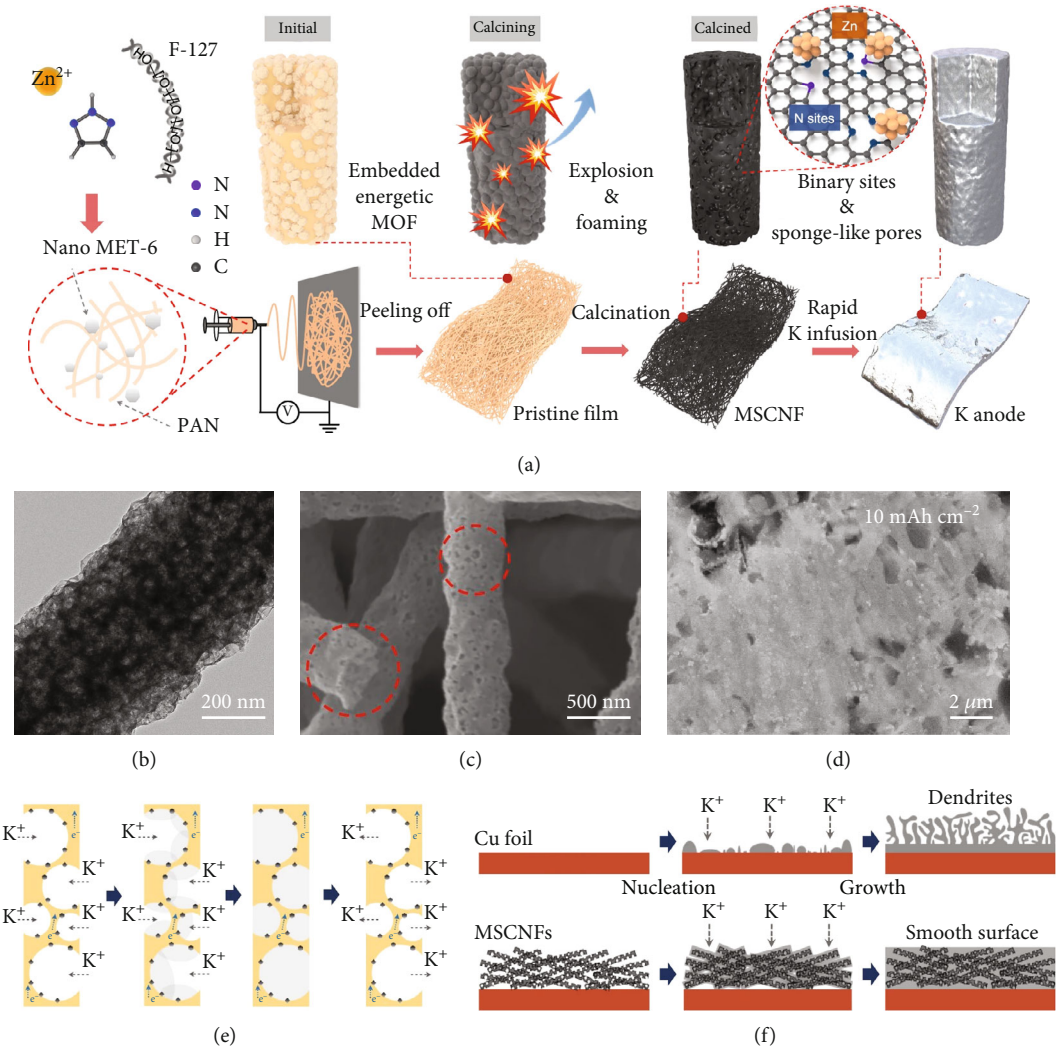

Figure 9: (a) Schematic of the fabrication process of MSCNFs and the K composite electrode. (b) TEM image of MSCNFs. (c) SEM image of MSCNFs. The porous structures of MSCNFs are highlighted in red dashed circles. (d) SEM image of MSCNFs after K deposition up to 10 mAh cm^{-2}. Schematic illustration of (e) K plating/stripping process on MSCNFs and (f) K deposition process on Cu and MSCNFs, reproduced with permission [106]. Copyright 2023, Springer Nature.

and plating over a hundred cycles [100, 131]. In those studies, the K ion preferentially deposits on noble metal surfaces and forms an alloy. This alloy formation serves as a buffer, effectively mitigating the volume expansion that occurs as a result of subsequent K deposition.

(5) Metal-Organic Frameworks to Fabricate Potassiophilic 3D Hosts. One of the effective methods to make the carbon substrate potassiophilic would be to use Metal-Organic Frameworks (MOFs) as the precursors for the introduction of potassiophilic nanoparticles [105, 122]. MOFs are crystalline porous materials that consist of metal ions and organic ligands [132]. MOFs are often adopted for energy-related applications due to their various advantages (e.g., providing active sites, tunability, porous structure, large surface area, and chemical stability). A noteworthy aspect is that metal composites can be synthesized using MOFs through a simple heat treatment process [122]. Recently, Li et al. synthesized porous carbon nanofibers with zinc (Zn) metal particles and nitrogen groups (MSCNF) using Zn-triazole MOF and MET-6 to polyacrylonitrile- (PAN-) based nanofibers (Figure 9(a)) [106]. Due to the presence of Zn and N sites, the sponge-like MSCNF gets highly potassiophilic, showing rapid K infusion.

Meanwhile, as stated in Section 2, K metal electrodes can experience large volume changes, and thus, it may be hard to confine a large amount of K metal on the host structure. Utilization of MOF, including ZIF, can open a new way to resolve it. In many cases, MOF often shows an open structure [133]. Also, for some MOFs, in the calcination process, gas emission occurs, thus indicating a hierarchically porous structure (Figure 9(b)). Those open structures or interconnected pores could provide a space for a large capacity of K deposition. Indeed, Xie et al. deposited K metal up to 10 mAh cm^{-2} without dendrite growth (Figures 9(c)–9(f)).

Despite the excellent performances of MOF-derived electrodes, there are only a few MOF-based electrode designs for K metal [101, 106, 122].

(6) A Rise of MXene. MXene, a two-dimensional material consisting of transition metal carbides or carbonitrides, has been adopted for the metallic framework owing to its high electronic conductivity and inherent surface terminations (e.g., O, F, OH, and Cl) that exhibit strong affinities toward alkali metal ions [134–136]. However, conventional two-dimensional MXenes show limited porosity to accommodate the metal deposition and self-restacking behavior, thereby leading to low capacity and inferior cycling stability [137]. In this regard, Tang et al. designed defect-rich and N-containing MXene with CNT scaffolds (DN-MXene/CNT) [72]. The 3D MXene/CNT freestanding scaffold with abundant interconnected voids could host a large amount of K deposition. Furthermore, potassiophilic MXenes played the role of "seed points" to induce preferential K plating, preventing direct deposition of K outside of the scaffold and exhibiting a dendrite-free behavior [72].

Research on MXene as a scaffold for K metal electrodes is still in its infancy compared to that on Li and Na [138, 139]. Concerning the advantages of MXenes, including high electrical conductivity and abundant terminal groups, MXenes may offer a broader range of possibilities for modifying host materials for the K metal.

(7) Miscellaneous Considerations in Hosts for Potassium Metal. Host structure with an extremely large surface area often deteriorates electrode stability. That is, high porosity can weaken the bulk mechanical properties, potentially causing the structural collapse of an electrode and losing the benefit of the reduced local current density by a large surface area [129]. In the worst case, broken fragments from the bulk electrodes may obstruct pores, leading to poor ion diffusion. Additionally, an internal short circuit could occur due to the broken fragment, which could pierce the separator. Moreover, extremely large surface areas necessitate a greater amount of electrolyte decomposition to cover the electrode surface [93]. Indeed, failure of metal batteries often occurred via electrolyte depletion [140]. Therefore, it is important to design an electrode with potassiophilicity rather than simply design with a large surface area.

Typically, alkali metal electrodes are fabricated via melt infusion or electrodeposition methods [67, 129]. As mentioned earlier, in order to enhance the wettability between molten metals and host materials, or to improve the deposition behavior of metals, the host material often require special treatments. These treatments can include the introduction of functional groups, surface coating, or introducing particles on the surface of the host material [71, 106]. However, these pretreatments might increase the production time and price of batteries. In this sense, a simple and cheap fabrication process should be essential.

To sum up, 3D potassiophilic hosts could suppress the rampant dendrite growth, improve the K^+ permeability into substrates, and lower interfacial resistance via providing potassiophilic nucleation sites. Three key points have been highlighted in common. First, the mechanical toughness of the host skeleton needs to be high enough to tolerate a large volume change during K deposition. Secondly, it is important to endow the structure with potassiophilicity via synthesizing the nucleation points. Lastly, the porous and interconnected structure should offer enough space to store a sufficient amount of K metal which is key to increase the volumetric capacity. Table 3 describes various potassiophilic hosts and their electrochemical performances. Despite enhanced performance compared to bare K metal electrodes, further research is needed to improve the rate and cycling performance. Therefore, to enhance the overall electrochemical performance of the K metal anode to the level of commercialization, comprehensive strategies such as optimizing electrolytes and designing a stable SEI layer should be urgently required (electrolyte and interfacial engineering will be discussed later).

3.1.2. K-Graphitic Intercalation Compounds. K ions are able to intercalate into graphite layers, forming K-graphite intercalation compounds (K-GICs, KC_x) without destroying the layered structure of graphite [18]. Among various K-GIC formations (e.g., KC_{24}, KC_{16}, KC_8, and KC_6), the KC_8 state is the most thermodynamically stable [141]. The K-GICs can store and release K ions through an insertion/deinsertion process, which provides the feasibility of K-GICs as a K metal electrode (Figure 10(a)). Furthermore, K ions exhibit a higher binding energy towards K-GICs compared to the K metal. This indicates that K ions would deposit on the K-GIC surface rather than on the K metal, leading to a uniform deposition without dendrite growth [142]. Due to the ability to store K ions and the potassiophilicity of K-GICs, K-GICs have been employed as a host for a uniform and dendrite-free K metal anode. Xiao et al. employed an aligned carbon fiber (ACF) film as a framework for K deposition [143]. During the initial stage of the deposition process, K ions continue to intercalate into ACF films, resulting in the formation of KC_x ($x \geq 8$) (Figure 10(b)). After the initial intercalation process, metallic K is uniformly plated outside of a potassiated ACF film due to its improved potassiophilicity via the formation of K-GIC. As a result, the K-GIC exhibited superior cycling stability with dendrite-free behavior [142, 143].

K-GICs can also be utilized as metal-free electrodes, thereby mitigating safety concerns associated with the high reactivity of the K metal [144]. This offers a potential solution to prevent safety issues like fire hazards in K metal batteries. Zhang et al. compared the reactivity between water and K metal and K-GIC by dropping them into water [144]. When a piece of K metal was dropped into water, it resulted in sparks and an explosion. In contrast, when the K-GIC was introduced to water, it transformed into black powder and dispersed without combustion (Figures 10(c) and 10(d)).

Alkali metals react strongly with humid air; therefore, a highly regulated environment is required for metal extrusion and assembly of cells with alkali metal electrodes [145]. This

Table 3: Various hosts for K metal and corresponding cycling performance of symmetric cells.

Strategy	Host	Electrolyte	Current density ($mA\ cm^{-2}$)	Stripping capacity ($mAh\ cm^{-2}$)	Overpotential[a] (mV) (h)	Ref.
Single carbon host	ACM	0.8 M KPF_6 EC/DEC	1	1	60 (233)	[102]
	CNF2800	1 M KFSI EC/DEC	0.5	0.5	200 (2000)	[99]
	rGO	0.8 M KPF_6 EC/DEC	2	1	40 (270)	[67]
	BVC	3 M KFSI DME	0.1	0.2	50 (1800)	[111]
Functional group	TCC	1 M KFSI DME	5	5	60 (1400)	[118]
	CBC	1 M KFSI DME	0.5	0.5	90 (1400)	[101]
	CC	0.8 M KFSI EC/DEC	1	1	120 (360)	[71]
	NGM	Mole ratio KFSI/DME = 0.5	1	1	52.3 (220)	[120]
	FCC	0.8 M KPF_6 EC/DEC	0.5	0.5	250 (300)	[297]
	OPCMs	3 M KFSI DME	1	1	40 (800)	[291]
Particle loading	PM/NiO	0.8 M KPF_6 EC/DEC	0.4	0.2	140 (200)	[73]
	SnS_2@CP	3 M KFSI DME	0.25	0.25	42.4 (800)	[129]
	CoZn@HCT	1 M KFSI DME	0.5	0.5	40 (1100)	[125]
	Ag-CC	0.8 M KPF_6 EC/DEC	0.5	0.5	180 (1400)	[121]
	Bi@CNT	1 M KFSI DME	0.5	0.5	50 (500)	[110]
	SA-Co@HC	3 M KFSI EC/DEC	0.5	0.5	130 (2500)	[126]
	Bi_{80}/N-rGO	3 M KFSI DME	0.2	0.1	50 (3000)	[293]
	rGO@3D-Cu	0.8 M KPF_6 EC/DEC	0.5	0.5	250 (200)	[75]
	Au/Cu foam	3 M KFSI DME	1	1	500 (350)	[108]
	NiCo@NOGC	1 M KFSI EC/DEC	0.2	0.2	70 (700)	[294]
	rGCA	0.8 M KPF_6 EC/DEC	0.2	0.2	280 (3200)	[295]
Surface coating	Sn@HNCP/G	Mole ratio KFSI/DME = 0.5	1	1	31 (100)	[127]
	PCNF@SnO_2	1 M KFSI DME	1	1	115 (1700)	[130]
	CC@SnO_2	1 M KFSI EC/DEC	0.5	1	100 (635)	[128]
	Cu_3Pt-Cu mesh	1 M KFSI DME	0.5	1	500 (320)	[131]
	Pd/Cu foam	3 M KFSI DME	1	1	500 (130)	[100]
	Cu@SKS	4 M KFSI DME	1	1	60 (900)	[82]
Metal-organic framework	Co-CNF	1 M KFSI DME	0.5	0.5	150 (1300)	[105]
	CC@CuO	1 M KFSI EC/DEC	0.5	0.5	200 (1200)	[122]
	MSCNF	1 M KFSI EC/DEC	1	1	100 (233)	[106]
MXene	DN-MXene/CNT	0.8 M KPF_6 EC/DEC	0.5	0.5	170 (300)	[72]
	MXene-MF	0.8 M KFSI EC/DEC	5	5	30 (800)	[139]
	a-Ti_3C_2	0.8 M KFSI EC/DEC	5	5	18 (800)	[292]
Graphite intercalation compounds	GIC	0.8 M KPF_6 EC/DEC	0.4	0.4	450 (700)	[144]
	ACF film	0.8 M KPF_6 EC/DEC	0.1	0.1	105.3 (610)	[143]
	KRG250	5 m KFSI EC/DEC	1	1	600 (2000)	[142]

[a]When the exact overpotential is not provided, the overpotential (positive overpotential) was evaluated from the voltage profiles.

process requirement would lead to additional costs such as the need for a costly dry room [146]. To improve the air stability of the Li metal, Shen et al. covered the Li surface with a protective layer consisting of graphite fluoride and lithium fluoride, exhibiting hydrophobicity [145]. Due to the hydrophobic layer, a long-term stability of the Li metal in ambient air was obtained. Meanwhile, a recent study on Na metal has successfully improved the air stability of the Na metal by artificially preforming a Na_2CO_3 layer on the surface of the Na metal [147]. As the Na ions show a higher diffusion barrier in Na_2CO_3, the further growth of the Na-oxide and carbonate layer has been effectively limited. Although there are

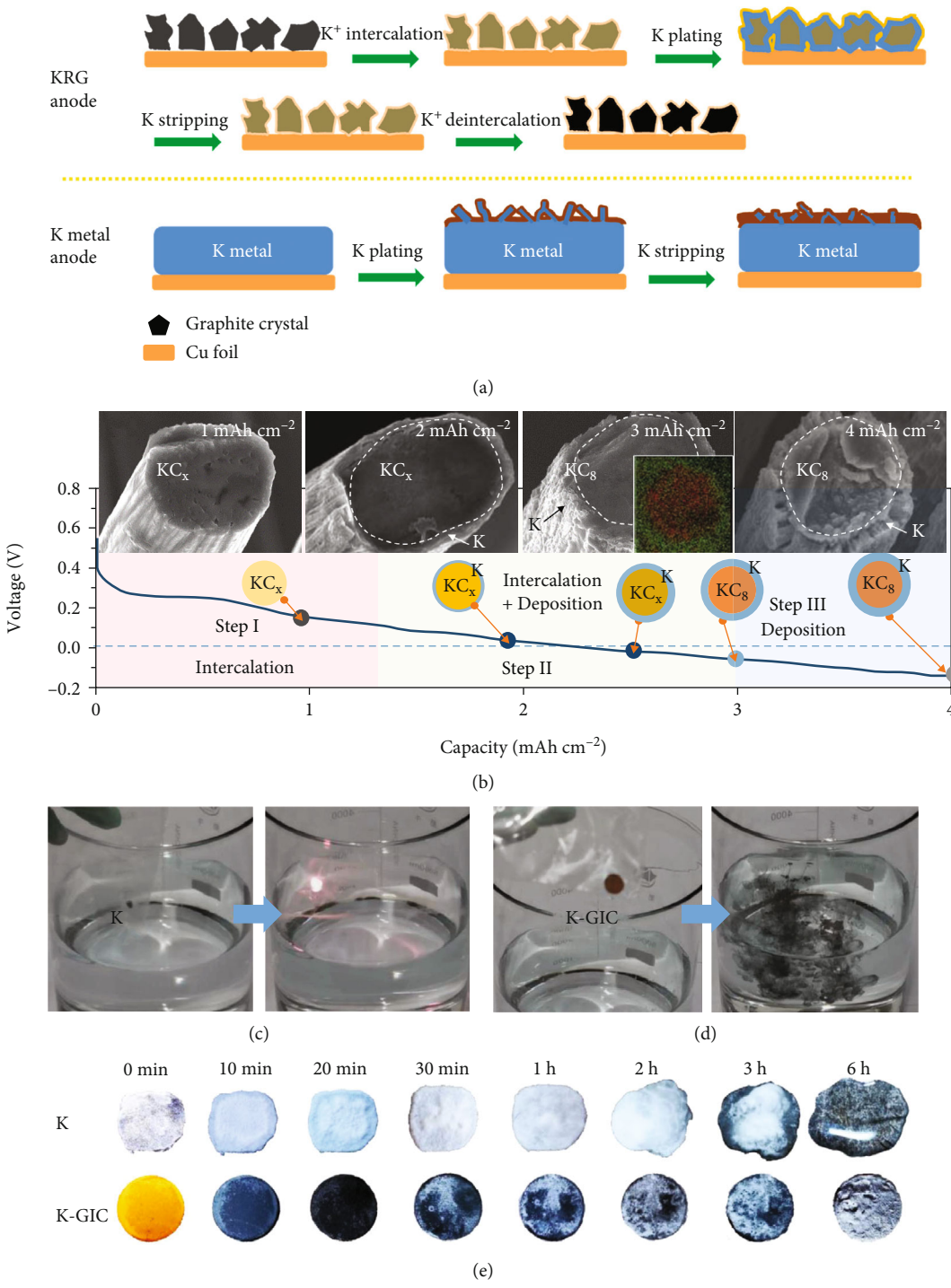

Figure 10: Continued.

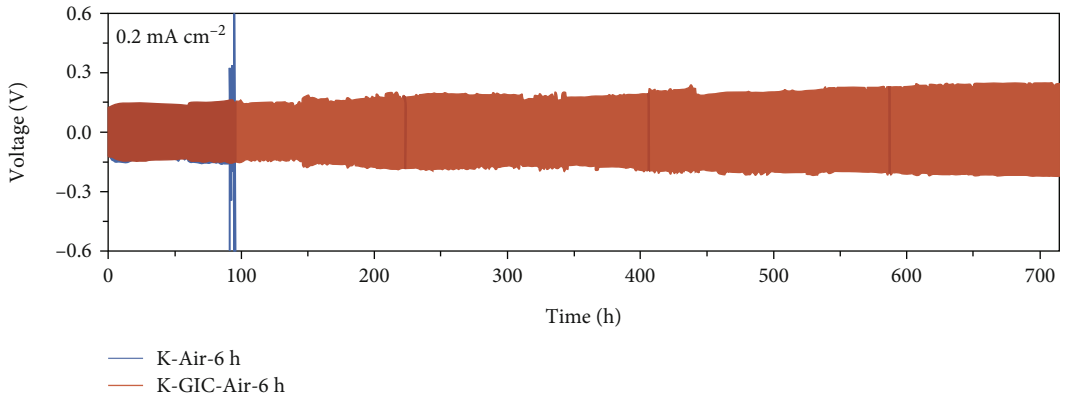

(f)

Figure 10: (a) Schematic illustration of plating/stripping processes in K-GIC electrode and K metal electrode, reproduced with permission [142]. Copyright 2023, Elsevier. (b) Ex situ SEM images of the aligned carbon fiber (ACF) film with different capacities of K deposits and the corresponding voltage profiles, reproduced with permission [143]. Copyright 2022, Elsevier. Digital photos of the reactions between water and (c) K metal and (d) K-GIC. (e) Snapshots for the appearance transition of K metal and K-GIC in ambient air at different time points. (f) Plating/stripping process of K and K-GIC which have been exposed to air for 6 h, reproduced with permission [144]. Copyright 2021, Elsevier.

few reports regarding the air stability of K metal, the K-GIC can also be an effective way to ensure the air stability of K metal electrodes. Zhang's group compared the environmental stability of K metal and K-GIC electrodes in the air environment [144]. During air exposure, the bare K metal loses its shine because air continuously reacts with the fresh K metal, forming K_2O on its surface, and finally becomes a liquid state owing to the spontaneous reaction with moisture (Figure 10(e)). On the other hand, though the color and morphology of K-GIC have changed, K-GIC could retain its solid state, suggesting the excellent air stability of K-GIC. Both air-exposed bare K and K-GIC electrodes were cycled, and the K-GIC electrode operated over 700 h while bare K displayed a much shorter lifetime, demonstrating the safety and environmental stability of K-GIC (Figure 10(f)).

In summary, K-GICs demonstrate remarkable environmental stability and safety, even when in contact with water. This could be attributed to the fact that K atoms are embedded within graphite layers. As a result, K-GICs provide a protective environment that mitigates the high reactivity of K metal and enhances the overall safety of PMBs. Also, K-GIC could provide convenience to manufacturers in handling K metal anodes.

3.1.3. K-Na Alloy. The solid-liquid interface of K metal electrodes would experience microcracking due to the repeated volume changes during plating/stripping processes. These microcracks contribute to the inhomogeneous K ion flux, thereby promoting dendrite growth. This challenge could be resolved by replacing the solid-liquid electrolyte interface with a liquid-liquid electrolyte interface. Indeed, theoretically, solid metallic dendrite cannot grow on the liquid-state electrode [148]. In addition, the formation of dendrites would be effectively suppressed due to the inherent liquidity of the electrode [149]. In this context, liquid-state electrodes, such as alloy-based electrodes, have garnered significant attention in recent years [150]. In particular, the K-Na alloy has been proposed as a viable alternative to bare K metal, as they spontaneously form an alloy around ambient temperature [151, 152]. It is noted that the K-Na alloy exhibits a unique combination of both metal and liquid properties. The K-Na alloy possesses a viscosity similar to that of liquid while maintaining the excellent electronic conductivity of the metal. Additionally, the K-Na alloy also could deliver a high specific capacity of 579 mAh g^{-1} for PMBs while remaining in the liquid state [153].

A notable characteristic of the K-Na alloy is its high surface tension, resulting in inferior wetting behavior on most substrates [154]. This property not only poses challenges for effective contact and interaction with electrode materials but also complicates the fabrication of the K-Na alloy into disk-shaped or sheet-shaped electrodes. In this aspect, Xue et al. tried to absorb the K-Na alloy into carbon paper for electrode fabrication and then successfully absorbed the K-Na alloy into carbon paper at 420°C (Figure 11(a)) [153]. Furthermore, Xue and coworkers reported a strategy to confine the liquid K-Na alloy within a porous substrate (e.g., carbon paper, Cu, Al, and Ni foam) through the use of vacuum infiltration at room temperature [148]. The successful infiltration of the K-Na alloy into various substrates indicates that the physical interaction between the substrate and the alloy can be improved under external conditions such as high temperature and high pressure. As a result, these conditions facilitate enhanced wetting and adhesion between the substrate and K-Na alloy, enabling effective integration and stabilization of the K-Na alloy electrode. The microstructure of substrates can also affect the interaction between the K-Na alloy and substrates. For instance, surface morphologies, roughness, and other structural characteristics of the substrate significantly impact the wetting behavior of the K-Na alloy [155]. Qin et al. enhanced the wettability of the K-Na alloy towards the carbon membrane by aligning the CNT membrane (CM) [156]. The presence of small gaps between CNTs under 200 nm results in a

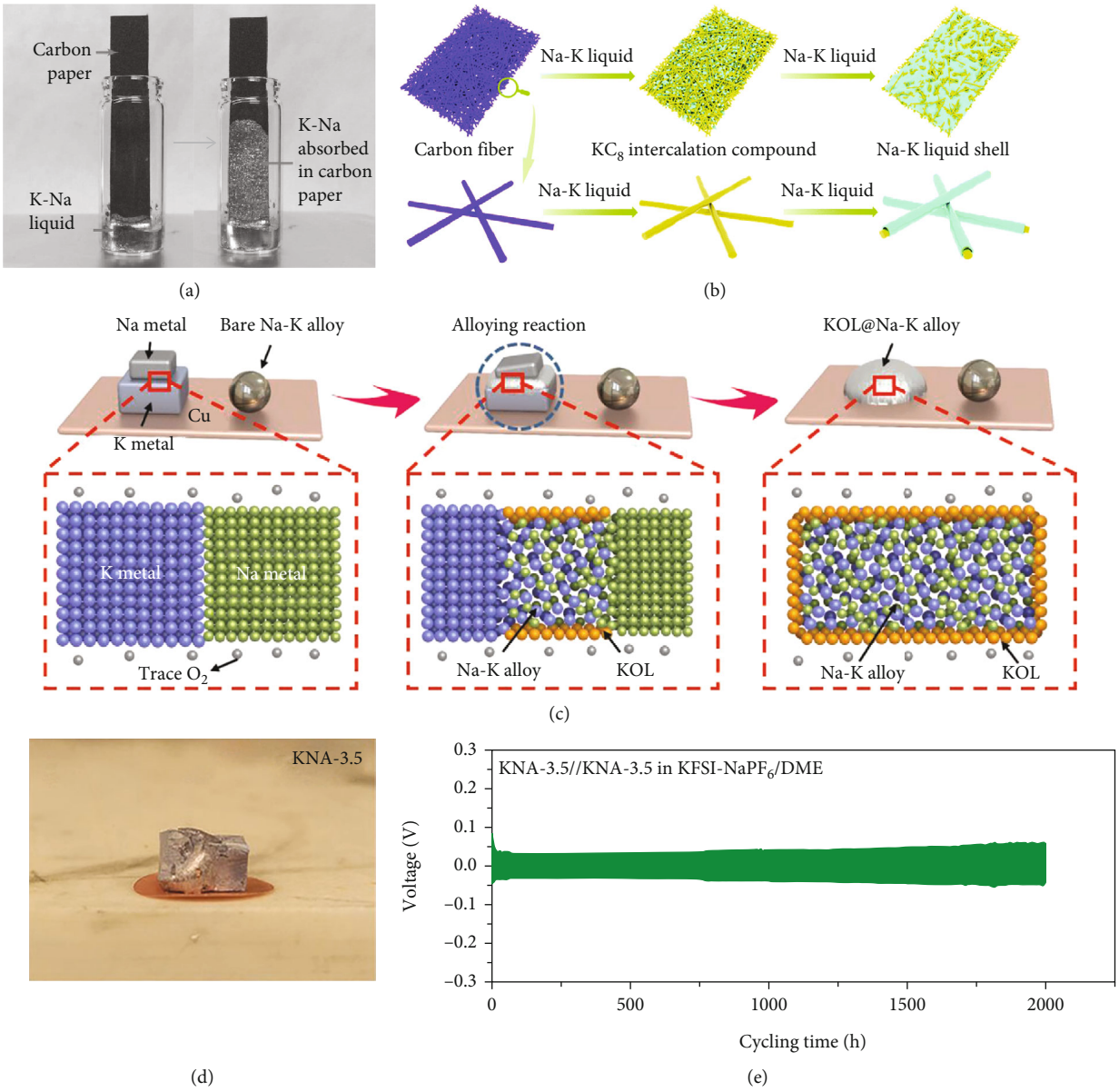

Figure 11: (a) Digital images of the absorbing process of K-Na alloy into a carbon paper at 420°C, reproduced with permission [153]. Copyright 2016, Wiley. (b) Schematic illustration of NaK-G-C electrode fabrication and preparation, reproduced with permission [149]. Copyright 2019, Royal Society of Chemistry. (c) Schematic illustration of the spontaneous fabrication process of KOL@Na-K alloy, reproduced with permission [37]. Copyright 2018, Wiley. (d) Photograph of KNA-3.5 on a copper foil. (e) Voltage profiles of KNA-3.5||KNA-3.5 cell in KFSI-$NaPF_6$/DME at a current density of 4 mA cm^{-2}, reproduced with permission [154]. Copyright 2021, Wiley.

strong capillary force which could drive absorption of the K-Na alloy into CM even at room temperature without any external conditions [155, 156].

When a potassiophilic free-standing electrode is immersed in molten K, it exhibits spontaneous infiltration of the molten K. This is due to its potassiophilicity of the electrode, enabling it to attract and absorb the molten K into its structure [71, 101]. Similarly, the chemical affinity between substrates and the K-Na alloy also can improve the poor wettability of the K-Na alloy. For instance, Zhang et al. reported that when the carbon fiber matrix was immersed in the K-Na alloy, K diffused into the carbon matrix, forming a GIC of KC_8 state (Figure 11(b)) [149]. As discussed in the K-GIC section, KC_8 formation exhibits potassiophilicity and can show enhanced wettability to the K-Na alloy [142]. As a result, GIC allows for the homogeneous integration of the K-Na alloy, facilitating the formation of a uniform electrode. Meanwhile, Cui et al. proposed uniformly distributed cobalt-single-atom carbon nanoarrays (Co-SACN) to confine the K-Na alloy within the substrate [152]. As K ions exhibit a strong affinity to Co nanoparticles, the presence of Co particles on the carbon substrate improved the wettability of the K-Na alloy [125, 126]. Benefiting from the excellent wetting behavior, Co-SACN@-NaK contributed to stable cycling at a high current of 10 mA cm^{-2} for 4000 h.

Table 4: Various electrodes for K-Na alloy and corresponding cycling performance of symmetric cells.

Electrode	Mass ratio of Na : K (wt%)	Electrolyte	Current density (mA cm^{-2})	Stripping capacity (mAh cm^{-2})	Overpotential[a] (mV) (h)	Ref.
KNC	33.7 : 66.3	1 M $NaClO_4$ EC/DEC	0.4	0.8	200 (2800)	[153]
CM@NaK	33.3 : 66.7	0.5 M KPF_6 DEGDME	1	1	100 (1600)	[156]
NaK-G-C	33.3 : 66.7	2 M KFSI EC/DEC	80	16	400 (1200)	[149]
KNA@C	22 : 78	0.8 M KPF_6 EC/DEC	8	4	160 (360)	[151]
CC@NaK	50 : 50	1 M $NaClO_4$PC + FEC 5 vol%	2	2	280 (1800)	[155]
KNA-3.5	3.5 : 96.5	0.4 M KFSI-$NaPF_6$ DME	4	2	60 (2000)	[154]
Na-K@rGO	44 : 56	0.8 M KPF_6 EC/DEC	1	0.25	90 (600)	[157]
Co-SACN@NaK	25 : 75	0.8 M KPF_6 EC/DEC	10	10	230 (4000)	[152]
CNT-2@NaK	22 : 78	0.8 M KPF_6 EC/DEC	8	4	300 (500)	[158]

[a]When the exact overpotential is not provided, the overpotential (positive overpotential) was evaluated from the voltage profiles.

Typically, the K-Na alloy has been absorbed or confined within a framework to be employed as an electrode [157]. However, it is important to note that if excessive pressure is applied to a K-Na alloy electrode beyond its tolerable limit, there is a risk of the K-Na alloy being forced out of the frameworks [152]. This can lead to unstable electrochemical properties and potentially give rise to safety concerns. Therefore, reducing the inherent high surface tension and fluidity of the K-Na alloy by modifying the alloy's properties is crucial in order to achieve stable liquid electrodes. Zhang et al. reported that the introduction of a K_2O layer (KOL) covering the K-Na alloy can enhance the intrinsic wettability of the K-Na alloy (Figure 11(c)) [37]. This KOL was spontaneously formed due to the oxidation of K by a trace of O_2 in the glove box. The KOL acts as a modifier, enhancing the interaction and wetting behavior between the alloy and electrode materials. Motivated by this work, Zhang et al. fabricated the K-Na alloy and Super P composite (KNA@C) [151]. Super P, which contains a significant amount of inherent moisture, can react with the K-Na alloy, resulting in the formation of hydroxides (KOH and NaOH) during the stirring process. The hydroxide compounds also improved the poor wettability of the K-Na alloy, thus enabling a host-free K-Na alloy electrode. These approaches indicate that modifying the chemical composition of the alloy can address the challenges associated with the high surface tension and fluidity of the K-Na alloy. While trace water and oxygen contribute to increase in wettability of the liquid K-Na alloy by forming hydroxides and oxides, it is important to note that they can also ruin the balance between electrolytes and electrodes [158]. Excessive moisture or oxygen can lead to undesired side reactions or degradation of the electrolyte and electrode, which can negatively impact the overall performance of batteries. In view of practical usage, it remains essential to find ways to reduce the flowable nature and high surface tension of the K-Na alloy without relying on composite electrodes with hosts or powders. Recently, the non-Newtonian state of the K-Na alloy, defined simply as a highly viscous liquid, was reported by Tai et al. [154]. The authors introduced only 3.5 wt% Na into K (KNA-3.5), which exhibits a quasiliquid state compared to the liquid state of the K-Na alloy (Na/K = 33.7/66.3 *w*/*w*) (Figure 11(d)). The quasiliquid state of the K-Na alloy enables its fabrication into a metallic electrode by markedly reducing its fluidity. Notably, the KNA-3.5 anode demonstrated its excellent cyclability up to 2000 h at a high current density of 4 mA cm^{-2} (Figure 11(e)).

Various K-Na alloy electrodes and their cycling performances are described in Table 4 for comparison. Overall, K-Na alloy electrodes exhibit an excellent rate capability and cycling stability compared to pristine K metal electrodes. However, it is worthwhile to limit the specific capacity of the K-Na alloy electrode to prevent its solidification. The K-Na alloy can maintain its liquid state only within a specific range of composition [152, 157]. Therefore, controlling the specific capacity is essential to ensure its desired properties as a liquid electrode. Moreover, the safety issue should be considered more due to their inherent high reactivity compared to solid K metals.

3.1.4. Modification of Current Collectors

(1) Modified-Cu Current Collectors. Current collectors provide a pathway for the electrical current generated at electrodes and establish a connection with external circuits [159]. Planar copper (Cu) foil has been regarded as the most suitable current collector for the anode due to its excellent electronic conductivity. Thereby, Cu foil has also been employed as an anode current collector in PMBs. However, the Cu foil shows an inherent low affinity to the K metal, thereby inducing a large overpotential for electrochemical deposition of K on the Cu foil [75]. Furthermore, weak interaction between Cu and the electrolyte could also lead to a nonuniform K^+ ion flux and further promote the formation of K metal islands on the substrate which could be the origin of dendritic growth [15].

Researchers have employed Cu foam or mesh for metal current collectors which possesses 3D structures [100, 160]. Such existing studies primarily focused on enlarging the surface area of the current collector. By increasing the surface area, the local current density is effectively reduced, delaying the emergence of the dendrite based on Sand's time [73]. However, structural modification alone still poses the challenge of inherently low interaction between the K metal and Cu. In this context, various approaches established for

K metal hosts have been expanded for current collectors, including the use of potassiophilic elements to cover the surface of the Cu current collector. For example, researchers have loaded rGO, Cu_3Pt alloy, Pd, Sn-K alloy, and gold (Au) elements on 3D-Cu current collectors, which display higher binding energy to the K ion compared to bare Cu [75, 82, 100, 108, 131]. All these distributed species on 3D-Cu improve the potassiophilicity and thus induce a uniform K deposition.

(2) Modified-Al Current Collectors. Aluminum (Al) foil, a traditional substrate for the cathode of Li-ion batteries, has been proposed as a current collector for K metal anodes because of the thermodynamic stability between Al and K [161]. Indeed, Al has slightly lower electrical conductivity compared to Cu. However, the density of Al ($2.7\,g\,cm^{-3}$) is approximately three times lower than that of Cu ($8.94\,g\,cm^{-3}$). This lower density allows for the reduction of weight in a battery when employing Al current collectors. Furthermore, the price of Al ($\$1.5\,lb^{-1}$) is cheaper than Cu ($\$4\,lb^{-1}$), as reported in the Mineral Commodity Summaries 2023 by the US Geological Survey [162]. This suggests that utilizing the Al foil as an anode current collector can contribute to cost-efficient electrochemical energy storage systems.

Despite the advantages, the commercial Al foil has limitations in terms of its nucleation resistance and low affinity to the K metal. The adsorption energy of the K atom on Al foil is relatively low, with a value of -0.51 eV, compared to Na atoms, which exhibit a much higher energy of -2.24 eV [72, 163]. This low adsorption energy of K on Al can result in reduced interaction between K and Al surfaces, leading to uneven K deposition, poor performance, and rampant dendrite growth. In this sense, Yi et al. reported that an Al current collector with potassiophilic moieties can induce uniform K ion flux and consequently mitigate dendrite growth [95]. The authors fabricated N-doped carbon@-graphdiyne with Cu Quantum Dot- (NC@GDY-) coated Al foil to improve the potassiophilicity of the Al current collector. K ions tend to nucleate uniformly on the NC@GDY-Al current collector due to its improved potassiophilicity. Furthermore, the NC@GDY-Al current collector can achieve a more uniform current distribution due to its regular hexagon morphologies (Figure 12(a)). Due to the synergetic effects of the chemical and morphological features of NC@GDY, the K@NC@GDY electrode delivered a low-voltage hysteresis of about 20 mV during the K plating/stripping process at $2\,mA\,cm^{-2}$ for 2400 h. In addition to the interaction between the K metal and Al foil, the interaction between the electrolyte and the current collector should be carefully considered. The nonwetted areas of the planar Al foil exhibit inactivity towards K deposition, which presumably leads to the formation of irregular SEI layers and island growth of K [164]. Therefore, surface modification of the Al current collector should be explored to control the electrolyte wetting behavior. To address the poor wettability of Al current collectors to electrolytes, Liu et al. introduced the aluminum-powder-sintered aluminum foil (Al@Al) [15]. The authors argued that greatly increased surface roughness can improve the wettability of electrolytes [165]. This result indicates that the wetting behavior of electrolytes to the current collector should also be considered for uniform K deposition (Figure 12(b)).

Meanwhile, researchers have regarded the early-stage electrochemical deposition of the K metal on a current collector as a thin film growth mode established in the classic theory of vacuum deposition [38, 75]. Types of growth mode are divided into the film growth mode, island growth mode, and film-island combination growth mode (Figure 12(c)). It is accepted that the film growth is determined by the surface energy difference between the substrate and the film [77]. For instance, when the surface energy of the substrate is particularly higher compared to that of the film, the film growth expands across the substrate. On the other hand, if the surface energy of the film exceeds that of the substrate, the film is likely to grow in the form of isolated islands. Motivated by this, Zhao et al. covered an Al foil with a thin graphene layer (Al@G) to increase the surface energy of the substrate [76]. The increase in surface energy is likely attributed to the numerous defects present in the graphene layer, which could result in higher binding energy to alkali ions [166, 167]. Because of the higher surface energy of Al@G in comparison to carbon-coated Al foil and bare Al foil, Al@G exhibits the smallest wetting angle to molten K (Figure 12(d)). Consequently, this property facilitates film growth on the substrate, thereby leading to stable cycling over 1000 h (Figure 12(e)).

As discussed, microengineering on both current collectors of Cu and Al could contribute to improved electrochemical performance. It is noteworthy that utilizing the current collector by itself as a framework for the K metal would be one of the effective strategies to elevate the total energy density of batteries while reducing their volume, thickness, and weight. Furthermore, in view of production, preparing active materials, slurry making and coating, and the drying process can be excluded from the production process. Therefore, the production process would lead to curtailed cost and production time [168]. Overall, modified current collectors exhibit superior performance compared to conventional current collectors such as Cu and Al foils (Table 5).

(3) Exploring Anode-Free Batteries. Anode-free batteries are a type of rechargeable metal battery, composed of a cathode, electrolyte, separator, and anode current collector [169]. They operate without an anode, its initial state. In the anode-free system, the cathode or electrolyte holds charge carriers (i.e., Li, Na, and K ions), and ions from the cathode accumulate on a bare current collector to form a metal electrode during the first charge cycle. As for discharging, ions are dissolved from the newly formed metal electrode and inserted back into the cathode. By eliminating the preexisting anode material, these batteries can effectively achieve much higher energy densities compared to a conventional battery's designs [169].

The anode-free systems have already been employed in Li and Na metal batteries. For instance, Chen et al. employed

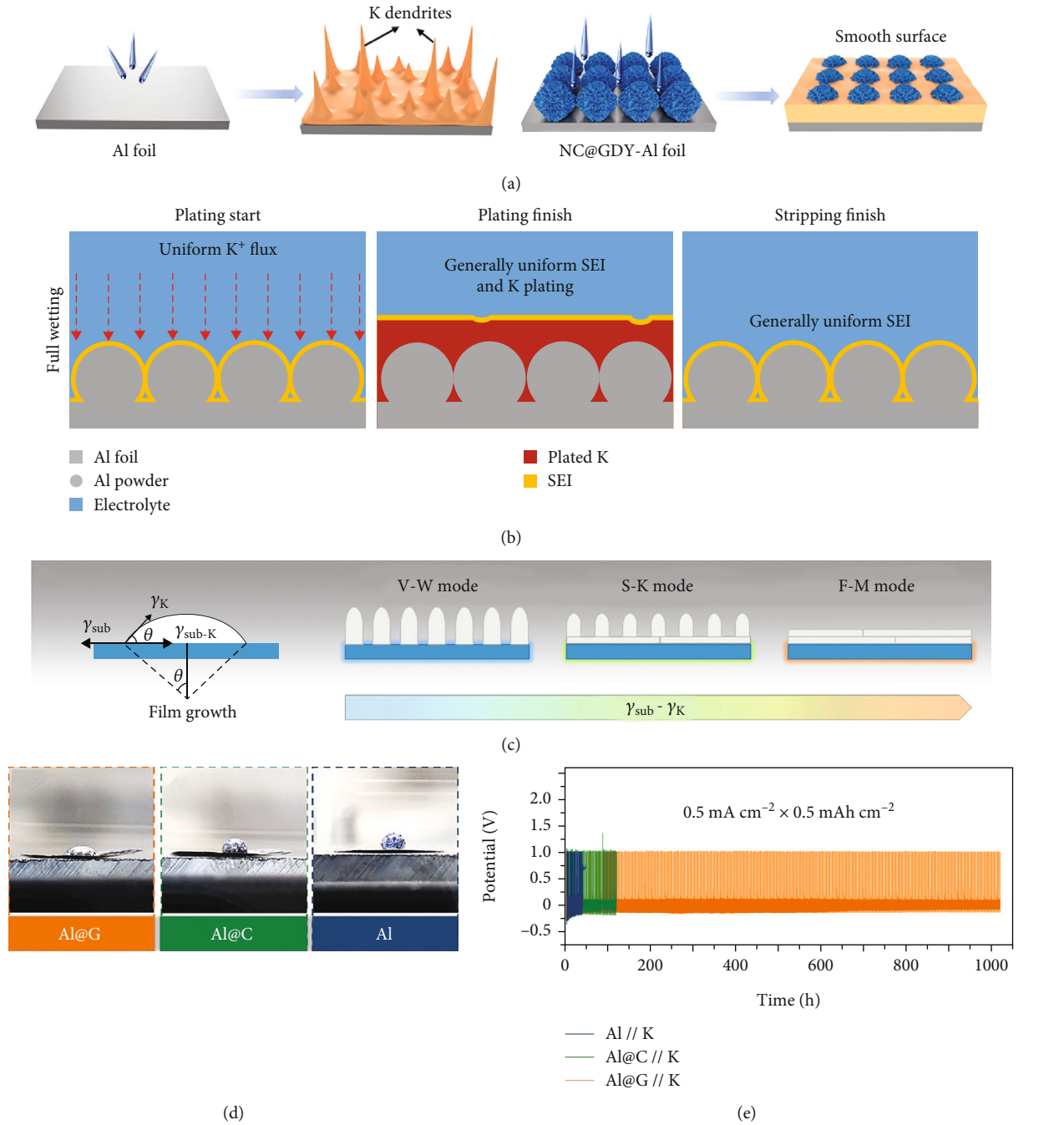

Figure 12: (a) Schematic illustration of K deposition behavior on Al foil and NC@GDY-Al foil, reproduced with permission [95]. Copyright 2022, Wiley. (b) Schematic diagram of enhanced wettability of electrolyte to Al@Al current collector, resulting in uniform K^+ flux, uniform SEI, and homogeneous K plating/stripping, reproduced with permission [15]. Copyright 2020, Wiley. (c) Scheme of film growth modes which rely on the surface energy differences between substrate and film. (d) Digital photos of wettability test of molten K metal to Al@G, Al@C, and Al current collectors. (e) Voltage profiles of K deposition/dissolution process with different current collectors, reproduced with permission [76]. Copyright 2022, Wiley.

an Au-decorated Cu foil as a current collector for anode-free batteries with Li_2S as the cathode and hence achieved a high energy density of 626 Wh kg^{-1} [170]. Meanwhile, Zhou et al. designed an anode-free SMB comprising a graphitic carbon-coated Al foil and a layered oxide-based $Na[Cu_{1/9}Ni_{2/9}Fe_{1/3}Mn_{1/3}]O_2$ with a dual-salt electrolyte of $NaPF_6$ and $NaBF_4$, obtaining a high energy density over 200 Wh kg^{-1} [171]. In spite of these achievements of the anode-free system in Li and Na, there are only a few reports about anode-free PMBs [76, 172, 173].

Several challenges impede the practical applications of anode-free PMBs. First, the planar Cu and Al are unable to accommodate the volume changes during the plating/stripping process due to the lack of any "cage" for metal

Table 5: Various current collectors for K metal electrode and corresponding cycling performance.

Current collector	Counter electrode	Electrolyte	Current density (mA cm^{-2})	Areal capacity (mAh cm^{-2})	CE[a] (cycles)	Ref.
Cu	K	0.8 M KPF_6 EC/DEC	0.5	0.5	30% (13)	[75]
Al	K	4 M KFSI DME	0.5	0.5	50.7% (20)	[76]
Al@Al	K	4 M KFSI DME	0.5	0.5	98.9% (1000)	[15]
NC@GDY-Al	K	4 M KFSI DME	0.2	0.2	99.93% (800)	[95]
Al@G	K	4 M KFSI DME	0.5	0.5	99% (500)	[76]

[a]When the exact CE is not provided, the CE was estimated from the figures.

deposition. In addition, the unstable SEI not only leads to low Coulombic efficiency during charge/discharge process but also promotes dendrite growth. Hence, comprehensive strategies should be devoted to realizing stable anode-free PMBs. Recently, Li et al. reported an anode-free PMB in a diluted high-concentration electrolyte (DHCE) with a mesoporous fibrous host (MCNF) [173]. DHCE contributed to the construction of an anion-derived SEI layer, which was more robust compared to that of 1 M KFSI/DME (further discussed in *(3) Highly Concentrated Electrolytes*). Moreover, MCNF could suppress the volume fluctuations with enough inner room for K storage, providing sufficient capacity of K. As a result, an anode-free MCNF full cell with $K_{1.18}Fe[Fe(CN)_6]_{0.82}{\cdot}0.47H_2O$ delivered a high energy density of 362 Wh kg^{-1} [173].

Overall, though anode-free PMBs show deficient electrochemical performances, they are still attractive due to their high energy and power density, low cost, and simplified manufacturing process. Therefore, many strategies such as electrolyte optimization to generate robust SEI layers, modifications on current collector, and engineering on the host for K deposition should be integrated to design anode-free PMBs.

3.1.5. Interface Engineering. The SEI layer acts as a protective coating on the metal surface. It is crucial for the SEI layer to possess excellent mechanical toughness to withstand the repeated volume fluctuations of metal that occur during the plating/stripping process. In the case of the K metal, which experiences significant volume expansion/shrinkage compared to Li and Na metals, the SEI layer should have superior mechanical properties to endure strain by repeated volume changes [12]. However, SEI layers on the K metal presumably possess insufficient mechanical properties to tolerate the volume expansion [66]. The mechanically poor SEI layer would be broken due to repeated volume changes; therefore, the fresh K metal beneath the SEI layer results in preferential deposition and promotes dendrite growth [60]. The continuous breakage of the SEI layer and formation of dendrites lead to low Coulombic efficiency and an increase in interfacial resistance [130]. To overcome these challenges, interface engineering such as constructing artificial SEI (ASEI) layers on metal electrodes has been proposed. The important features of the ASEI layer are excellent mechanical integrity, high K ionic conductivity, low electronic conductivity, and superior chemical passivation to prevent side reactions between the K metal and electrolytes [174]. Typically, ASEI can be formed by covering the K metal with sheet material [175], dropping compounds that can react with the K metal spontaneously [94], or dipping the K metal into a liquid solution [31]. Recently reported ASEI will be described with categorization via fabrication methods.

(1) Covering Potassium Metal with Carbonaceous Materials. One approach is to cover the metal electrode with a carbonaceous material, such as carbon paper (CP) and CNT [176, 177]. Li et al. introduced CP on the K metal as a protective layer [176]. The CP significantly reduced the local current density due to its large surface area. The carbonaceous material can also act as a barrier to inhibit direct contact between the metal electrode and electrolyte. Wang et al. covered the K metal with CNT film (K/CNT) [177]. The spontaneous potassiation of the CNT film occurred when the K/CNT electrode was immersed in the electrolyte, thereby leading to an increase in the potassiophilicity of CNT. Due to the improved potassiophilicity of CNT, the SEI layer was formed on the potassiated CNT film rather than on the K metal surface. As a result, the artificial SEI (ASEI) layer not only acts as the interface protecting the K metal from electrolyte corrosion but also plays the role of the K metal host which could induce uniform K deposition. Additionally, due to the excellent mechanical properties of the CNT, the ASEI layer tightly adhered to the K metal and could accommodate the volume changes without the breakage of the SEI layer. Hu et al. used the freestanding 3D sulfur-doped porous graphene (S-doped graphene) as a protective layer in K-O_2 battery systems to prevent parasitic reactions of the K metal induced by superoxide anions (O_2^-) and dissolved O_2 (Figures 13(a)–13(c)) [178]. With the reactive behavior of S-dopants on graphene to O_2^-/O_2 species, S-doped graphene drove preferential accumulation of KO_2 byproducts on its outer surface, acting as a sacrificial layer [179].

(2) Spreading Precursors to Generate ASEI. Another strategy to construct an ASEI layer on the metal electrode is by spreading precursors of a protective layer on fresh K metal [93, 94, 180]. The ASEI layer is formed as the result of the spontaneous reactions between precursors and the K metal [181]. For instance, it is well-known that mercury (Hg) is able to form alloys with large amounts of metals, resulting in amalgams. Indeed, Yang et al. coated the K metal with Hg to stabilize the K metal surface by forming K-Hg alloys (e.g., K_7Hg_{31} and K_2Hg_7) [93]. The K-Hg alloy layer probably possesses low activation energy for surface diffusion, which facilitates rapid transportation of K ions at the interface [182]. As a result, the protective amalgam layers

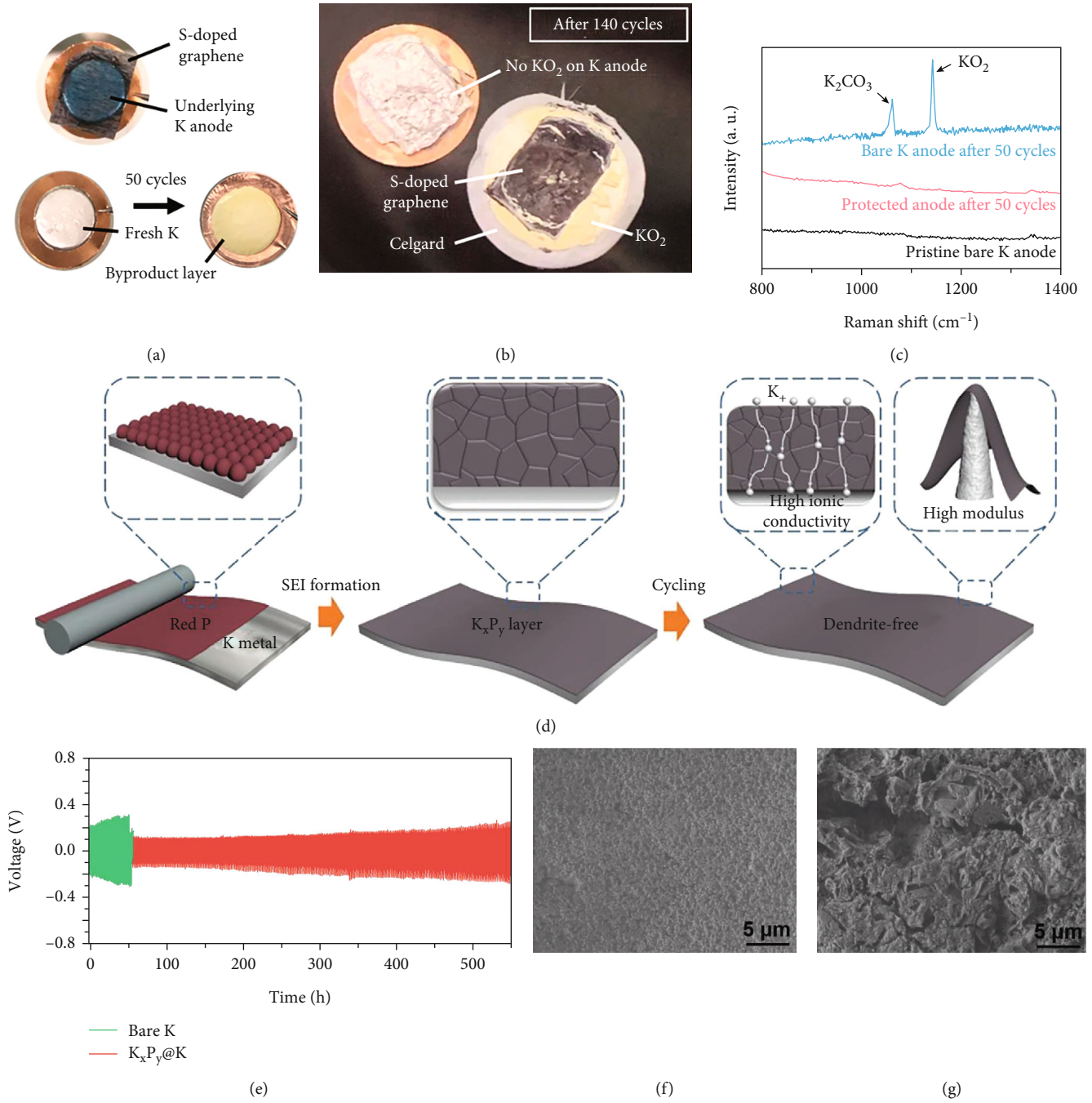

Figure 13: Digital pictures of (a) K anode covered by a S-doped graphene sheet, a pristine K anode, the 50th cycled K anode, and (b) the protected K anode by S-doped graphene after 140 cycles. (c) Raman spectra of cycled K anode, protected K anode by S-doped graphene, and pristine K, reproduced with permission [178]. Copyright 2020, American Chemical Society. (d) Schematic illustration of the fabrication process and properties of the K_xP_y@K electrode. (e) Voltage profiles of galvanostatic cycling of K and K_xP_y@K symmetric cells. SEM images of (f) K_xP_y@K electrode and (g) bare K electrode after cycles, reproduced with permission [180]. Copyright 2020, Wiley.

prevented metal electrodes from further decomposition of electrolytes and provided better kinetics and cycling stability. Meanwhile, Shi et al. fabricated red phosphorous- (P-) derived protective layers on the K metal by rolling red P powders on the K metal surface, and thus, K_xP_y layers were formed on the metal surface (K_xP_y@K) through the spontaneous reaction between the K metal and red P (Figure 13(d)) [180]. The K_xP_y layer exhibits a densely packed crystal structure, which is likely to enhance Young's modulus of the artificial protective layer. Moreover, the K_xP_y layer demonstrates high ionic conductivity presumably ascribed to its similarity to the crystal structure of Na_3P, thus offering various 3D diffusion ion pathways [180]. The K_xP_y@K displayed prolonged cycling stability and reduced polarization

Table 6: Various types of interface engineering of K metal electrode and corresponding cycling overpotential.

Interface (K)	Counter electrode	Electrolyte	Current density ($mA\,cm^{-2}$)	Stripping capacity ($mAh\,cm^{-2}$)	Overpotential[a] (mV) (cycles)	Ref.
K/CP	K/CP	1 M KPF_6 EC/DMC	5	1	30 (3000)	[176]
Polished K	Polished K	1 M KTFSI DME	0.1	0.02	~150 (200)	[43]
K/CNT	K/CNT	0.5 M KPF_6 EC/DEC	5	4	~150 (1230)	[177]
K-Hg	K-Hg	1 M KFSI DME	0.2	0.2	~60 (300)	[93]
K_xP_y@K	K_xP_y@K	1 M KTFSI EC/DEC	0.5	0.5	260 (225)	[180]
K@K_2Te	K@K_2Te	1 M KFSI EC/DEC	0.5	0.5	~350 (400)	[94]
PVA-borax@K	PVA-borax@K	3 M KFSI DME	1	0.5	~140 (250)	[175]
PPS-treated K	PPS-treated K	1 M KFSI DME	1	1	~330 (550)	[183]
K_3OCl/K_3Bi@K	K_3OCl/K_3Bi@K	1 M KFSI EC/DEC	0.5	0.5	101 (4000)	[296]
K@MES	K@MES	3 M KFSI DME	0.5	0.5	~80 (2300)	[298]

[a]When the exact overpotential is not provided, the overpotential (positive overpotential) was evaluated from the voltage profiles.

during the K plating/stripping process over 550 h compared to bare K (Figure 13(e)). Besides, K_xP_y@K presented obviously smooth and dendrite-free surface morphology, whereas bare K exhibited microcracks on its surface with a porous structure (Figures 13(f) and 13(g)).

The ASEI layer on the K metal can be formed by the liquid solution method. Typically, in this strategy, ASEI has been introduced by dropping the liquid organic solution on the K metal or immersing the K metal in the solution [31, 42, 183]. ASEI can be also constructed through the spontaneous reaction between the K metal and the components presented in a solution. For example, Park et al. treated the K metal with a liquid solution of potassium polysulfide (PPS) in diethylene glycol dimethyl ether (DEGDME) [183]. The spontaneous reaction between the K metal and the PPS solution results in the formation of K_2S on the K metal. The authors revealed that K_2S exhibits a lower K ion diffusion energy barrier compared to KF compounds known to improve the stability of the SEI layer. As a result, the symmetric cell with PPS-treated K metal was cycled over 400 h at $4\,mA\,cm^{-2}$, while the bare K metal electrode showed a dramatic increase of polarization up to 1 V around 75 h [183].

To date, various types of artificial layers for the K metal have been reported. Table 6 provides the details of interface-engineered K metal and the corresponding electrochemical performance for comparison. Overall, several key properties of the ASEI layer for the K metal are identified as superior mechanical properties, uniform, fast K ion transport, and the passivation to K-electrolyte side reactions. For the actual application of K metal electrodes, the areal capacity should be above $3\,mAh\,cm^{-2}$, which most interface-engineered K electrodes fall behind [177].

(3) Self-Healing Property of Potassium Metal. It is well known that dendrite growth is more promoted at a high current density based on the space charge model [72]. In 2018, however, Li et al. reported the opposite [184]. When a high current density over $9\,mA\,cm^{-2}$ is applied on the Li metal surface, the Joule heating effect occurs, and then, Li surface migration is promoted. This surface diffusion can heal the dendrites and flatten the Li metal surface [185]. Tough dendrites still grow; they are fused and merged by Joule heating and then eventually combined as a dendritic layer. This observation suggests that the dendritic problems at the interface could be prevented by the controlled charge/discharge rates without any pretreatment of the metal electrode. Later, Hundekar and coworkers showed that the K metal has a superior self-healing capability compared to the Li metal, even at a lower current density of $2\,mA\,cm^{-2}$ [78]. The authors found that the K metal possesses a higher rate constant and lower activation barrier for surface diffusion compared to the Li metal, which facilitates self-diffusion of the K metal when the same current density is applied (~0.1 eV of K metal and ~0.15 eV of Li metal) (Figures 14(a) and 14(b)). Also, surface morphologies of the K metal electrode cycled at a low current density of $0.01\,mA\,cm^{-2}$ exhibited isolated hemispherical deposits, while a smooth and compact surface at a high current density of $2\,mA\,cm^{-2}$ due to the excellent self-diffusion of the K metal (Figures 14(c) and 14(d)). The self-healing performances of dendrites in Li and K metal electrodes were further confirmed by Li et al. [80]. Figures 14(e) and 14(f) display the overpotential profiles of Li and K symmetric cells. The overpotential of Li cells is almost the same, indicating that the current density of $2\,mA\,cm^{-2}$ is insufficient to drive the self-healing of the dendrite. On the other hand, K cells displayed an obvious decrease in overpotential right after high current density promotion, which is the result of the intrinsic self-healing of K dendrites.

It is worth mentioning that the self-healing of dendrites takes place at a relatively high current density. Although self-healing occurs at a lower temperature than the melting point of the K metal, the local temperature would exceed the melting point of the K metal, resulting in disastrous failure by thermal runaway. In addition, high current density usually delivers decreased capacity in full-cell configuration. Therefore, an effective battery management system to control internal temperature should be developed for the practical application of self-healing of K dendrites.

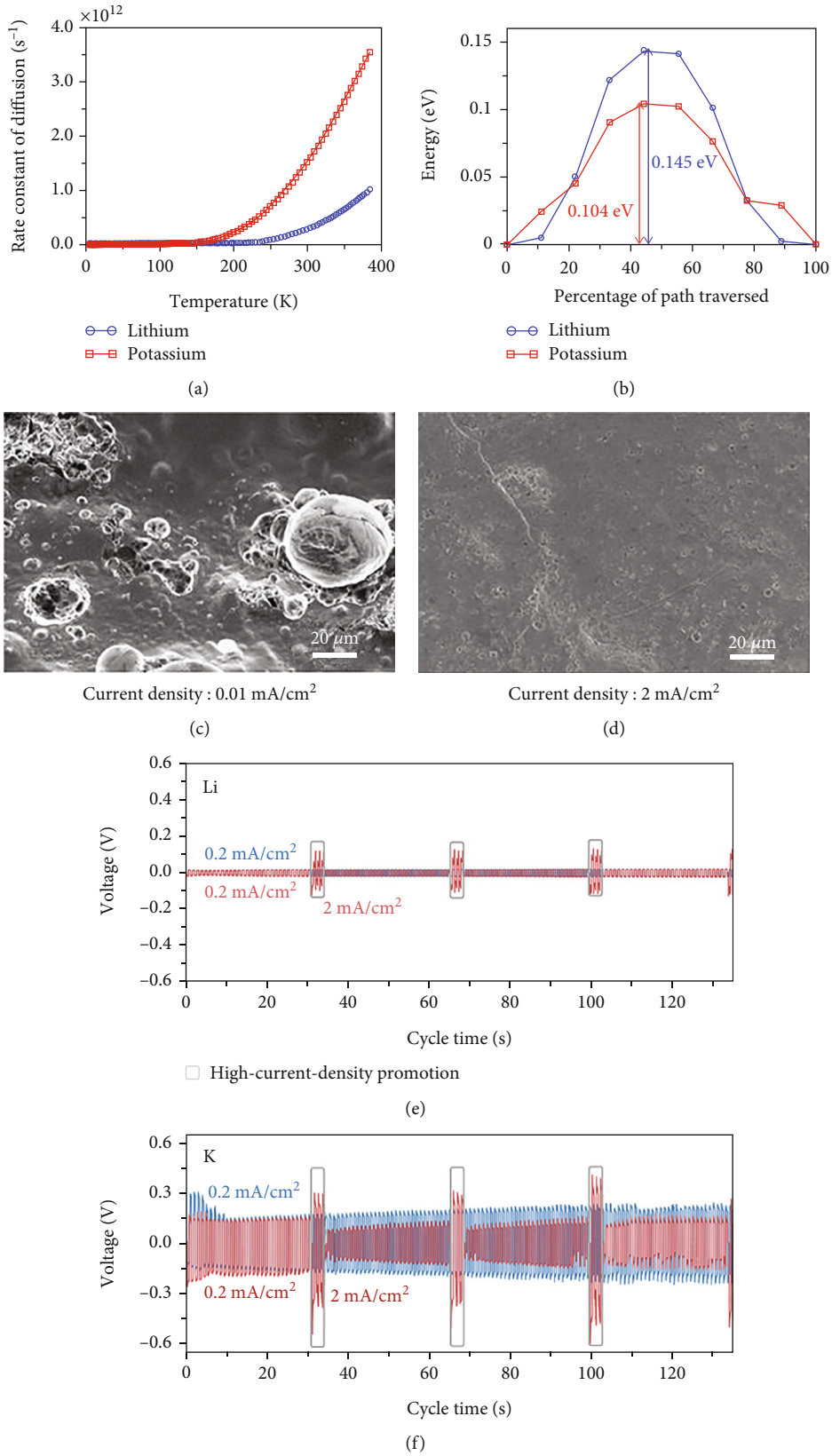

Figure 14: (a) Calculation results of the diffusion rate constant of Li and K along with temperature. (b) Calculation of activation energy barrier of Li and K for diffusion at the surface. (c, d) SEM images showing the surface morphologies of K metal anode cycled at current densities of 0.01 mA cm^{-2} and 2 mA cm^{-2}, respectively, reproduced with permission [78]. Copyright 2020, National Academy Sciences. (e, f) Galvanostatic cycling curves of Li and K symmetric cells, respectively, reproduced with permission [80]. Copyright 2021, Wiley.

3.2. Indirect Engineering of an Electrode

3.2.1. Functionalized Separators. The pivotal role of a separator is to prevent a direct connection of the anode to the cathode. Nowadays, polyethylene (PE) and polypropylene (PP) separators have been employed for the standard battery manufacturing of LIBs [186]. PE and PP separators have sufficient thermal and mechanical stability and a thickness of less than 25 μm [187]. Recently, with the rising attention of Li metal electrodes, separators have new requirements to ensure their safe operation. In response to the demand for safety, commercial separators have been modified with rigid layers on their surface [188]. For instance, Liang et al. covered a separator with a layer of SiO_2 spheres [189]. By incorporating these shield-like SiO_2 layers, the catastrophic piercing of the separator by the dendrite was effectively prevented. This strategy has further evolved, leading to the replacement of the separator with a solid-state electrolyte, which will be discussed in the solid-state electrolyte section.

The separator provides ion diffusion pathways across its pores while isolating each electrode physically. Concerning this, it is crucial to thoroughly evaluate properties related to ion transport, such as porosity and electrolyte wettability. These factors play a significant role in ion migration within the battery system and even affect the deposition behavior of metal. For example, when ions are unevenly distributed due to electrolyte enrichment near pores, this can trigger random nucleation and plating of ions, leading to the formation of dendrites [190]. Therefore, it is necessary to homogenize the ion flux after crossing the separator to promote uniform deposition. By achieving a more uniform ion distribution, the probability of uneven plating and dendritic growth can be decreased. Based on this idea, Zhao et al. fabricated an Al-doped $Li_{6.75}La_3Zr_{1.75}Ta_{0.25}O_{12}$- (LLZTO-) coated PP [190]. Due to the copious 3D ion conduction channels in the LLZTO-coating layer, the Li-ion flux can be homogenized after it passes through the separators. As a result, the Li metal is plated uniformly without dendrite growth, thereby improving the cycling stability of the battery.

So far, commercial PE and PP separators have also been employed often for K-based batteries as separators [68, 101, 125]. However, due to the more severe dendrite growth of the K metal, the PP separator seems to be more easily penetrated by K dendrites as compared to Li dendrites [66]. Furthermore, PE and PP separators exhibit insufficient wetting behavior to electrolytes, which is likely to cause uneven metal deposition [191]. Liu et al. synthesized the AlF_3 double-side-coated separator (AlF_3@PP) to enhance the wettability between the separator and electrolyte, eventually promoting a rapid and uniform K ion flux (Figure 15) [164]. The AlF_3 coating on PP improved interfacial tension between the PP separator and liquid electrolyte due to increased surface roughness [165]. As a result, the modified separator exhibited a complete wetting behavior to the electrolyte, thus inducing uniform K ion distribution. Besides, AlF_3 layers also contributed to the formation of inorganic-rich (e.g., KF, Al_2O_3, and AlF_3) SEI layers presumably due to the electrochemical reaction between the AlF_3 and semicarbonates of the original SEI layer. Consequently, K metal batteries assembled with the AlF_3@PP separator displayed stable cycling stability without dendrite growth compared to those of PP.

It is worth noting that the most widely used separator for K-based batteries is a glass fiber (GF) membrane [102, 142, 155, 180, 192]. The GF separator is composed of randomly arranged inorganic nonmetallic fibers with diameters smaller than 2 μm, resulting in the formation of a three-dimensional network and large pores in the macroscale range [193]. GF has been regarded as the most suitable separator for K-based batteries due to its high degree of porosity with excellent thermal stability. Moreover, GF exhibits superior wettability to electrolytes, which could improve ionic conductivity and thus facilitate ion transport [83]. However, employing GF as a separator does not guarantee the stable cycling of K metal batteries. GF/D, a type of glass fiber, can easily be pierced and filled with K dendritic particles due to its low mechanical cohesion and high degree of porosity [68]. The propagated separator could induce uneven K deposition thereby accelerating the cell failure. Thus, researchers have modified the surface of the GF separator, exploiting the strategies established in PE or PP separators. For instance, Wang et al. coated lithium niobate/graphene ($LiNbO_3$@G) compounds on commercial GF via vacuum filtration [172]. The $LiNbO_3$@G layer has a porous structure and a thickness of less than 1 μm with ferroelectricity. It is noted that ferroelectric materials possess spontaneous polarization due to their asymmetric crystal structure, which can manipulate the transport kinetics of K ions and ion concentration distribution through the interaction between ferroelectric dipoles and adsorbed ions [194]. Due to the regulated K ion flux, K was plated and stripped reversibly on the Cu current collector during the charge/discharge process. Additionally, it would be desirable to load nanomaterials which exhibit a high conductivity onto the surface of the separator facing the anode side [195]. For instance, 2D nanosheets of graphene can be coated on GF for improving the electrical conductivity of separators [196]. A conductive reduced graphene oxide layer on the separator (rGO@GF) has the ability to "reactivate" electrically isolated dead K which was detached from the bulk K electrode [197].

Overall, it is obvious that pretreated separators not only suppress the dendrite growth but also enhance the electrochemical performance. Two major points should be of concern for an ideal separator. The one is the sufficient mechanical properties to suppress dendritic growth. The next one is to distribute ions uniformly via its pores during cycling, thereby promoting uniform deposition of K. Consequently, the development of a functionalized separator would open up a new avenue for overcoming many challenges of the K metal anode without direct engineering or modification on the metal electrode.

3.2.2. Liquid Electrolytes. Electrolytes, the essential lifeblood of batteries, serve dual critical roles. Primarily, they function as the charge carrier between electrodes, facilitating the fundamental mechanism of energy storage and delivery. Additionally, they are decomposed and contribute to the formation of SEI, a pivotal layer that significantly impacts

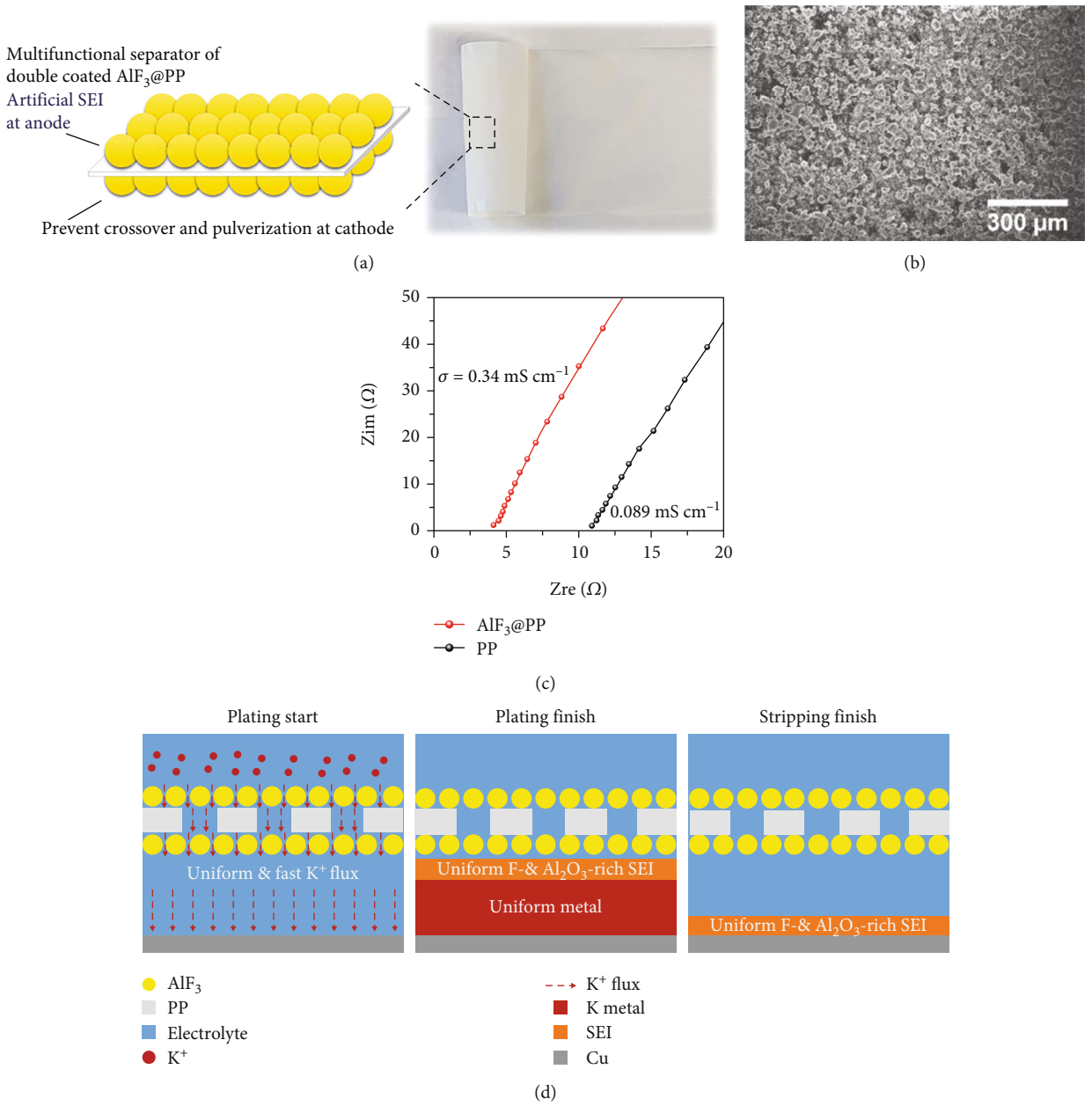

Figure 15: (a) Illustration and photograph of double-coated PP with multifunctional AlF_3 layer. (b) Top-view SEM image of AlF_3@PP separator. (c) EIS Nyquist plots with different separators displaying the ionic conductivities. (d) Schematic of the role of AlF_3@PP separator during K plating/stripping process, reproduced with permission [164]. Copyright 2022, Wiley.

battery performance and lifespan [61]. Given that potassium metal anodes experience substantial and repetitive stress change, the formation of a stable SEI layer through electrolyte engineering emerges as a particularly significant area of interest in the realm of K metal anodes [44].

The initial focus of our discussion is salts, which act as the main conductive component with electrolytes. Next, we turn to solvent, the carrier for the salt within the electrolyte. These components not only influence the cycling stability of the battery but also play a role in forming the vital SEI layer. Our discussion then shifts to additives, substances introduced into the electrolyte to optimize battery performance. Subsequently, ionic liquids are introduced. Finally, recent advances in solid electrolytes will be explored. By breaking down each component in this sequence, the objective of this section is to provide an insightful and comprehensive view of the intricate dynamics involved in electrolyte engineering. A special emphasis will be placed on the formation of a stable SEI layer on potassium metal anodes, an area of pressing importance given the inherent stress changes experienced by these anodes.

(1) Salt Engineering. Salt anions play a pivotal role in designing the chemical and physical properties of the SEI layer, influencing its mechanical strength, ionic conductivity, and passivation ability [198]. It is understood that inorganic

phases (for instance, LiF) within the SEI layer are more robust compared to organic phases, thereby offering effective protection to Li metal anodes [199]. In LIBs, it has been reported that a LiF-rich SEI layer is formed when lithium bis(fluorosulfonyl)imide (LiFSI) or lithium bis(trifluoromethanesulfonyl)imide (LiTFSI) salts are employed [200, 201]. Due to the low LUMO energy of LiFSI and LiTFSI, they are decomposed prior to solvents at the beginning of the SEI formation process [202]. Also, the dissociation energy of LiFSI and LiTFSI is lower than that of $LiPF_6$ [200]. This observation logically extended to PMBs, employing potassium bis(fluorosulfonyl)imide (KFSI) or potassium bis(trifluoromethanesulfonyl)imide (KTFSI) [43, 57, 69, 149, 203]. For instance, Wang et al. investigated the influence of KFSI on K metal anodes [204]. The KFSI electrolyte exhibited not only extended cycling performance but also good rate capability compared to the KPF_6 electrolyte. The authors revealed that inorganic components dominate the SEI layer, perhaps providing better mechanical strength to accommodate volume change. Despite FSI (-N-SO_2-F) and TFSI (-N-SO_2-CF_3) possessing similar chemical structures (Figure 16(a)), TFSI often shows inferior electrochemical performances [205–207]. Xiao et al. compared the Coulombic efficiency of 1 M KPF_6-DME, 0.8 M KPF_6-EC/DEC, and 1 M KTFSI-DME for K metal anodes and observed that all the electrolytes failed within 10~20 cycles while showing stable cyclability in the use of KFSI-DME [205–207]. The different results between KFSI and KTFSI might be originated from the different SEI structure formations [38]. It is generally understood that the SEI on the anode surface is created through the reductive decomposition of electrolytes, and the LUMO energy of these electrolytes is thought to be closely related to their decomposition. The FSI^- anion's LUMO energy level is just marginally lower than that of the EC solvent. However, the LUMO energy levels of the $TFSI^-$ and PF_6^- anions are significantly higher than those of the EC solvent, suggesting that the EC solvent can be easily reduced on the surface of the anode (Figure 16(b)). That is, in the case of KTFSI, anion decomposition might contribute less to the SEI formation on the anode surface [38, 208]. Recently, Hu et al. proposed the potassium hexafluoropropane-1,3-disulfonimide (KHFDF) salt which is a modified form of KTFSI salt [208]. The $HFDF^-$ anion exhibits a cyclic structure (Figure 16(a)), which might be more effective in passivating both anode and cathode surfaces compared to the linear structure anions such as FSI^- and $TFSI^-$, forming an inorganic-rich SEI layer [209].

Overall, recent studies about salt engineering argue that it is crucial to form an inorganic-rich SEI layer by anion decomposition in three aspects. Inorganic-rich SEI, indicating low density surface film formation and dendrite growth, could help to compact the surface structure [199, 200]. In addition, it could suppress the side reaction with HF coming from PF_5 [210]. Moreover, inorganic-rich SEI layers can retard electron transfer and facilitate Li^+ migration [211]. It is worth mentioning that the inorganic-rich (especially KF) might not be an ideal solution. In LIBs, the electrochemical performance of graphite anodes has improved at a mild use of FEC while unexpected granules were found on the graphite surface at a high concentration of FEC (10 vol%), thus increasing surface impedance [204, 212].

Although KFSI showed better performances than KPF_6, they are not without shortcomings for several reasons. (i) For instance, they tend to initiate corrosion on the Al foil [213]. This is similar to the Al corrosion cases of LiFSI, which might be attributed to the F-S bonds in FSI^- or the residual impurities such as chloride originating from the synthesis process [214, 215]. (ii) Additionally, KFSI tends to show larger overpotential than KPF_6 electrolytes during the plating/stripping process [204, 216]. This is presumably attributed to different SEI layer compositions of KPF_6 and KFSI or different solvation energies of each electrolyte, which should be further investigated [40, 204, 217]. To avoid these shortcomings, researchers have reported strategies to (i) use a highly concentrated electrolyte or employ an additive [206, 218]. For instance, KFSI and KTFSI salts up to 5 M are used to reduce the corrosion at the Al foil. KFSA, which also shows highly corrosive behavior to Al foil, worked for PMBs in concentrated conditions [219]. Researchers expected that highly concentrated electrolytes reduce the number of free solvent molecules in K ion electrolytes, thereby potentially inhibiting the corrosion of Al foils, similar to the effect observed in Li and Na. As a result, both highly concentrated electrolytes exhibited anticorrosive behavior at a high voltage [206]. The effects of high concentration electrolytes will be discussed further in the section on highly concentrated electrolytes. (ii) In addition, Kang et al. reported that adding potassium nitrate (KNO_3) in the KFSI electrolyte also could achieve noncorrosion of Al current collector and reduced onset overpotential, which will be discussed later.

Meanwhile, in salt design, the salt should have high solubility and ionic conductivity. Potassium perchlorate ($KClO_4$) and potassium tetrafluoroborate (KBF_4) have been tried for K electrolytes; they are rarely adopted due to their low solubility and poor ionic conductivity [23, 219–221]. For instance, the overpotential of the K||K cell showed high overpotential up to 1 V in early cycles in the electrolyte of 0.1 M $KClO_4$ PC [222].

(2) Solvent Engineering. Solvents, one of the main components of electrolytes, also play a decisive role in the formation of the SEI layer and in determining the electrochemical performance of PMBs. The solvent molecules are decomposed during the early charge/discharge process, and the decomposed products are deposited on the anode surface, forming the SEI layer [223]. The mixture of cyclic carbonates (EC and PC) and linear carbonates (DMC and DEC) has been widely employed as electrolyte solvents for the K metal anode [12, 18, 72, 75, 102, 204]. It is noted that the high dielectric constant of cyclic carbonates contributes to the formation of SEI layers, whereas the low viscosity of linear carbonates enhances the mobility of K ions [224]. Hosaka et al. compared the overpotential behavior of K symmetric cells filled with KPF_6-EC/DEC, KPF_6-PC, KPF_6-EC/DMC, and KPF_6-EC/PC for investigating the electrolyte compatibility with the K metal [98]. All cells showed

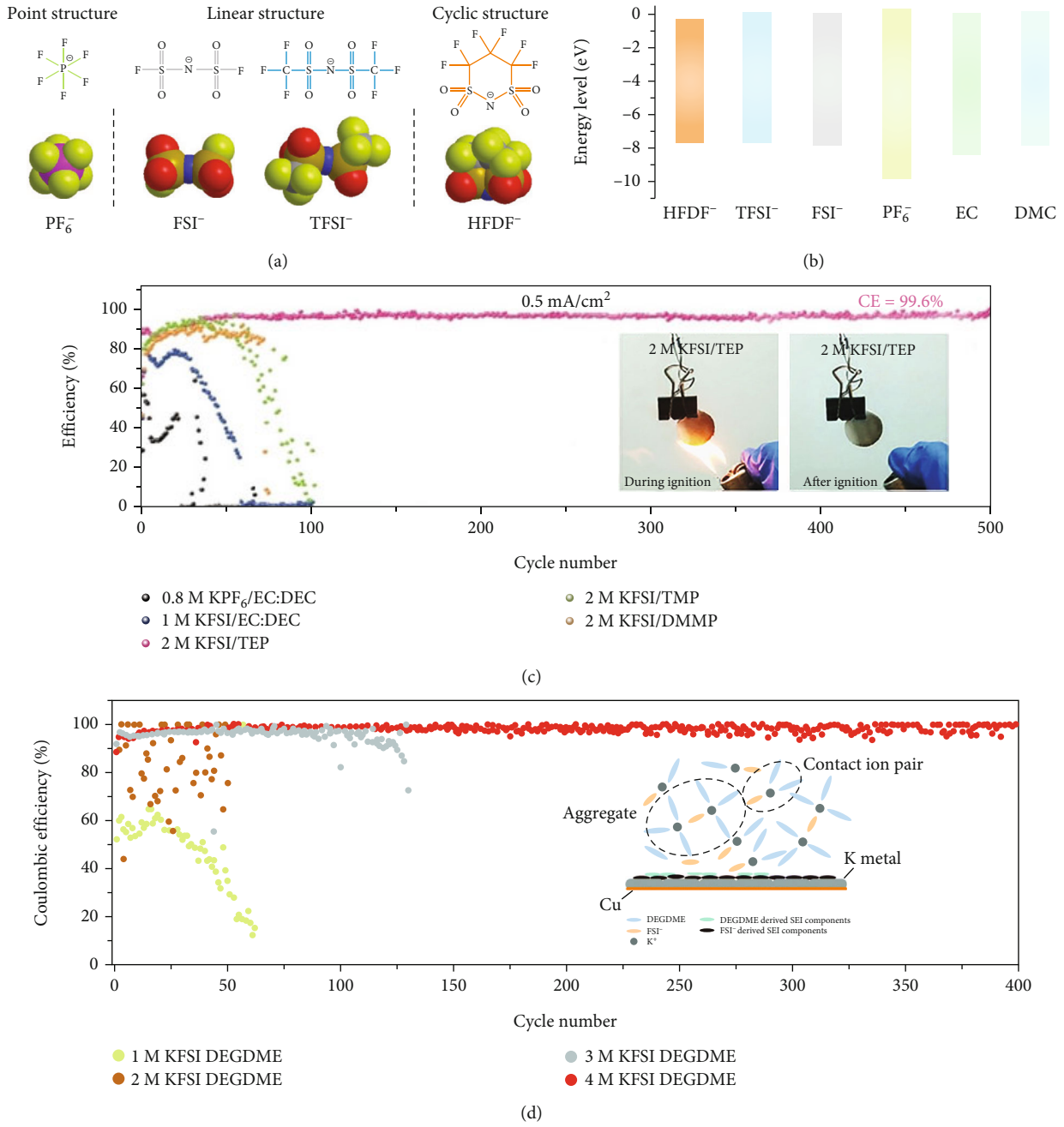

Figure 16: Continued.

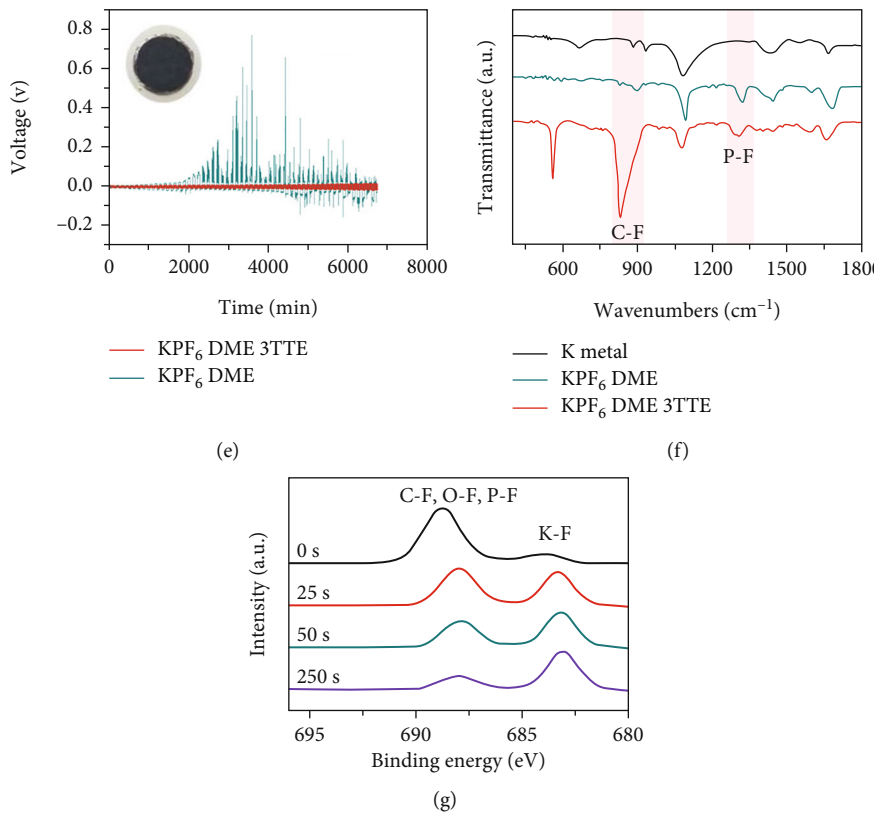

Figure 16: (a) Design illustrations and molecular structures of PF_6^-, FSI^-, $TFSI^-$, and $HFDF^-$ anions. (b) The HOMO and LUMO energy diagram of various anions and carbonate solvents, reproduced with permission [208]. Copyright 2022, Oxford University Press. (c) Coulombic efficiencies of K||Cu cells filled with various electrolytes during cycling. Inset: flame test of separator soaked with TEP-based electrolyte, reproduced with permission [233]. Copyright 2020, Wiley. (d) Cycling performance of K||Cu cells in KFSI-DEGDME electrolytes with various concentrations. Inset: scheme of the role of highly concentrated electrolyte, reproduced with permission [225]. Copyright 2021, Royal Society of Chemistry. (e) Overpotentials of K||K cells in 1 M KPF_6-DME with and without 3TTE electrolytes. Inset: digital photo of the K metallic electrode from the cycled cell in electrolyte with 3TTE. (f) FTIR spectra of fresh K metal and cycled K metals in different electrolytes. (g) F 1 s XPS depth profiles of K metal cycled in 1 M KPF_6-DME-3TTE, reproduced with permission [239]. Copyright 2022, Wiley.

large overpotentials of >500 mV. Notably, the KPF_6-PC cell exhibited a continuous increase in overpotential during cycles, which is presumably due to the continuous reduction of electrolytes and the accumulation of decomposed products on the K metal. These results suggest that the highly reactive K metal anodes immersed in carbonate-based electrolytes usually lead to the formation of unstable SEI, resulting in a low CE-severe dendritic growth [57, 225, 226].

Compared with carbonate-based electrolytes, it is noteworthy to point out that ether-based electrolytes exhibit higher solvation energy to K ion, resulting in a higher degree of solvation molecules and thus inhibiting the side reaction between free solvent molecules and the K metal anode [204]. This is because the polar ether group (-C-O-C-) of ether solvents which possess the O atoms with lone pairs can strongly attract the K ion through electrostatic interaction [227]. Meanwhile, Hosaka and coworkers also investigated the overpotentials of K symmetric cells with KFSA-PC, KFSA-EC/DEC, and KFSA-DME [98]. The carbonate-based electrolytes exhibited a large overpotential, whereas KFSA-DME electrolytes showed a low overpotential of 50 mV. The reduced overpotential is ascribed to the lower resistive and durable SEI layer on the K metal [205]. To examine the difference in the SEI layer formed in the ether- and carbonate-based electrolytes, Li et al. investigated the LUMO and HOMO energy levels of FSI^-, DME, EC, and DEC solvents [228]. They argued that the LUMO energy level of FSI^- is significantly lower than that of DME solvents, promoting the prior decomposition of FSI^- to the DME solvent. The decomposed products of FSI^- are inorganic compounds, constructing an inorganic-rich SEI layer on the K metal [204]. Notably, the inorganic-rich SEI layer has been demonstrated to be significantly impermeable to the solvent, consequently reducing the subsequent decomposition of DME solvents [228, 229]. On the other hand, the LUMO energy levels of FSI^-, EC, and DEC are relatively close. Consequently, the simultaneous decomposition of FSI^-, EC, and DEC forms random distribution of inorganic and organic compounds in the SEI layer. Decomposition of electrolytes would be continued and thus leads to the formation of a thicker SEI layer which is likely to raise the cell impedance [230]. Overall, ether-based electrolytes can contribute to the improvement of CE and cycling life by forming a robust

Table 7: Various electrolytes for K metal anodes and associated cycling performance.

Working electrode	Counter electrode	Electrolyte	Current density ($mA\ cm^{-2}$)	Areal capacity ($mAh\ cm^{-2}$)	CE (cycles)	Ref.
K	Cu	1 M KFSI TEP	0.5	0.5	99.2% (650)	[57]
K	Cu	1 M KFSI DME	0.05	0.15	99% (100)	[205]
K	Cu	4 M KFSI DEGDME	0.25	0.25	98.3% (400)	[225]
K	Cu	2.3 M KFSI DEGDME/TFETFE	0.15	0.15	98.2% (300)	[236]
K	Cu	1 M KFSI DEE	0.2	0.4	98.1% (100)	[232]
K	Cu	0.5 M KFSI EC/DEC	0.5	0.5	97.2% (100)	[192]
K	Cu	0.8 M KHFDF EC/DMC	0.25	0.5	94.3% (200)	[208]

SEI layer compared to carbonate-based electrolytes [205, 231, 232].

Despite various advantages of ether-based electrolytes, they suffer from limited oxidation stability which makes it difficult to meet the need for high-voltage K metal batteries [225]. This might be attributed to the higher HOMO energy level of the ether solvent compared to carbonate solvents, thereby easily losing their electrons when the high voltage is applied [204]. This poor oxidation stability can be enhanced by increasing the concentration of electrolytes or incorporating postoxidative additives, expanding on the strategies established for salt engineering [206, 218].

Battery safety issues are getting more attention in the public recently. For the practical application of metal anodes, in particular, fire issues of the battery should be resolved. There are two major causes associated with fire problems of K metal anodes—high reactivity of the K metal and high flammability of organic electrolytes [5]. Commonly employed organic solvents for K ion electrolytes including EC, DEC, and DME are highly flammable, which could eventually lead to fire or explosion of batteries. Therefore, using nonflammable electrolytes can be a promising method to ensure the safety of K metal anodes. Liu's group reported a nonflammable K ion electrolyte by using triethyl phosphate (TEP) and trimethyl phosphate (TMP) solvents [216, 233]. TEP and TMP solvents did not show any flame during the fire test due to their nonflammable nature, while carbonate electrolytes were easily ignited. Furthermore, phosphate-based electrolytes show higher CE and reduced overpotential during the K plating/stripping process compared to carbonate-based electrolytes (Figure 16(c)) [216, 233]. This is probably attributed to the SEI layer formed in phosphate-based electrolytes forming large patches of inorganic compounds (e.g., KPO_3), which can effectively passivate the surface of the K metal [57]. As a result, organic phosphate-based electrolytes not only exhibit a nonflammable behavior but also lead to the formation of a robust and thin SEI layer.

(3) Highly Concentrated Electrolytes. Building on the foundational understanding of how highly concentrated electrolytes enhance lithium metal anodes' performance, there is increasing interest in exploring this approach for potassium (K) metal anodes. The benefit of highly concentrated electrolytes on metal anodes lies in their ability to modulate the solvation sheath of alkali ions (i.e., the protective layer that forms around alkali ions in an electrolyte solution) and suppress dendritic growth, which opens up new possibilities for addressing similar challenges in K metal anodes [234]. In typical dilute electrolytes, alkali metal ions are surrounded by a sheath composed of solvent molecules, but in highly concentrated electrolytes, alkali metal ions would be coordinated with anions instead of solvent molecules and thus make it difficult for them to aggregate into dendrites [60, 225, 235]. In line with the rationale, it has been tried to implant the appealing properties of the concentrated electrolytes on K metal anodes. In 2017, a notable investigation by Xiao et al. elucidated that concentrated KFSI-DME (mole ratio = 0.5) increases the reversibility of K plating/stripping [205]. Recently, long-term cycling over 400 cycles with a high average CE of 98.3% was achieved using 4 M KFSI-diethylene glycol dimethyl ether (DEGDME) (Figure 16(d)) [225]. The mechanism underpinning these results lies in the unique chemistry of highly concentrated electrolytes. By decreasing free solvent molecules in electrolytes, these electrolytes foster the formation of contact ion pairs (CIPs) and aggregates (AGGs). These structures involve an anion coordinated with one or more K ions [60]. A resultant effect is the formation of an inorganic-rich solid electrolyte interphase (SEI) layer, which resists the decomposition of free solvents [225]. In another study, Hosaka et al. leveraged a highly concentrated potassium bis(fluorosulfonyl)amide (KFSA) salt in DME, achieving significantly reduced polarization without any voltage spike compared to KPF_6 in carbonate solvents [98]. It is notable that highly concentrated electrolytes typically enhance performance in ether-based electrolytes, but this enhancement does not necessarily translate to carbonate-based electrolytes despite their higher ionic [192].

Instead of the concentrated electrolytes, a practical solution would be localized high concentration electrolytes (LHCEs) that employ an inert diluent as a cosolvent [236]. This strategy allows for the maintenance of the solvation structure of high concentration electrolytes while reducing viscosity and improving ionic conductivity. For instance, electrolytes composed of 2.3 M KFSI-DEGDME along with 1,1,2,2-tetrafluoro-1-(2,2,2-trifluoroethoxy)ethane (TFETFE) have shown enhancements in the cycling lifespan and potential window up to 5 V [236]. Table 7 provides a

comprehensive summary of different electrolytes and the associated cycling stability they exhibit on potassium metal anodes.

(4) Additives for Liquid Electrolytes. The application of additives in electrolytes would be an efficacious approach to bolster the cyclability of potassium (K) metal electrodes [237]. This strategy, inspired by advances in lithium-ion battery (LIB) technology, is fundamentally aimed at controlling the formation of the SEI layer on metal anode surfaces [238]. In LIBs, additives like fluoroethylene carbonate (FEC) have proven instrumental in the prevention of excessive solvent reduction, due to their lower relative LUMO energy than that of conventional solvents like EC and DEC [199]. These additives are reduced preferentially during SEI layer formation, effectively passivating the metallic anode surface, and preventing detrimental side reactions. Encouraged by these successes in LIBs, researchers have sought to implement similar strategies in K-ion electrolytes. However, the path has been fraught with challenges. Most additives trialed thus far have led to degraded electrochemical performance, indicating that the passivating efficacy of additives in LIBs does not necessarily translate to K metal anodes [69]. For example, a series of additives known for their beneficial effects on LIBs and SIBs, including FEC, difluoroethylene carbonate (DFEC), vinylene carbonate (VC), ethylene sulfite (ES), and trimethylene sulfate (TMS), increased the overpotentials of K symmetric cells in the conventional carbonate electrolyte 0.8 M KPF_6-EC/DEC [96, 98].

Despite the contrary results of the additives in carbonate-based electrolytes, moderate-concentration ether electrolytes such as 2.3 M KFSI-DME with 50 mM potassium nitrate (KNO_3) have shown promise [218]. The relatively low LUMO energy level of KNO_3 facilitates the formation of a N/F-containing inorganic-rich SEI layer during initial cycles. This additive served a dual purpose: it promotes more uniform K plating and also improves the typically poor oxidation stability of ether-based electrolytes, making them stable up to 4.5 V [218]. In another noteworthy paper, Chen et al. achieved rapid K ion desolvation at a low temperature of -40°C by employing 1 M KPF_6-DME with 1,1,2,2-tetrafluoroethyl-2,2,3,3-tetrafluoropropyl ether (TTE) additives [239]. The authors found that the TTE formed a passivation layer on the K metal via the spontaneous reactions and helped to form an inorganic-rich SEI layer (Figures 16(e)–16(g)).

Drawing from these studies, it would be that while the efficacy of additives in LIBs and SIBs does not directly translate to K metal anodes, the principle of forming an inorganic-rich SEI layer on K metal surfaces could still be a powerful strategy [96].

(5) Exploring Ionic Liquids. Ionic liquids (ILs) are essentially molten salts characterized by organic cations and either organic or inorganic anions [240]. The appeals of ILs as a safer electrolyte system rest on their nonvolatility, nonflammability, and superior thermal stability [241]. With their respectable ionic conductivity, one of the most significant advantages of ILs is their inherent broad voltage window. This wide electrochemical stability window arises from the low nucleophilicity of the anions and low electrophilicity of the cations, which resist oxidation and reduction, respectively [242]. This attribute suggests their potential suitability for high-voltage battery applications that could extend up to 6 V [242]. In 2019, Yoshii et al. employed an IL electrolyte, consisting of 0.5 M potassium bis(trifluoromethanesulfonyl)amide (KTFSA) in 1-butyl-1-methylpyrrolidinium bis(trifluoromethanesulfonyl)imide (Pyr_{14}TFSA) for high-voltage K metal batteries [242]. However, the IL electrolyte revealed limited cycling capability only at a modest current density of 6.4 $\mu A\,cm^{-2}$ due to a moderate ionic conductivity of 2.1 $mS\,cm^{-1}$ at 25°C by bulky cations and anions such as Pyr and TFSI. Thus, Sun et al. proposed 1-ethyl-3-methylimidazolium chloride ([EMIm]Cl)/$AlCl_3$/KCl/KFSI (buffered K-Cl-IL) IL [243]. The buffered electrolyte exhibited enhanced ionic conductivity of 13.1 $mS\,cm^{-1}$ at 25°C and delivered superior cycling performance over 820 cycles. Owing to the diverse inorganic anions present in the buffered K-Cl-IL, an effective passivation layer-incorporating KF, AlF_3, Al_2O_3, and KCl was established on the K metal anode [243].

Although ILs offer distinct advantages, their practical implementation in energy storage systems is hampered by their high cost and industrial-scale production challenges. Additional hurdles for ILs include their high viscosity and relatively low conductivity at room temperature. Despite these impediments, ILs remain a strong contender compared to traditional electrolytes in the context of safety. With their unique advantage of a wide voltage window, ILs have the potential to redefine the boundaries of high-voltage applications.

3.2.3. Solid-State Electrolytes. Rechargeable battery systems have traditionally employed liquid electrolytes due to their high ionic conductivity and excellent electrode-wetting characteristics. Despite the successful commercial application of these liquid electrolytes, they pose safety risks including electrolyte leakage, fire, and gas generation [244]. Also, SEI formation via liquid electrolyte decomposition may not be a fundamental solution to the suppression of dendrite growth. In response to these safety concerns as well as the stable operation of metal batteries, scientists are exploring safer and more stable electrolyte alternatives [144, 233, 243]. Among them, solid-state electrolytes (SSEs) are gaining huge scientific attention recently [245]. In view of mechanical stability, SSEs are fundamentally favorable to mitigate severe safety hazards like dendrite growth due to their solid-state nature. Moreover, most of the SSEs can inherently offer a wider electrochemical stability window, contributing to higher energy densities [246]. Despite these advantages, the remaining requirements are still challenging. Many SSEs often exhibit lower ionic conductivity at room temperature as well as unsatisfactory electrode compatibility [247].

For the uptake of SSEs, the imminent requirement would be high ionic conductivity ($>10^{-3}\,S\,cm^{-1}$), of course, ultralow electronic conductivity ($<10^{-10}\,S\,cm^{-1}$), wide working

Table 8: Ionic conductivity and activation energy of various SSEs for K ion.

Type	Compound	Ionic conductivity (mS cm^{-1})	Activation energy (eV)	Temperature[a] (°C)	Ref.
Polymers	PEO-KI-ZnS	0.31	0.15	25	[251]
	PPC-KFSI	0.014	—	20	[252]
	PEO-KTFSI	0.27	—	60	[253]
	PMMA-KPF_6	4.3	0.27	25	[264]
	P(EO/MEEGE/AGE)-KFSA	0.02	—	25	[254]
	PEO-KFSI	0.036	—	25	[246]
	PEO-KDFTFSI	0.053	—	70	[261]
	K-SPE750-K	0.98	—	80	[262]
	V_{34}/PSS-K-1	4.55	0.59	25	[263]
	PVDF-HFP-KFSI@PAN	0.36	—	25	[265]
Oxide	K-β-alumina	0.065	0.29	25	[299]
	K-β''-alumina	1-2	0.2	25	[255]
	$K_2Fe_4O_7$	50	0.08	25	[256]
Antiperovskite	$K_{2.9}Ba_{0.05}OI$	3.5	0.36	257[a]	[258]
Borohydrides	$KCB_{11}H_{12}$	0.32	0.82	88	[260]
	KB_3H_8	0.0003	0.44	150	[259]
	$KB_{11}H_{14}$	0.12	1.9	150	[276]
	$KB_3H_8{\cdot}NH_3B_3H_7$	0.13	0.44	55	[247]

[a]When the exact temperature is not specified, the temperature was estimated.

potential (>3~4 V), chemical stability, robust mechanical strength, thermal stability, as well as excellent interface impedance (often pointed out as a culprit of cell failure) and compatibility (i.e., wettability) to metal anodes [248]. Also, the HOMO of the SSEs should be lower than that of the cathode potential [249]. That is, SSEs literally play the role of *solid electrolyte*: the electrolyte only acts as a robust ion conductor like an ultrastable SEI. Although the developed SSEs still need to be improved further, a couple of recent studies showed the feasibility of SSEs for K metal anodes, showing noticeable ionic conductivity at room temperature [250].

(1) Polymer-Based Solid Electrolytes. K-ion SSEs for PMBs reported so far fall into four groups: solid polymer electrolytes (SPEs) [251–254], oxides [255–257], antiperovskites [258], and borohydrides [247, 259, 260]. The most intensively studied SSEs for PMBs are SPEs. SPEs are generally synthesized by dissociating salts in a polymer host. So far, various polymer frameworks such as poly(ethylene oxide) (PEO) [246, 261, 262], poly(propylene carbonate) (PPC) [252], poly(styrene sulfonate) (PSS) [263], poly(methyl methacrylate) (PMMA) [264], and polyacrylonitrile (PAN) [265] have been used as precursors to prepare the SPEs. In particular, PEO has been most widely investigated for Li and Na due to its low glass transition temperature ($T_g \approx -60$°C), wide electrochemical stability, and superior compatibility with several alkali metal salts even at high concentrations [266]. With an optimal molar ratio of ethylene oxide to K, PEO-KTFSI showed 3.56×10^{-5} S cm^{-1}, still falling behind the ionic conductivity of liquid electrolytes [246]. Meanwhile, Gao et al. reported a polymer-gel-type electrolyte with a high ionic conductivity of 4.3×10^{-3} S cm^{-1} at room temperature which is developed by cross-linking PMMA and tetraethylene glycol dimethacrylate (TEGDMA) [264]. Although there has been noticeable progress in SPEs, most of the SPEs still exhibit low ionic conductivities (<10^{-5} S cm^{-1}), which fall short of the required ionic conductivities for practical applications (>10^{-3} S cm^{-1}) (Table 8) [244]. Also, a key feature of SPEs is that their ionic conductivity has a trade-off relationship to mechanical properties. Considering that one of the primary goals of SSEs is inhibiting dendrite growth, tuning the electrochemical property of SPEs should be done with sophisticated calculations or experiments of mechanical properties.

(2) Oxide-Based Solid Electrolyte. Oxide-based SSEs have received great attention for LMBs due to their high ionic conductivity, tunability, mechanical modulus, and electrochemical stability [248]. Recently, K ion conductors that are based on oxides have also been the focus of extensive research. In particular, β''-Al_2O_3 has been the representative oxide-based fast ionic conductor. In β''-Al_2O_3, ions diffuse through 2D conduction slabs between spinel blocks, which are comprised of four layers of oxygen ions with aluminum ions [267]. K-β''-Al_2O_3, where K ions replace Na ions in the conduction slab, delivers high ionic conductivity up to 8×10^{-4} S cm^{-1} at room temperature, which is superior compared to usual SSEs (<10^{-4} S cm^{-1}) [268].

It is noted that the conductivity of K-β''-Al_2O_3 is lower than that of Na-β''-Al_2O_3. This is presumably a larger ionic size of K (1.38 Å) compared to Na (1.02 Å), which results in greater difficulty for K ions to migrate in solids [269]. For

instance, Lu's group reported that the conductivity of Na-β''-Al_2O_3 is significantly higher than that of K-β''-Al_2O_3 across a wide range of temperatures (Figure 17(a)) [270]. This leads to limited feasible structures for K ion SSEs. For instance, the larger size of K ions makes it difficult to migrate through the quadrangular O_4 sites, while Na ions could diffuse through O_4 sites such as $Na_2M_2TeO_6$("M" is either Ni, Co, Zn, or Mg) [269]. Therefore, the K ion solid conductors should provide larger sites such as hexagonal O_6 or octagonal O_8 sites [256, 271]. Yuan et al. synthesized a 3D open-framework ferrite $K_2Fe_4O_7$, which is composed of a 2D layer formed by FeO_6 octahedral and FeO_4 tetrahedral units and K ions [256]. The $K_2Fe_4O_7$ provides two directions of ion diffusion channels parallel to *a*- or *b*-axis and *c*-axis (Figures 17(b) and 17(c)). The channels parallel to the *a*-axis have an open and wide structure which can mainly contribute to the fast K ion migration through the solids. However, the channels parallel to the *c*-axis are obstructed by the FeO_4 tetrahedral units, resulting in K ions facing difficulty in diffusing along the *c*-axis as compared to the *a*-axis. This indicates that large and expanded lattices are advantageous for facilitating the larger size of K ions through the SSEs.

(3) Antiperovskite-Based Solid Electrolytes. The body-centered cubic (bcc) anion sublattice has a less packed structure compared to the other sublattices such as face-centered cubic (fcc) or hexagonal closed-packed (hcp). The bcc anion sublattice can provide a large diffusion channel with weakened interactions between the anion and the metal cation, facilitating the fast ion migration. This has been demonstrated by antiperovskites for Li and Na (e.g., Li_3OCl and Na_3OBr) [272, 273], which possess similar atomic topology to a perovskite, whereas with a reversed ionic arrangement [244]. Zheng et al. reported a potassium antiperovskite of K_3OI for K ion SSEs, which possesses a larger lattice volume compared to other potassium antiperovskites [258]. The authors argued that K ions migrate through the vacancies of K sites and disordered I-O sites, which is anticipated to improve the K ion diffusion (Figure 17(d)). Based on this, the barium (Ba) ion was doped in K_3OI to introduce K vacancies, and thus, the ionic conductivity was effectively increased (Figure 17(e)) [258].

(4) Borohydride-Based Solid Electrolytes. Borohydrides have recently attracted attention as a promising candidate for SSEs due to their special properties [274]. They possess negligible grain boundary barriers and excellent physical and chemical durability with light weight. Meanwhile, it is reported that borohydrides undergo a reversible structural transition at a certain temperature. For example, monoclinic KB_3H_8 undergoes a two-step polymorphic transition along the temperature increase. The transition from monoclinic to orthorhombic occurs at 15°C and from orthorhombic to cubic occurs at 30°C (Figure 17(f)) [259]. This transition results in a high degree of disordered $B_3H_8^-$ anion with a rotation state, which can enhance the mobility of the K ion in this material [275]. As a result, the ionic conductivity of KB_3H_8 is 3.4×10^{-7} S cm^{-1} at 150°C [259]. Recently, Zhang et al. synthesized the $KB_3H_8{\cdot}NH_3B_3H_7$ complex by incorporating neutral molecules of $NH_3B_3H_7$ in KB_3H_8 to increase ionic conductivity further [247]. The incorporation of neutral molecules enlarges the volume of KB_3H_8, which can also expand the space around K ions and consequently contribute to higher ionic conductivity. Therefore, $KB_3H_8{\cdot}NH_3B_3H_7$ can deliver enhanced ionic conductivity of 1.3×10^{-4} S cm^{-1} at 55°C compared to KB_3H_8 [247]. The borohydride-based SSEs show a superionic conductivity at high temperatures and a potential for stabilization of ionic conductivity at ambient temperature [276].

(5) Challenge of Solid Electrolytes: Void Formation. Meanwhile, one of the challenges of solid-state batteries (SSBs) is to maintain stable electrical contact between metal surfaces and SSEs. It is generally accepted that the interface impedance of SSBs generally depends on a charge transfer process and a contact condition between electrodes and SSEs [277]. During the stripping process at a K metal electrode, the K atom at the interface changes into K ions and diffuses into SSEs, leaving vacancies. When the current density or areal capacity is applied with a higher value, the formation of voids will be promoted, thereby yielding a high interfacial resistance [278]. Spencer Jolly et al. observed that K metal SSBs with K-β''-alumina significantly increase overpotential during cycling at the voids between the K metal and SSEs [257]. Therefore, the operating condition of SSBs such as current density and areal capacity should be considered to inhibit void formation at the interface. Recently, Wu's group employed a K metal composite electrode with reduced graphene oxide (K-10%RGO) for SSBs to construct a 3D-interconnected interface [245]. The K-RGO composite electrode exhibits a higher diffusion coefficient, surpassing even that of K metal (Figure 17(g)). This enables it to rapidly fill K atom vacancies formed at the interface by the K atom diffusing from the inside of the metal electrode. Consequently, the interfacial structure remains well-intact after the K stripping process with the areal capacity of 6 mAh cm^{-2}, and the formation of the voids was inhibited (Figures 17(h) and 17(i)). This result suggests that to enhance the electrochemical performance of K metal SSBs, comprehensive strategies (e.g., host electrode and interface engineering) are also required.

4. Summary and Outlook

Potassium (K) metal has been identified as a promising anode material for next-generation batteries due to its high theoretical specific capacity, low cost, and abundant availability. However, similar to Li and Na, K metal anodes suffer from their high reactivity, unstable SEI, and dendrite growth as well as safety concerns. In this review, we have organized strategies for dendrite suppression into two categories: direct modification of the electrodes and indirect approaches that involve engineering other components surrounding the electrodes. Despite significant advancements, there is still a substantial gap to uptake of PMBs for commercial uses. For the successful employment of K metal anodes, a couple of aspects require further exploration.

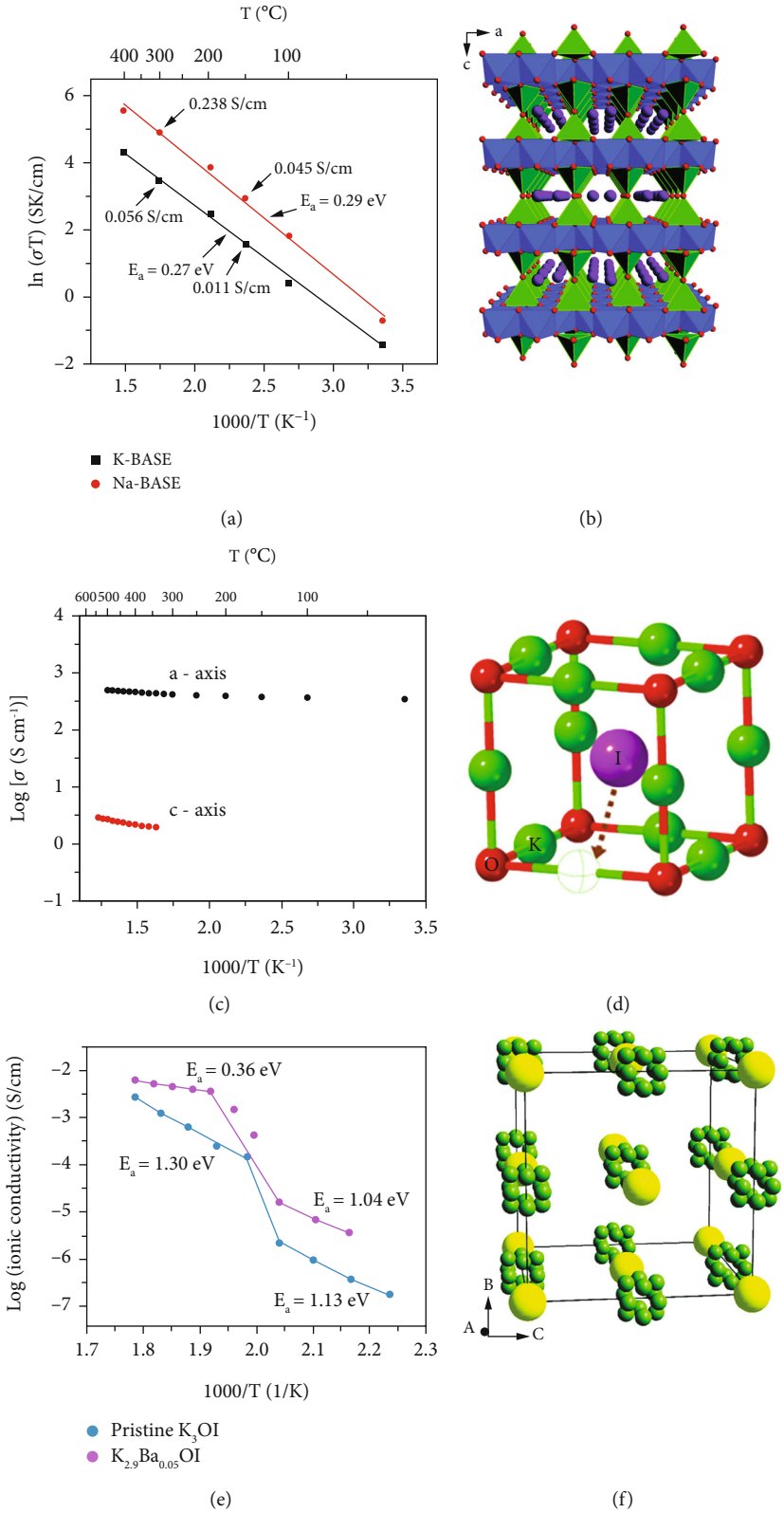

Figure 17: Continued.

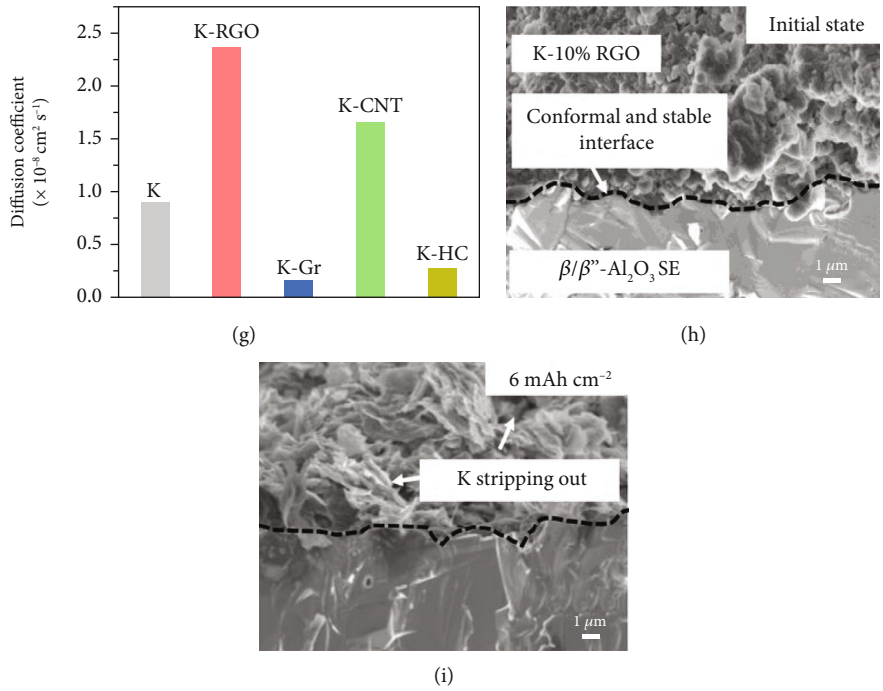

Figure 17: (a) Arrhenius conductivity plot of K- and Na-beta alumina SSEs, reproduced with permission [270]. Copyright 2015, Wiley. (b) 3D open framework structure and intersection of $K_2Fe_4O_7$ (O, red; K, purple; FeO_6, blue; and FeO_4, green). (c) Arrhenius plot of ionic conductivity of $K_2Fe_4O_7$ along the *a*- and *c*-axes, reproduced with permission [256]. Copyright 2015, Royal Society of Chemistry. (d) Structure of K_3OI antiperovskite and the phase transition forming I-O disordered site (O, red; I, purple; and K, green). (e) Arrhenius plots of conductivity of K_3OI and $K_{2.9}Ba_{0.05}OI$, reproduced with permission [258]. Copyright 2021, American Chemical Society. (f) The cubic crystal structure of KB_3H_8 after the polymorphic transition, reproduced with permission [259]. Copyright 2019, Royal Society of Chemistry. (g) Comparison of K self-diffusion coefficient in K metal and various carbon allotropes. SEM images of K-10%RGO/K-β''-alumina interface at different states, (h) initial and (i) after 6 mAh cm^{-2} stripping of K, reproduced with permission [245]. Copyright 2023, Wiley.

4.1. Unveiling Potassium Deposition Mechanism. It is essential for achieving stability of K metal electrodes to investigate the underlying mechanisms of K deposition and its subsequent electrochemical decay. In the case of the Li metal, several models have been proposed to explain the dendrite growth mechanism (e.g., space-charge model and film growth model) [70]. These models have been adopted to illustrate the K dendrite growth behavior as the K metal belongs to the alkali metal group. However, this leaves open the question: whether the models established for Li dendrite growth are applicable to K dendrites. As discussed earlier (Table 1), the dissimilarities in physical, mechanical, and chemical features result in variations in electrochemical properties such as the stability of the SEI layer, ion kinetics, and ion nucleation behaviors. These different features definitely influence the deposition behavior and the mechanism of dendrite growth. For instance, the K metal might show a tendency for the deposition of smoother surfaces compared to Li under high current density conditions due to the lower surface diffusion barrier of the K metal [78, 80]. This may indicate that the K metal follows the pathway away from the Li deposition models. Therefore, the theory for illustrating K metal deposition is required, considering the inherent characteristics of K.

To landscape the K deposition behavior, including the dendrite growth mode and SEI formation, advanced characterization (e.g., *operando* techniques) would be helpful [279, 280]. For instance, in situ AFM or in situ TEM would allow the elucidation of surface morphology on the K metal electrode as well as K dendrite growth [281]. Indeed in Li metal anodes, researchers have investigated Li dendrite growth in real time using the peak-force-tapping mode of AFM under inert gas and have suggested a particle growth model [282]. Also, in situ TEM could be utilized to elucidate the morphology development of the K metal surface further in detail. In Li metal anodes, those advanced techniques helped to visually show that Li grows in a shape of fiber-like, including branch-like, rather than mossy and film-like structure [283]. However, in K metal anodes, real-time observation of K growth, including the early stage of K growth, has not been reported yet. That might be due to the difficulty of the K metal's low threshold to electron beam coming from the low bonding energy of the K metal [67]. Thus, the surface of K metal anodes should be characterized under a highly regulated environment such as ultralow temperature (e.g., cryo-TEM and cryo-EM). For instance, cryo-TEM is benign when handling a sensitive material such as alkali metals and was utilized to reveal that there are two dendrite types coexisting on the Li electrode [280, 284]. Considering that the K growth mode is likely to be more complicated, it would be helpful for developing a stable K anode to thoroughly investigate the entire K growth process using

Table 9: Analytical techniques to characterize K metal anodes.

Technique	Information provided	Scan condition	Capability	Ref.
SEM	Morphology	Ex situ	High-resolution investigation of structure and morphology of K metal anode	[71, 75, 126, 295]
TEM	Morphology Composition	Ex situ	Examine structure and thin SEI layer on K metal anode. Provide local elemental distribution and bonding environment with energy-dispersive spectroscopy (EDS)	[37, 151, 177]
AFM	Morphology	Ex situ	Provide a 3D surface profile of K metal anode with mechanical properties of SEI layer	[66, 99, 180, 192]
XRD	Composition	Ex situ and in situ	Provide the crystal structure and chemical composition of bulk SEI layers on K metal anode	[72, 106, 144, 154]
XPS	Composition	Ex situ	Analyze surface chemistry and provide chemical bond level and electronic state information of SEI layer	[15, 82, 127, 293]
Optical imaging	Morphology	In situ	Provide a direct imaging of structural evolution of the surface of K metal anode	[73, 74, 158]
Cryo-TEM	Morphology Composition	Ex situ	Provide high-resolution imaging, while preserving the initial structure and morphology of K metal anode at extremely low temperatures	[57, 217]
X-ray tomography	Morphology	Ex situ	Visualize a 3D morphology of the electrodeposited K metal anode	[297]
ToF-SIMS	Composition	Ex situ	Analyze the quantitative elemental composition and distribution of a SEI layer on K metal anode	[183, 208, 245]
^{1}H-NMR	Composition	Ex situ	Probe the local structure and electronic structure of the surface of K metal anode	[203]
FTIR	Composition	Ex situ	Detect the chemical composition or changes at the electrolyte/electrode interfaces	[239]

advanced characterization techniques. And the recent characterization techniques for the K metal anode are summarized in Table 9 through selected examples. This might be a useful reference point for further exploration of the K metal anode.

4.2. Host Design. In recent potassiophilic host designs, carbon materials or Cu current collectors have been tailored with heterogeneous materials. In the fabrication process of those hosts, harmful and expensive precursors are often employed. In addition, certain hosts necessitate a prolonged synthesis period. For instance, cobalt is doped on the host structure to increase potassiophilicity [125, 126]. Recently, the price of cobalt has experienced a significant increase due to its geographically concentrated reserves and the growing demand as a cathode material [7]. Moreover, $CoCl_2$, which is one of the representative Co precursors, can cause cancer [285]. Therefore, cost efficiency, environmental friendliness, and facileness are desired for the mass production of the K metal host.

The 3D potassiophilic hosts usually exhibit a porous structure, which can provide sufficient space for K accommodation. Porous structures also play a beneficial role in withstanding volume fluctuations of K electrodes, which appear to be more severe due to a higher volume per mole compared to those of Li and Na metals [12]. However, if the pore volume is too large, this presumably leads to inferior battery performance. For instance, the highly porous structure could seriously collapse due to poor stiffness of the host and fatigue by the large volume change of the K metal. Further research is necessary to elucidate the correlation between the mechanical stability of hosts and their electrochemical behavior, considering a range of pore structures. Meanwhile, it may be important to find an optimal surface area of a host with the consideration of the required electrolyte amount. The porous structure typically presents a large surface area. The large surface increases the contact area between the electrode and electrolyte and thus requires a large amount of electrolyte decomposition. This excessive consumption of electrolytes presumably drives the exhaustion of liquid electrolytes, leading to a rapid rise in cell impedance for K ion diffusion. Indeed, cell failure is often observed via electrolyte exhaustion [140].

4.3. Separators. Empirically, GF has been preferentially used for K-based batteries as a separator rather than PE/PP. However, the question, which one is more effective among GF and PE/PP, still remains. The reason to employ GF is its ability to prevent dendrite penetration and its excellent wettability to the electrolyte. When the PE/PP separator is used for K metal batteries, batteries could readily face short circuit even at initial cycles [66]. This is presumably due to granular

morphologies of K deposits ranging in size from nanometers to micrometers which easily pass through the nanopores of PE/PP [66]. Hence, it seems that a thicker GF separator has been employed for the K metal electrode. Moreover, compared to Li-ion electrolytes, K ones typically possess a high viscosity, and GF, which has a large pore, is forced for K batteries [286–288]. Considering these characteristics of a separator, the required research can be summarized as follows: (i) reducing the viscosity of K ion electrolytes, (ii) achieving a small pore size with high permeability to electrolytes, and (iii) designing a thin and impenetrable separator.

4.4. Electrolyte Engineering. Electrolyte optimization has been regarded as a viable solution to tackle the interfacial challenges of PMBs. This is a relatively simple approach that does not require any modifications of the existing battery components and could be easily implemented. In a cell operation, one of the electrolytes' primary roles is to form a passivation layer on the metal surface. To form a stable SEI layer, the use of additives would be an effective way. Indeed, commercial LIBs also often employ electrolytes with additives (e.g., $LiPF_6$ – EC/DEC + FEC) [289]. However, only a few studies, mostly showing a negative effect on K metal anodes, have been reported, and the exact reason for their failure remains unresolved. The primary reason may be the different contributions of additives to the formation of the SEI structure on the K metal. Therefore, it is important to establish the mechanism of SEI formation based on the chemical composition of additives, using in situ advanced techniques discussed earlier.

Meanwhile, research on achieving stable battery operation in a wide range of temperatures has progressed. LMBs also worked at a high temperature of 100°C by inducing strong coordination in the solvated structure of electrolytes [84]. Furthermore, the operation of LMBs at an extremely low temperature of -60°C has been reported by tailoring the SEI structure [290]. By comparison, the electrochemical performances of PMBs are generally evaluated under room temperatures and laboratory conditions. This may be due to the high chemical reactivity of the K metal, limiting commercialization. If the SEI layer maintains chemical stability across a broad temperature range, though the K metal is highly reactive, it would enable PMBs to be cycled in a wide range of temperatures. Therefore, it is necessary to design the SEI layer to be stable even over a wide temperature range.

It is important to pay attention to the safety considerations for PMBs, which significantly rely on electrolyte systems. In this regard, the design of electrolytes possessing nonflammable characteristics with a substantial wide operational temperature range would be useful. LMBs also worked at a high temperature of 100°C by inducing strong coordination in the solvated structure of electrolytes [84]. Furthermore, the operation of LMBs at an extremely low temperature of -60°C has been reported by tailoring the SEI structure [290].

The suitable electrolyte also stabilizes the cathode materials at a high voltage. However, research on the compatibility between K ion electrolytes and cathode materials is still in the initial state. Additionally, there is a lack of understanding regarding the formation of the cathode electrolyte interphase (CEI), and its association with the performance of full-cell PMBs remains unexplored. To fill this gap, the K ion electrolytes for advanced PMBs may be an important research direction in the future.

4.5. Solid-State Electrolytes. Besides high ionic conductivity, other properties such as mechanical strength and a wide electrochemical window should be the first criteria in the development of a new SSE. (i) The K metal experiences large volume fluctuations during the plating/stripping process. These volume changes could impose stress/strain evolution on SSEs, probably bringing cracks and fractures to SSEs. Due to the softness of the K metal, the K metal is more prone to show that the K dendrite grows by filling microcracks in SSEs and eventually causes a short circuit. Despite the softness of the K metal, the SSEs for the K metal should exhibit high yield strength and strain. (ii) Electrochemical stability is another important property. The voltage window is the range in which SSEs retain their chemical/physical structure without oxidation/reduction. Once the voltage exceeds this window, the material initiates the insertion and extraction of K ions. In other words, the SSEs can be reduced at the anode side by metal with the uptake of K ions. It is noted that the K metal may act as a strong reducing agent toward SSEs due to its hyperreactivity [70].

All in all, the commercialization of PMBs seems to be far away. However, PMBs are gaining more attention as an alternative to LMBs due to potassium's low cost and low redox potential [38]. PMBs, for instance, can be developed as a low-cost and large-scale energy storage such as an energy storage system (ESS). That is, the K metal-based ESS can contribute to the stabilization of the electrical grid and thus smooth out fluctuations in supply and demand, reducing the likelihood of the blackout. Furthermore, large-scale PMBs can be installed on a vessel and provide a sustainable energy originating from solar energy, presumably reducing the dependence on diesel power generators. It is noteworthy that the flowability of the K-Na alloy makes it suitable for applications in stretchable and flexible energy storage systems, which can be utilized in wearable devices, flexible displays, etc. Thus, considerable endeavors should be devoted to fundamental research, material design, and comprehensive strategies for the suppression of dendrites to realize the practical application of PMBs. Table 2 presents a selected electrochemical performance of state-of-the-art PMBs. This could serve as a valuable reference for further investigations into PMBs. We hope that this review of current research on PMBs provides fruitful insights and thus contributes to the progress of PMB technology.

Data Availability

The data are available on request from the authors.

Conflicts of Interest

The authors declare that they have no known competing financial interests or personal relationships that could have appeared to influence the work reported in this paper.

Authors' Contributions

Seunghwi Baek, Taeksoo Jung, and Sunghyun Jie were responsible for the design concept of this article and writing its draft. Myeongjin Kim provided supervision and critical review and wrote and edited the draft. Byeongyong Lee provided supervision and critical review and wrote and edited the draft.

Acknowledgments

This research was supported by the Basic Science Research Program through the National Research Foundation of Korea (NRF) funded by the Ministry of Science, ICT & Future Planning (2021R1C1C1004570). This work was partly supported by the Korea Institute of Energy Technology Evaluation and Planning (KETEP) grant funded by the Korea government (MOTIE) (20214000000140, Graduate School of Convergence for Clean Energy Integrated Power Generation).

References

[1] M. Armand and J. M. Tarascon, "Building better batteries," *Nature*, vol. 451, no. 7179, pp. 652–657, 2008.

[2] R. Kaur, V. A. Chhabra, V. Chaudhary et al., "Metal-organic frameworks and their derivatives as anode material in lithium-ion batteries: recent advances towards novel configurations," *International Journal of Energy Research*, vol. 46, no. 10, 13204 pages, 2022.

[3] Y. Li, Y. X. Lu, P. Adelhelm, M. M. Titirici, and Y. S. Hu, "Intercalation chemistry of graphite: alkali metal ions and beyond," *Chemical Society Reviews*, vol. 48, no. 17, pp. 4655–4687, 2019.

[4] J. Qian, W. A. Henderson, W. Xu et al., "High rate and stable cycling of lithium metal anode," *Nature Communications*, vol. 6, no. 1, p. 6362, 2015.

[5] J. Park, J. Lee, M. H. Alfaruqi, W.-J. Kwak, J. Kim, and J.-Y. Hwang, "Initial investigation and evaluation of potassium metal as an anode for rechargeable potassium batteries," *Journal of Materials Chemistry A*, vol. 8, no. 33, pp. 16718–16737, 2020.

[6] B. Lee, E. Paek, D. Mitlin, and S. W. Lee, "Sodium metal anodes: emerging solutions to dendrite growth," *Chemical Reviews*, vol. 119, no. 8, pp. 5416–5460, 2019.

[7] R. Schmuch, R. Wagner, G. Hörpel, T. Placke, and M. Winter, "Performance and cost of materials for lithium-based rechargeable automotive batteries," *Nature Energy*, vol. 3, no. 4, pp. 267–278, 2018.

[8] M. Kim, G. D. Park, and Y. C. Kang, "Investigation of the potassium-ion storage mechanism of nickel selenide materials and rational design of nickel selenide-C yolk-shell structure for enhancing electrochemical properties," *International Journal of Energy Research*, vol. 46, no. 5, 5810 pages, 2021.

[9] Y.-S. Hu and Y. Li, "Unlocking sustainable Na-ion batteries into industry," *ACS Energy Letters*, vol. 6, no. 11, pp. 4115–4117, 2021.

[10] K. M. Abraham, "How comparable are sodium-ion batteries to lithium-ion counterparts?," *ACS Energy Letters*, vol. 5, no. 11, pp. 3544–3547, 2020.

[11] S. Dhir, S. Wheeler, I. Capone, and M. Pasta, "Outlook on K-ion batteries," *Chem*, vol. 6, no. 10, pp. 2442–2460, 2020.

[12] C. Wei, Y. Tao, H. Fei et al., "Recent advances and perspectives in stable and dendrite-free potassium metal anodes," *Energy Storage Materials*, vol. 30, pp. 206–227, 2020.

[13] C. Grosjean, P. H. Miranda, M. Perrin, and P. Poggi, "Assessment of world lithium resources and consequences of their geographic distribution on the expected development of the electric vehicle industry," *Renewable and Sustainable Energy Reviews*, vol. 16, no. 3, pp. 1735–1744, 2012.

[14] S. Liu, S. Tang, X. Zhang, A. Wang, Q. H. Yang, and J. Luo, "Porous Al current collector for dendrite-free Na metal anodes," *Nano Letters*, vol. 17, no. 9, pp. 5862–5868, 2017.

[15] P. Liu, Y. Wang, H. Hao et al., "Stable potassium metal anodes with an all-aluminum current collector through improved electrolyte wetting," *Advanced Materials*, vol. 32, no. 49, article e2002908, 2020.

[16] Z. Jian, W. Luo, and X. Ji, "Carbon electrodes for K-ion batteries," *Journal of the American Chemical Society*, vol. 137, no. 36, pp. 11566–11569, 2015.

[17] H. Moriwake, A. Kuwabara, C. A. J. Fisher, and Y. Ikuhara, "Why is sodium-intercalated graphite unstable?," *RSC Advances*, vol. 7, no. 58, pp. 36550–36554, 2017.

[18] J. Zhao, X. Zou, Y. Zhu, Y. Xu, and C. Wang, "Electrochemical intercalation of potassium into graphite," *Advanced Functional Materials*, vol. 26, no. 44, pp. 8103–8110, 2016.

[19] S. He, S. Huang, S. Wang, I. Mizota, X. Liu, and X. Hou, "Considering critical factors of silicon/graphite anode materials for practical high-energy lithium-ion battery applications," *Energy & Fuels*, vol. 35, no. 2, pp. 944–964, 2021.

[20] M. N. Obrovac and V. L. Chevrier, "Alloy negative electrodes for Li-ion batteries," *Chemical Reviews*, vol. 114, no. 23, pp. 11444–11502, 2014.

[21] M. Sha, L. Liu, H. P. Zhao, and Y. Lei, "Anode materials for potassium-ion batteries: current status and prospects," *Carbon Energy*, vol. 2, no. 3, pp. 350–369, 2020.

[22] X. Min, J. Xiao, M. Fang et al., "Potassium-ion batteries: outlook on present and future technologies," *Energy & Environmental Science*, vol. 14, no. 4, pp. 2186–2243, 2021.

[23] K. Kubota, M. Dahbi, T. Hosaka, S. Kumakura, and S. Komaba, "Towards K-ion and Na-ion batteries as "beyond Li-ion"," *The Chemical Record*, vol. 18, no. 4, pp. 459–479, 2018.

[24] S. Komaba, T. Hasegawa, M. Dahbi, and K. Kubota, "Potassium intercalation into graphite to realize high-voltage/high-power potassium-ion batteries and potassium-ion capacitors," *Electrochemistry Communications*, vol. 60, pp. 172–175, 2015.

[25] T. A. Pham, K. E. Kweon, A. Samanta, V. Lordi, and J. E. Pask, "Solvation and dynamics of sodium and potassium in ethylene carbonate from ab initio molecular dynamics simulations," *The Journal of Physical Chemistry C*, vol. 121, no. 40, pp. 21913–21920, 2017.

[26] M. Okoshi, Y. Yamada, S. Komaba, A. Yamada, and H. Nakai, "Theoretical analysis of interactions between potassium ions and organic electrolyte solvents: a comparison with lithium, sodium, and magnesium ions," *Journal of the Electrochemical Society*, vol. 164, no. 2, pp. A54–A60, 2017.

[27] Y. Li, Y. Yang, Y. Lu et al., "Ultralow-concentration electrolyte for Na-ion batteries," *ACS Energy Letters*, vol. 5, no. 4, pp. 1156–1158, 2020.

[28] Y. Li, L. Zhou, F. Xie et al., *Ester- and Ether-Based Electrolytes for Na-Ion Batteries*, Wiley, 2022.

[29] "Lithium-ion batteries need to be greener and more ethical," *Nature*, vol. 595, no. 7865, p. 7, 2021.

[30] L. Leyssens, B. Vinck, C. Van Der Straeten, F. Wuyts, and L. Maes, "Cobalt toxicity in humans–a review of the potential sources and systemic health effects," *Toxicology*, vol. 387, pp. 43–56, 2017.

[31] N. Xiao, J. Zheng, G. Gourdin, L. Schkeryantz, and Y. Wu, "Anchoring an artificial protective layer to stabilize potassium metal anode in rechargeable K–O_2 batteries," *ACS Applied Materials & Interfaces*, vol. 11, no. 18, pp. 16571–16577, 2019.

[32] X. Y. Zhao, Y. Lu, Z. F. Qian, R. H. Wang, and Z. P. Guo, "Potassium-sulfur batteries: status and perspectives," *EcoMat*, vol. 2, no. 3, article e12038, 2020.

[33] N. Xiao, X. Ren, W. D. McCulloch, G. Gourdin, and Y. Wu, "Potassium superoxide: a unique alternative for metal-air batteries," *Accounts of Chemical Research*, vol. 51, no. 9, pp. 2335–2343, 2018.

[34] X. Ren and Y. Wu, "A low-overpotential potassium-oxygen battery based on potassium superoxide," *Journal of the American Chemical Society*, vol. 135, no. 8, pp. 2923–2926, 2013.

[35] Q. Zhao, Y. Hu, K. Zhang, and J. Chen, "Potassium-sulfur batteries: a new member of room-temperature rechargeable metal-sulfur batteries," *Inorganic Chemistry*, vol. 53, no. 17, pp. 9000–9005, 2014.

[36] N. Nitta, F. Wu, J. T. Lee, and G. Yushin, "Li-ion battery materials: present and future," *Materials Today*, vol. 18, no. 5, pp. 252–264, 2015.

[37] L. Zhang, X. Xia, Y. Zhong et al., "Exploring self-healing liquid Na-K alloy for dendrite-free electrochemical energy storage," *Advanced Materials*, vol. 30, no. 46, article 1804011, 2018.

[38] P. Liu and D. Mitlin, "Emerging potassium metal anodes: perspectives on control of the electrochemical interfaces," *Accounts of Chemical Research*, vol. 53, no. 6, pp. 1161–1175, 2020.

[39] W. Liu, P. Liu, and D. Mitlin, "Review of emerging concepts in SEI analysis and artificial SEI membranes for lithium, sodium, and potassium metal battery anodes," *Advanced Energy Materials*, vol. 10, no. 43, article 2002297, 2020.

[40] J. Xie, X. Li, H. Lai et al., "A robust solid electrolyte interphase layer augments the ion storage capacity of bimetallic-sulfide-containing potassium-ion batteries," *Angewandte Chemie*, vol. 131, no. 41, pp. 14882–14889, 2019.

[41] H. Wang, D. Yu, C. Kuang et al., "Alkali metal anodes for rechargeable batteries," *Chem*, vol. 5, no. 2, pp. 313–338, 2019.

[42] Y. Cheng, X. Yang, M. Li et al., "Enabling ultrastable alkali metal anodes by artificial solid electrolyte interphase fluorination," *Nano Letters*, vol. 22, no. 11, pp. 4347–4353, 2022.

[43] Y. Gu, W. W. Wang, Y. J. Li et al., "Designable ultra-smooth ultra-thin solid-electrolyte interphases of three alkali metal anodes," *Nature Communications*, vol. 9, no. 1, p. 1339, 2018.

[44] J. Popovic, "Review—recent advances in understanding potassium metal anodes," *Journal of The Electrochemical Society*, vol. 169, no. 3, article 030510, 2022.

[45] A. Dey, "Electrochemical alloying of lithium in organic electrolytes," *Journal of The Electrochemical Society*, vol. 118, no. 10, p. 1547, 1971.

[46] E. Peled, "Film forming reaction at the lithium/electrolyte interface," *Journal of Power Sources*, vol. 9, no. 3, pp. 253–266, 1983.

[47] J. B. Goodenough and Y. Kim, "Challenges for rechargeable Li batteries," *Chemistry of Materials*, vol. 22, no. 3, pp. 587–603, 2010.

[48] E. Peled and S. Menkin, "Review—SEI: past, present and future," *Journal of The Electrochemical Society*, vol. 164, no. 7, pp. A1703–A1719, 2017.

[49] A. Yoshino, "The birth of the lithium-ion battery," *Angewandte Chemie International Edition*, vol. 51, no. 24, pp. 5798–5800, 2012.

[50] D. Lin, Y. Liu, and Y. Cui, "Reviving the lithium metal anode for high-energy batteries," *Nature Nanotechnology*, vol. 12, no. 3, pp. 194–206, 2017.

[51] S. S. Zhang, "Problem, status, and possible solutions for lithium metal anode of rechargeable batteries," *ACS Applied Energy Materials*, vol. 1, no. 3, pp. 910–920, 2018.

[52] S. Chen, F. Dai, and M. Cai, "Opportunities and challenges of high-energy lithium metal batteries for electric vehicle applications," *ACS Energy Letters*, vol. 5, no. 10, pp. 3140–3151, 2020.

[53] B. Scrosati, J. Hassoun, and Y.-K. Sun, "Lithium-ion batteries. A look into the future," *Energy & Environmental Science*, vol. 4, no. 9, pp. 3287–3295, 2011.

[54] F. Hao, A. Verma, and P. P. Mukherjee, "Mechanistic insight into dendrite–SEI interactions for lithium metal electrodes," *Journal of Materials Chemistry A*, vol. 6, no. 40, pp. 19664–19671, 2018.

[55] Y.-S. Hong, N. Li, H. Chen, P. Wang, W.-L. Song, and D. Fang, "In operando observation of chemical and mechanical stability of Li and Na dendrites under quasi-zero electrochemical field," *Energy Storage Materials*, vol. 11, pp. 118–126, 2018.

[56] J. H. Cho, X. Xiao, K. Guo, Y. Liu, H. Gao, and B. W. Sheldon, "Stress evolution in lithium metal electrodes," *Energy Storage Materials*, vol. 24, pp. 281–290, 2020.

[57] Q. Zhang, B. Han, Y. Zou et al., "Enabling atomic-scale imaging of sensitive potassium metal and related solid electrolyte interphases using lltralow-dose cryo-TEM," *Advanced Materials*, vol. 33, no. 43, article e2102666, 2021.

[58] E. Peled, D. Golodnitsky, and G. Ardel, "Advanced model for solid electrolyte interphase electrodes in liquid and polymer electrolytes," *Journal of The Electrochemical Society*, vol. 144, no. 8, p. L208, 1997.

[59] M. Moshkovich, Y. Gofer, and D. Aurbach, "Investigation of the electrochemical windows of aprotic alkali metal (Li, Na, K) salt solutions," *Journal of The Electrochemical Society*, vol. 148, no. 4, p. E155, 2001.

[60] H. Wang, D. Zhai, and F. Kang, "Solid electrolyte interphase (SEI) in potassium ion batteries," *Energy & Environmental Science*, vol. 13, no. 12, pp. 4583–4608, 2020.

[61] T. Hosaka, K. Kubota, A. S. Hameed, and S. Komaba, "Research development on K-ion batteries," *Chemical Reviews*, vol. 120, no. 14, pp. 6358–6466, 2020.

[62] N. Yabuuchi, K. Kubota, M. Dahbi, and S. Komaba, "Research development on sodium-ion batteries," *Chemical Reviews*, vol. 114, no. 23, pp. 11636–11682, 2014.

[63] X. Chen, H. R. Li, X. Shen, and Q. Zhang, "The origin of the reduced reductive stability of ion-solvent complexes on alkali

and alkaline earth metal anodes," *Angewandte Chemie International Edition*, vol. 57, no. 51, pp. 16643–16647, 2018.

[64] A. Bouibes, N. Sakaki, and M. Nagaoka, "Microscopic analysis of the mechanical stability of an SEI layer structure depending on the FEC additive concentration in Na-ion batteries: maximum appearance in Vickers hardness at lower FEC concentrations," *ACS Omega*, vol. 8, no. 19, pp. 16570–16578, 2023.

[65] Y. Gao, X. Du, Z. Hou et al., "Unraveling the mechanical origin of stable solid electrolyte interphase," *Joule*, vol. 5, no. 7, pp. 1860–1872, 2021.

[66] J. Hu, H. Wang, S. Wang et al., "Electrochemical deposition mechanism of sodium and potassium," *Energy Storage Materials*, vol. 36, pp. 91–98, 2021.

[67] Z. Wei, A. Wang, X. Guan et al., "Processable potassium metal anode for stable batteries," *Energy & Environmental Materials*, vol. 5, no. 4, pp. 1278–1284, 2022.

[68] L. Ni, M. Osenberg, H. Liu et al., "In situ visualizing the interplay between the separator and potassium dendrite growth by synchrotron X-ray tomography," *Nano Energy*, vol. 83, article 105841, 2021.

[69] W. Zhang, W. K. Pang, V. Sencadas, and Z. Guo, "Understanding high-energy-density Sn_4P_3 anodes for potassium-ion batteries," *Joule*, vol. 2, no. 8, pp. 1534–1547, 2018.

[70] H. Liu, X.-B. Cheng, Z. Jin et al., "Recent advances in understanding dendrite growth on alkali metal anodes," *EnergyChem*, vol. 1, no. 1, article 100003, 2019.

[71] J. Meng, H. Zhu, Z. Xiao et al., "Amine-wetting-enabled dendrite-free potassium metal anode," *ACS Nano*, vol. 16, no. 5, pp. 7291–7300, 2022.

[72] X. Tang, D. Zhou, P. Li et al., "MXene-based dendrite-free potassium metal batteries," *Advanced Materials*, vol. 32, no. 4, article e1906739, 2020.

[73] Y. Li, L. Zhang, S. Liu et al., "Original growth mechanism for ultra-stable dendrite-free potassium metal electrode," *Nano Energy*, vol. 62, pp. 367–375, 2019.

[74] B. Ma, P. Sittisomwong, J. Ma, and P. Bai, "Effects of interfacial solvation structures on the morphological stability of potassium metal anodes revealed by operando diagnosis," *ACS Applied Energy Materials*, vol. 5, no. 6, pp. 7124–7133, 2022.

[75] P. Liu, Y. Wang, Q. Gu, J. Nanda, J. Watt, and D. Mitlin, "Dendrite-free potassium metal anodes in a carbonate electrolyte," *Advanced Materials*, vol. 32, no. 7, article e1906735, 2020.

[76] Y. Zhao, B. Liu, Y. Yi et al., "An anode-free potassium-metal battery enabled by a directly grown graphene-modulated aluminum current collector," *Advanced Materials*, vol. 34, no. 29, article e2202902, 2022.

[77] D. Wang, W. Zhang, W. Zheng, X. Cui, T. Rojo, and Q. Zhang, "Towards high-safe lithium metal anodes: suppressing lithium dendrites via tuning surface energy," *Advanced Science*, vol. 4, no. 1, article 1600168, 2017.

[78] P. Hundekar, S. Basu, X. Fan et al., "In situ healing of dendrites in a potassium metal battery," *Proceedings of the National Academy of Sciences*, vol. 117, no. 11, pp. 5588–5594, 2020.

[79] P. Hundekar, S. Basu, J. Pan et al., "Exploiting self-heat in a lithium metal battery for dendrite healing," *Energy Storage Materials*, vol. 20, pp. 291–298, 2019.

[80] Y. Li, L. Zhang, J. Zhang et al., "Self-healing properties of alkali metals under "high-energy conditions" in batteries," *Advanced Energy Materials*, vol. 11, no. 21, article 2100470, 2021.

[81] P. Bai, J. Guo, M. Wang et al., "Interactions between lithium growths and nanoporous ceramic separators," *Joule*, vol. 2, no. 11, pp. 2434–2449, 2018.

[82] J. Xie, Y. Ji, L. Ma et al., "Bifunctional alloy/solid-electrolyte interphase layer for enhanced potassium metal batteries via prepassivation," *ACS Nano*, vol. 17, no. 2, pp. 1511–1521, 2023.

[83] J. Zhu, M. Yanilmaz, K. Fu et al., "Understanding glass fiber membrane used as a novel separator for lithium-sulfur batteries," *Journal of Membrane Science*, vol. 504, pp. 89–96, 2016.

[84] T. Chen, Z. Jin, Y. Liu et al., "Stable high-temperature lithium-metal batteries enabled by strong multiple ion-dipole interactions," *Angewandte Chemie International Edition*, vol. 61, no. 35, article e202207645, 2022.

[85] N. Mei, X. Xu, and R. Li, "Heat dissipation analysis on the liquid cooling system coupled with a flat heat pipe of a lithium-ion battery," *ACS Omega*, vol. 5, no. 28, pp. 17431–17441, 2020.

[86] X. Chen, X. Shen, B. Li et al., "Ion-solvent complexes promote gas evolution from electrolytes on a sodium metal anode," *Angewandte Chemie International Edition*, vol. 57, no. 3, pp. 734–737, 2018.

[87] X. Chen, T.-Z. Hou, B. Li et al., "Towards stable lithium-sulfur batteries: mechanistic insights into electrolyte decomposition on lithium metal anode," *Energy Storage Materials*, vol. 8, pp. 194–201, 2017.

[88] U. Mattinen, M. Klett, G. Lindbergh, and R. Wreland Lindström, "Gas evolution in commercial Li-ion battery cells measured by on-line mass spectrometry – effects of C-rate and cell voltage," *Journal of Power Sources*, vol. 477, article 228968, 2020.

[89] M. Onuki, S. Kinoshita, Y. Sakata et al., "Identification of the source of evolved gas in Li-ion batteries using ^{13}C-labeled solvents," *Journal of the Electrochemical Society*, vol. 155, no. 11, pp. A794–A797, 2008.

[90] R. Imhof and P. Novak, "In situ investigation of the electrochemical reduction of carbonate electrolyte solutions at graphite electrodes," *Journal of the Electrochemical Society*, vol. 145, no. 4, pp. 1081–1087, 1998.

[91] H. Zhao, J. Wang, H. Shao, K. Xu, and Y. Deng, "Gas generation mechanism in Li-metal batteries," *Energy & Environmental Materials*, vol. 5, no. 1, pp. 327–336, 2022.

[92] P. Liu, L. Yang, B. Xiao et al., "Revealing lithium battery gas generation for safer practical applications," *Advanced Functional Materials*, vol. 32, no. 47, article 2208586, 2022.

[93] Q. Yang, Y. Ding, and G. He, "An amalgam route to stabilize potassium metal anodes over a wide temperature range," *Chemical Communications*, vol. 56, no. 24, pp. 3512–3515, 2020.

[94] H. Yang, F. He, M. Li et al., "Design principles of sodium/potassium protection layer for high-power high-energy sodium/potassium-metal batteries in carbonate electrolytes: a case study of Na_2Te/K_2Te," *Advanced Materials*, vol. 33, no. 48, article e2106353, 2021.

[95] Y. Yi, J. Li, Z. Gao et al., "Highly potassiophilic graphdiyne skeletons decorated with Cu quantum dots enable dendrite-free potassium-metal anodes," *Advanced Materials*, vol. 34, no. 29, article e2202685, 2022.

[96] T. Hosaka, T. Fukabori, T. Matsuyama, R. Tatara, K. Kubota, and S. Komaba, "1,3,2-Dioxathiolane 2,2-dioxide as an electrolyte additive for K-metal cells," *ACS Energy Letters*, vol. 6, no. 10, pp. 3643–3649, 2021.

[97] S. Baek, S. Jie, and B. Lee, "Effects of fluoroethylene carbonate additive on potassium metal anode," *Journal of Mechanical Science and Technology*, vol. 37, pp. 3657–3665, 2023.

[98] T. Hosaka, S. Muratsubaki, K. Kubota, H. Onuma, and S. Komaba, "Potassium metal as reliable reference electrodes of nonaqueous potassium cells," *The Journal of Physical Chemistry Letters*, vol. 10, no. 12, pp. 3296–3300, 2019.

[99] R. Zhou, H. Tan, Y. Gao, Z. Hou, X. Du, and B. Zhang, "Constructing resilient solid electrolyte interphases on carbon nanofiber film for advanced potassium metal anodes," *Carbon*, vol. 186, pp. 141–149, 2022.

[100] J. Wang, W. Yan, and J. Zhang, "High area capacity and dendrite-free anode constructed by highly potassiophilic Pd/Cu current collector for low-temperature potassium metal battery," *Nano Energy*, vol. 96, article 107131, 2022.

[101] M. Zhou, W. Qi, Z. Hu et al., "Highly potassiophilic carbon nanofiber paper derived from bacterial cellulose enables ultra-stable dendrite-free potassium metal anodes," *ACS Applied Materials & Interfaces*, vol. 13, no. 15, pp. 17629–17638, 2021.

[102] L. Qin, Y. Lei, H. Wang et al., "Capillary encapsulation of metallic potassium in aligned carbon nanotubes for use as stable potassium metal anodes," *Advanced Energy Materials*, vol. 9, no. 29, article 1901427, 2019.

[103] Q. Zhang, Y. Lu, M. Zhou, J. Liang, Z. Tao, and J. Chen, "Achieving a stable Na metal anode with a 3D carbon fibre scaffold," *Inorganic Chemistry Frontiers*, vol. 5, no. 4, pp. 864–869, 2018.

[104] Q. Lu, Y. Jie, X. Meng et al., "Carbon materials for stable Li metal anodes: challenges, solutions, and outlook," *Carbon Energy*, vol. 3, no. 6, pp. 957–975, 2021.

[105] L. Wang, H. Wang, M. Cheng et al., "Metal–organic framework@polyacrylonitrile-derived potassiophilic nanoporous carbon nanofiber paper enables stable potassium metal anodes," *ACS Applied Energy Materials*, vol. 4, no. 6, pp. 6245–6252, 2021.

[106] S. Li, H. Zhu, Y. Liu et al., "Codoped porous carbon nanofibres as a potassium metal host for nonaqueous K-ion batteries," *Nature Communications*, vol. 13, no. 1, p. 4911, 2022.

[107] Z. Sun, S. Jin, H. Jin et al., "Robust expandable carbon nanotube scaffold for ultrahigh-capacity lithium-metal anodes," *Advanced Materials*, vol. 30, no. 32, article e1800884, 2018.

[108] H. Li, Y. Liu, J. Wang, W. Yan, and J. Zhang, "Robust 3D copper foam functionalized with gold nanoparticles as anode for high-performance potassium metal batteries," *Chemistry: An Asian Journal*, vol. 17, no. 15, article e202200430, 2022.

[109] P. Bai, J. Li, F. R. Brushett, and M. Z. Bazant, "Transition of lithium growth mechanisms in liquid electrolytes," *Energy & Environmental Science*, vol. 9, no. 10, pp. 3221–3229, 2016.

[110] G. Cheng, S. Liu, Y. Su et al., "Bi@hollow carbon tube enabled high performance potassium metal batteries," *Journal of Alloys and Compounds*, vol. 913, article 165329, 2022.

[111] H. Ding, Y. Feng, J. Zhou, X. Yu, L. Fan, and B. Lu, "Superstable potassium metal batteries with a controllable internal electric field," *Fundamental Research*, vol. 3, no. 5, pp. 813–821, 2023.

[112] K. Yan, Z. Lu, H.-W. Lee et al., "Selective deposition and stable encapsulation of lithium through heterogeneous seeded growth," *Nature Energy*, vol. 1, no. 3, article 16010, 2016.

[113] M. Boshir Ahmed, J. Alom, M. S. Hasan et al., "General doping chemistry of carbon materials," *ChemNanoMat*, vol. 9, no. 4, article e202200482, 2022.

[114] R. Zhang, X. R. Chen, X. Chen et al., "Lithiophilic sites in doped graphene guide uniform lithium nucleation for dendrite-free lithium metal anodes," *Angewandte Chemie International Edition*, vol. 56, no. 27, pp. 7764–7768, 2017.

[115] G. Wang, T. Liu, X. Fu, Z. Wu, M. Liu, and X. Xiong, "Lithiophilic amide-functionalized carbon nanotube skeleton for dendrite-free lithium metal anodes," *Chemical Engineering Journal*, vol. 414, article 128698, 2021.

[116] M.-g. Kim, B. Lee, M. Li et al., "All-soft supercapacitors based on liquid metal electrodes with integrated functionalized carbon nanotubes," *ACS Nano*, vol. 14, no. 5, pp. 5659–5667, 2020.

[117] A. K. Nanjundan, R. R. Gaddam, A. H. Farokh Niaei et al., "Potassium-ion storage in cellulose-derived hard carbon: the role of functional groups," *Batteries & Supercaps*, vol. 3, no. 9, pp. 953–960, 2020.

[118] Y. Xie, J. Hu, Z. Han et al., "Ultra-stable K metal anode enabled by oxygen-rich carbon cloth," *Nano Research*, vol. 13, no. 11, pp. 3137–3141, 2020.

[119] X. Chen, Y.-K. Bai, X. Shen, H.-J. Peng, and Q. Zhang, "Sodiophilicity/potassiophilicity chemistry in sodium/potassium metal anodes," *Journal of Energy Chemistry*, vol. 51, pp. 1–6, 2020.

[120] J. Xiong, M. Ye, Z. Wang et al., "Fast and homogeneous ion regulation toward a 4 V, high-rate and dendrite-free potassium metal battery," *Chemical Engineering Journal*, vol. 442, article 135927, 2022.

[121] J. Zhang, Y. Li, L. Zhu, X. Wang, and J. Tu, "Potassiophilic skeleton achieving highly stable potassium metal anode," *Chemical Engineering Journal*, vol. 449, article 137659, 2022.

[122] S. Liu, Y. Yang, Y. Qian et al., "MOF-derived potassiophilic CuO nanoparticles on carbon fiber cloth as host for stabilizing potassium metal anode," *ChemElectroChem*, vol. 9, no. 3, article e202101561, 2022.

[123] M. Lei, J. G. Wang, L. Ren et al., "Highly lithiophilic cobalt nitride nanobrush as a stable host for high-performance lithium metal anodes," *ACS Applied Materials & Interfaces*, vol. 11, no. 34, pp. 30992–30998, 2019.

[124] Y. Li, P. Xu, J. Mou et al., "Single cobalt atoms decorated N-doped carbon polyhedron enabled dendrite-free sodium metal anode," *Small Methods*, vol. 5, no. 11, article e2100833, 2021.

[125] G. Cheng, S. Liu, X. Wang et al., "CoZn nanoparticles@hollow carbon tubes enabled high-performance potassium metal batteries," *ACS Applied Materials & Interfaces*, vol. 14, no. 40, pp. 45364–45372, 2022.

[126] D. Zhang, X. Ma, L. Wu et al., "Coupling low-tortuosity carbon matrix with single-atom chemistry enables dendrite-free potassium-metal anode," *Advanced Energy Materials*, vol. 13, no. 2, article 2203277, 2022.

[127] M. Ye, J. Y. Hwang, and Y. K. Sun, "A 4 V class potassium metal battery with extremely low overpotential," *ACS Nano*, vol. 13, no. 8, pp. 9306–9314, 2019.

[128] F. Qiao, J. Meng, J. Wang et al., "Building carbon cloth-based dendrite-free potassium metal anodes for potassium metal

pouch cells," *Journal of Materials Chemistry A*, vol. 9, no. 40, pp. 23046–23054, 2021.

[129] M. Han, J. Jiang, S. Lu et al., "Moderate specific surface areas help three-dimensional frameworks achieve dendrite-free potassium-metal anodes," *ACS Applied Materials & Interfaces*, vol. 14, no. 1, pp. 900–909, 2022.

[130] X. Zhao, F. Chen, J. Liu et al., "Enhanced surface binding energy regulates uniform potassium deposition for stable potassium metal anodes," *Journal of Materials Chemistry A*, vol. 8, no. 11, pp. 5671–5678, 2020.

[131] J. Wang, J. Yuan, C. Chen et al., "Cu_3Pt alloy-functionalized Cu mesh as current collector for dendritic-free anodes of potassium metal batteries," *Nano Energy*, vol. 75, article 104914, 2020.

[132] L. Kong, M. Zhong, W. Shuang, Y. Xu, and X. H. Bu, "Electrochemically active sites inside crystalline porous materials for energy storage and conversion," *Chemical Society Reviews*, vol. 49, no. 8, pp. 2378–2407, 2020.

[133] R. Mehek, N. Iqbal, T. Noor et al., "Metal-organic framework based electrode materials for lithium-ion batteries: a review," *RSC Advances*, vol. 11, no. 47, pp. 29247–29266, 2021.

[134] X. Sang, Y. Xie, M. W. Lin et al., "Atomic defects in monolayer titanium carbide ($Ti_3C_2T_x$) MXene," *ACS Nano*, vol. 10, no. 10, pp. 9193–9200, 2016.

[135] Y. Fang, Y. Zhang, K. Zhu et al., "Lithiophilic three-dimensional porous $Ti_3C_2T_x$-rGO membrane as a stable scaffold for safe alkali metal (Li or Na) anodes," *ACS Nano*, vol. 13, no. 12, pp. 14319–14328, 2019.

[136] C. Bao, J. Wang, B. Wang et al., "3D sodiophilic Ti_3C_2 MXene@g-C_3N_4 hetero-interphase raises the stability of sodium metal anodes," *ACS Nano*, vol. 16, no. 10, pp. 17197–17209, 2022.

[137] R. Ma, Z. Chen, D. Zhao et al., "$Ti_3C_2T_x$ MXene for electrode materials of supercapacitors," *Journal of Materials Chemistry A*, vol. 9, no. 19, pp. 11501–11529, 2021.

[138] N. Lucero, D. Vilcarino, D. Datta, and M.-Q. Zhao, "The roles of MXenes in developing advanced lithium metal anodes," *Journal of Energy Chemistry*, vol. 69, pp. 132–149, 2022.

[139] H. Shi, M. Yue, C. J. Zhang et al., "3D flexible, conductive, and recyclable $Ti_3C_2T_x$ MXene-melamine foam for high-areal-capacity and long-lifetime alkali-metal anode," *ACS Nano*, vol. 14, no. 7, pp. 8678–8688, 2020.

[140] S. Wei, S. Choudhury, J. Xu, P. Nath, Z. Tu, and L. A. Archer, "Highly stable sodium batteries enabled by functional ionic polymer membranes," *Advanced Materials*, vol. 29, no. 12, article 1605512, 2017.

[141] W. Luo, J. Wan, B. Ozdemir et al., "Potassium ion batteries with graphitic materials," *Nano Letters*, vol. 15, no. 11, pp. 7671–7677, 2015.

[142] Y. Lei, S. Zhang, J. Dong et al., "Potassium-enriched graphite for use as stable hybrid anodes in high-efficiency potassium batteries," *Carbon*, vol. 201, pp. 1030–1037, 2023.

[143] K. Xiao, J.-F. Wu, H. Yan et al., "Intercalation-deposition mechanism induced by aligned carbon fiber toward dendrite-free metallic potassium batteries," *Energy Storage Materials*, vol. 51, pp. 122–129, 2022.

[144] J. Zhang, Y. Li, L. Zhu, X. Wang, and J. Tu, "An intercalation compound for high-safe K metal batteries," *Energy Storage Materials*, vol. 41, pp. 606–613, 2021.

[145] X. Shen, Y. Li, T. Qian et al., "Lithium anode stable in air for low-cost fabrication of a dendrite-free lithium battery," *Nature Communications*, vol. 10, no. 1, p. 900, 2019.

[146] J. Zhao, G. Zhou, K. Yan et al., "Air-stable and freestanding lithium alloy/graphene foil as an alternative to lithium metal anodes," *Nature Nanotechnology*, vol. 12, no. 10, pp. 993–999, 2017.

[147] Y. Li, Q. Liu, S. Wu et al., "Unraveling the reaction mystery of Li and Na with dry air," *Journal of the American Chemical Society*, vol. 145, no. 19, pp. 10576–10583, 2023.

[148] L. Xue, W. Zhou, S. Xin et al., "Room-temperature liquid Na-K anode membranes," *Angewandte Chemie International Edition*, vol. 57, no. 43, pp. 14184–14187, 2018.

[149] L. Zhang, S. Peng, Y. Ding et al., "A graphite intercalation compound associated with liquid Na–K towards ultra-stable and high-capacity alkali metal anodes," *Energy & Environmental Science*, vol. 12, no. 6, pp. 1989–1998, 2019.

[150] X. Xu, D. Zhou, X. Qin et al., "A room-temperature sodium-sulfur battery with high capacity and stable cycling performance," *Nature Communications*, vol. 9, no. 1, p. 3870, 2018.

[151] L. Zhang, Y. Li, S. Zhang et al., "Non-Newtonian fluid state K–Na alloy for a stretchable energy storage device," *Small Methods*, vol. 3, no. 10, article 1900383, 2019.

[152] J. Cui, B. Jin, A. Xu, J. Li, and M. Shao, "Single-atom metallophilic sites for liquid NaK alloy confinement toward stable alkali-metal anodes," *Advanced Science*, vol. 10, no. 8, article e2206479, 2023.

[153] L. Xue, H. Gao, W. Zhou et al., "Liquid K-Na alloy anode enables dendrite-free potassium batteries," *Advanced Materials*, vol. 28, no. 43, pp. 9608–9612, 2016.

[154] Z. Tai, Y. Li, Y. Liu et al., "Novel quasi-liquid K-Na alloy as a promising dendrite-free anode for rechargeable potassium metal batteries," *Advanced Science*, vol. 8, no. 16, article e2101866, 2021.

[155] Y. Xie, J. Hu, and Z. Zhang, "A stable carbon host engineering surface defects for room-temperature liquid Na K anode," *Journal of Electroanalytical Chemistry*, vol. 856, article 113676, 2020.

[156] L. Qin, W. Yang, W. Lv et al., "Room-temperature liquid metal-based anodes for high-energy potassium-based electrochemical devices," *Chemical Communications*, vol. 54, no. 58, pp. 8032–8035, 2018.

[157] T. Luo, Q. Zhao, Y. Liu et al., "High-rate and dendrite-free liquid alloy anode for high energy potassium metal batteries," *EcoMat*, vol. 4, no. 5, article e12203, 2022.

[158] W. Yuan, T. Ding, P. Mou et al., "Semi-solid CNT@NaK anode for potassium metal battery," *Advanced Functional Materials*, vol. 33, no. 4, article 2209774, 2022.

[159] P. Zhu, D. Gastol, J. Marshall, R. Sommerville, V. Goodship, and E. Kendrick, "A review of current collectors for lithium-ion batteries," *Journal of Power Sources*, vol. 485, article 229321, 2021.

[160] X.-Y. Hu, P. Xu, S. Deng et al., "Inducing ordered Li deposition on a PANI-decorated Cu mesh for an advanced Li anode," *Journal of Materials Chemistry A*, vol. 8, no. 33, pp. 17056–17064, 2020.

[161] C. Wang, T. Chen, Y. Liu et al., "Common capacity fade mechanisms of metal foil alloy anodes with different compositions for lithium batteries," *ACS Energy Letters*, vol. 8, no. 5, pp. 2252–2258, 2023.

[162] U. S. G. Survey, *Mineral Commodity Summaries 2023*, U.S. Geological Survey, 2023.

[163] M. Li, B. Sun, Z. Ao, T. An, and G. Wang, "Atomic-scale identification of influencing factors of sodium dendrite growth on different current collectors," *Journal of Materials Chemistry A*, vol. 8, no. 20, pp. 10199–10205, 2020.

[164] P. Liu, H. Hao, H. Celio et al., "Multifunctional separator allows stable cycling of potassium metal anodes and of potassium metal batteries," *Advanced Materials*, vol. 34, no. 7, article e2105855, 2022.

[165] Y. Sun and Z. Guo, "Recent advances of bioinspired functional materials with specific wettability: from nature and beyond nature," *Nanoscale Horizons*, vol. 4, no. 1, pp. 52–76, 2019.

[166] B. Lee, M. Kim, S. Kim et al., "High capacity adsorption—dominated potassium and sodium ion storage in activated crumpled graphene," *Advanced Energy Materials*, vol. 10, no. 17, article 1903280, 2020.

[167] H. He, D. Sun, Y. Tang, H. Wang, and M. Shao, "Understanding and improving the initial coulombic efficiency of high-capacity anode materials for practical sodium ion batteries," *Energy Storage Materials*, vol. 23, pp. 233–251, 2019.

[168] R. Weber, M. Genovese, A. J. Louli et al., "Long cycle life and dendrite-free lithium morphology in anode-free lithium pouch cells enabled by a dual-salt liquid electrolyte," *Nature Energy*, vol. 4, no. 8, pp. 683–689, 2019.

[169] Y. Tian, Y. An, C. Wei et al., "Recently advances and perspectives of anode-free rechargeable batteries," *Nano Energy*, vol. 78, article 105344, 2020.

[170] J. Chen, J. Xiang, X. Chen, L. Yuan, Z. Li, and Y. Huang, "Li_2S-based anode-free full batteries with modified Cu current collector," *Energy Storage Materials*, vol. 30, pp. 179–186, 2020.

[171] Y. Li, Q. Zhou, S. Weng et al., "Interfacial engineering to achieve an energy density of over 200 Wh kg^{-1} in sodium batteries," *Nature Energy*, vol. 7, no. 6, pp. 511–519, 2022.

[172] J. Wang, Y. Zuo, M. Chen et al., "Bifunctional separator with a light-weight coating for stable anode-free potassium metal batteries," *Electrochimica Acta*, vol. 433, article 141211, 2022.

[173] S. Li, H. Zhu, C. Gu et al., "Customized electrolyte and host structures enabling high-energy-density anode-free potassium–metal batteries," *ACS Energy Letters*, vol. 8, no. 8, pp. 3467–3475, 2023.

[174] Z. Yu, Y. Cui, and Z. Bao, "Design principles of artificial solid electrolyte interphases for lithium-metal anodes," *Cell Reports Physical Science*, vol. 1, no. 7, article 100119, 2020.

[175] S. Wang, Y. Yan, D. Xiong et al., "Towards dendrite-free potassium-metal batteries: rational design of a multifunctional 3D polyvinyl alcohol-borax layer," *Angewandte Chemie International Edition*, vol. 60, no. 47, pp. 25122–25127, 2021.

[176] P. Li, T. Xu, P. Ding et al., "Highly reversible Na and K metal anodes enabled by carbon paper protection," *Energy Storage Materials*, vol. 15, pp. 8–13, 2018.

[177] H. Wang, J. Hu, J. Dong et al., "Artificial solid-electrolyte interphase enabled high-capacity and stable cycling potassium metal batteries," *Advanced Energy Materials*, vol. 9, no. 43, article 1902697, 2019.

[178] K. Hu, L. Qin, S. Zhang et al., "Building a reactive armor using S-doped graphene for protecting potassium metal anodes from oxygen crossover in K–O_2 batteries," *ACS Energy Letters*, vol. 5, no. 6, pp. 1788–1793, 2020.

[179] J. Han, X. Guo, Y. Ito et al., "Effect of chemical doping on cathodic performance of bicontinuous nanoporous graphene for Li-O_2 batteries," *Advanced Energy Materials*, vol. 6, no. 3, article 1501870, 2016.

[180] P. Shi, S. Zhang, G. Lu et al., "Red phosphorous-derived protective layers with high ionic conductivity and mechanical strength on dendrite-free sodium and potassium metal anodes," *Advanced Energy Materials*, vol. 11, no. 5, article 2003381, 2020.

[181] P. Zhai, L. Liu, X. Gu, T. Wang, and Y. Gong, "Interface engineering for lithium metal anodes in liquid electrolyte," *Advanced Energy Materials*, vol. 10, no. 34, article 2001257, 2020.

[182] G. He, Q. Li, Y. Shen, and Y. Ding, "Flexible amalgam film enables stable lithium metal anodes with high capacities," *Angewandte Chemie International Edition*, vol. 58, no. 51, pp. 18466–18470, 2019.

[183] J. Park, Y. Jeong, M. H. Alfaruqi et al., "Stable solid electrolyte interphase for long-life potassium metal batteries," *ACS Energy Letters*, vol. 7, no. 1, pp. 401–409, 2022.

[184] L. Li, S. Basu, Y. Wang et al., "Self-heating–induced healing of lithium dendrites," *Science*, vol. 359, no. 6383, pp. 1513–1516, 2018.

[185] J. Jiao, G. Lai, L. Zhao et al., "Self-healing mechanism of lithium in lithium metal," *Advanced Science*, vol. 9, no. 12, article e2105574, 2022.

[186] S. Luiso and P. Fedkiw, "Lithium-ion battery separators: recent developments and state of art," *Current Opinion in Electrochemistry*, vol. 20, pp. 99–107, 2020.

[187] H. Lee, M. Yanilmaz, O. Toprakci, K. Fu, and X. Zhang, "A review of recent developments in membrane separators for rechargeable lithium-ion batteries," *Energy & Environmental Science*, vol. 7, no. 12, pp. 3857–3886, 2014.

[188] W. Ren, Y. Zheng, Z. Cui, Y. Tao, B. Li, and W. Wang, "Recent progress of functional separators in dendrite inhibition for lithium metal batteries," *Energy Storage Materials*, vol. 35, pp. 157–168, 2021.

[189] J. Liang, Q. Chen, X. Liao et al., "A nano-shield design for separators to resist dendrite formation in lithium-metal batteries," *Angewandte Chemie International Edition*, vol. 59, no. 16, pp. 6561–6566, 2020.

[190] C. Z. Zhao, P. Y. Chen, R. Zhang et al., "An ion redistributor for dendrite-free lithium metal anodes," *Science Advances*, vol. 4, no. 11, article eaat3446, 2018.

[191] R. Pan, X. Xu, R. Sun et al., "Nanocellulose modified polyethylene separators for lithium metal batteries," *Small*, vol. 14, no. 21, article e1704371, 2018.

[192] Y. Gao, Z. Hou, R. Zhou et al., "Critical roles of mechanical properties of solid electrolyte interphase for potassium metal anodes," *Advanced Functional Materials*, vol. 32, no. 17, article 2112399, 2022.

[193] B. Dang, Q. Li, Y. Luo, R. Zhao, J. Li, and F. Wu, "Metal-organic framework-based glass fiber separator as an efficacious polysulfide barrier and dendrite suppressor for lithium-sulfur batteries," *Journal of Alloys and Compounds*, vol. 915, article 165375, 2022.

[194] T. Chen, F. Huang, Y. Wang, Y. Yang, H. Tian, and J. M. Xue, "Unveiling the synergistic effect of ferroelectric polarization and domain configuration for reversible zinc metal

anodes," *Advanced Science*, vol. 9, no. 14, article e2105980, 2022.

[195] J. Y. Wang, M. H. Chen, Z. C. Lu, Z. D. Chen, and L. P. Si, "Robust potassium metal anodes realized by ferroelectricity and high conductivity separator," *Materials Science in Semiconductor Processing*, vol. 151, article 107001, 2022.

[196] W. Luo, L. Zhou, K. Fu et al., "A thermally conductive separator for stable Li metal anodes," *Nano Letters*, vol. 15, no. 9, pp. 6149–6154, 2015.

[197] L. Si, J. Wang, and X. Xu, "Reduced graphene oxide-coated separator to activate dead potassium for efficient potassium batteries," *Materials*, vol. 15, no. 16, p. 5505, 2022.

[198] H. Sonoki, M. Matsui, and N. Imanishi, "Effect of anion species in early stage of SEI formation process," *Journal of the Electrochemical Society*, vol. 166, no. 15, pp. A3593–A3598, 2019.

[199] X.-Q. Zhang, X.-B. Cheng, X. Chen, C. Yan, and Q. Zhang, "Fluoroethylene carbonate additives to render uniform Li deposits in lithium metal batteries," *Advanced Functional Materials*, vol. 27, no. 10, article 1605989, 2017.

[200] G. Yang, Y. Li, S. Liu, S. Zhang, Z. Wang, and L. Chen, "LiFSI to improve lithium deposition in carbonate electrolyte," *Energy Storage Materials*, vol. 23, pp. 350–357, 2019.

[201] X. Fan, L. Chen, X. Ji et al., "Highly fluorinated interphases enable high-voltage Li-metal batteries," *Chem*, vol. 4, no. 1, pp. 174–185, 2018.

[202] Z. Jiang, J. Mo, C. Li et al., "Anion-regulated weakly SolvatingElectrolytes forHigh-VoltageLithium metal batteries," *Energy & Environmental Materials*, no. article e12440, 2022.

[203] X. Ren, M. He, N. Xiao, W. D. McCulloch, and Y. Wu, "Greatly enhanced anode stability in K-oxygen batteries with an in situ formed solvent- and oxygen-impermeable protection layer," *Advanced Energy Materials*, vol. 7, no. 1, article 201601080, 2016.

[204] H. Wang, D. Yu, X. Wang et al., "Electrolyte chemistry enables simultaneous stabilization of potassium metal and alloying anode for potassium-ion batteries," *Angewandte Chemie International Edition*, vol. 58, no. 46, pp. 16451–16455, 2019.

[205] N. Xiao, W. D. McCulloch, and Y. Wu, "Reversible dendrite-free potassium plating and stripping electrochemistry for potassium secondary batteries," *Journal of the American Chemical Society*, vol. 139, no. 28, pp. 9475–9478, 2017.

[206] J. Touja, P. N. Le Pham, N. Louvain, L. Monconduit, and L. Stievano, "Effect of the electrolyte on K-metal batteries," *Chemical Communications*, vol. 56, no. 93, pp. 14673–14676, 2020.

[207] X. Liu, G. A. Elia, X. Gao, B. Qin, H. Zhang, and S. Passerini, "Highly concentrated KTFSI : Glyme electrolytes for K/bilayered-V_2O_5 Batteries," *Batteries & Supercaps*, vol. 3, no. 3, pp. 261–267, 2020.

[208] Y. Hu, L. Fan, A. M. Rao et al., "Cyclic-anion salt for high-voltage stable potassium-metal batteries," *National Science Review*, vol. 9, no. 10, article nwac134, 2022.

[209] Q. Zheng, Y. Yamada, R. Shang et al., "A cyclic phosphate-based battery electrolyte for high voltage and safe operation," *Nature Energy*, vol. 5, no. 4, pp. 291–298, 2020.

[210] K. H. Kim, J. H. Cho, J. U. Hwang, J. S. Im, and Y.-S. Lee, "A key strategy to form a LiF-based SEI layer for a lithium-ion battery anode with enhanced cycling stability by introducing a semi-ionic C-F bond," *Journal of Industrial and Engineering Chemistry*, vol. 99, pp. 48–54, 2021.

[211] M. Wang, Z. Peng, W. Luo et al., "Tailoring lithium deposition via an SEI-functionalized membrane derived from LiF decorated layered carbon structure," *Advanced Energy Materials*, vol. 9, no. 12, article 1802912, 2019.

[212] Z. Zhu, Y. Tang, Z. Lv et al., "Fluoroethylene carbonate enabling a robust LiF-rich solid electrolyte interphase to enhance the stability of the MoS(2) anode for lithium-ion storage," *Angewandte Chemie International Edition*, vol. 57, no. 14, pp. 3656–3660, 2018.

[213] L. Qiao, U. Oteo, M. Martinez-Ibanez et al., "Stable non-corrosive sulfonimide salt for 4-V-class lithium metal batteries," *Nature Materials*, vol. 21, no. 4, pp. 455–462, 2022.

[214] C.-l. Li, S.-w. Zeng, P. Wang et al., "Mechanism of aluminum corrosion in LiFSI-based electrolyte at elevated temperatures," *Transactions of Nonferrous Metals Society of China*, vol. 31, no. 5, pp. 1439–1451, 2021.

[215] L. Zhang, L. Chai, L. Zhang et al., "Synergistic effect between lithium bis(fluorosulfonyl)imide (LiFSI) and lithium bis-oxalato borate (LiBOB) salts in $LiPF_6$-based electrolyte for high-performance Li-ion batteries," *Electrochimica Acta*, vol. 127, pp. 39–44, 2014.

[216] S. Liu, J. Mao, L. Zhang, W. K. Pang, A. Du, and Z. Guo, "Manipulating the solvation structure of nonflammable electrolyte and interface to enable unprecedented stability of graphite anodes beyond 2 years for safe potassium-ion batteries," *Advanced Materials*, vol. 33, no. 1, article e2006313, 2021.

[217] J. Park, G. Oh, U. H. Kim et al., "Regulating the solvation structure of electrolyte via dual-salt combination for stable potassium metal batteries," *Advanced Science*, vol. 10, no. 16, article e2301201, 2023.

[218] H. Wang, J. Dong, Q. Guo et al., "Highly stable potassium metal batteries enabled by regulating surface chemistry in ether electrolyte," *Energy Storage Materials*, vol. 42, pp. 526–532, 2021.

[219] T. Hosaka, T. Matsuyama, K. Kubota, R. Tatara, and S. Komaba, "KFSA/glyme electrolytes for 4 V-class K-ion batteries," *Journal of Materials Chemistry A*, vol. 8, no. 45, pp. 23766–23771, 2020.

[220] L. Xue, Y. Li, H. Gao et al., "Low-cost high-energy potassium cathode," *Journal of the American Chemical Society*, vol. 139, no. 6, pp. 2164–2167, 2017.

[221] A. Eftekhari, "Potassium secondary cell based on Prussian blue cathode," *Journal of Power Sources*, vol. 126, no. 1-2, pp. 221–228, 2004.

[222] C. Zhang, J. Chen, X. Yin et al., "Optimal utilization of fluoroethylene carbonate in potassium ion batteries," *Chemical Communications*, vol. 57, no. 13, pp. 1607–1610, 2021.

[223] J. Wu, M. Ihsan-Ul-Haq, Y. Chen, and J.-K. Kim, "Understanding solid electrolyte interphases: advanced characterization techniques and theoretical simulations," *Nano Energy*, vol. 89, article 106489, 2021.

[224] Z. Feng, R. Chen, R. Huang, F. Zhang, W. Liu, and S. Liu, "Electrolyte solvation structure manipulation and synthetic optimization for enhanced potassium storage of tin phosphide/carbon alloy-based electrode," *Metals*, vol. 13, no. 4, p. 658, 2023.

[225] W. Xu, H. Wang, J. Hu et al., "A highly concentrated electrolyte for high-efficiency potassium metal batteries," *Chemical Communications*, vol. 57, no. 8, pp. 1034–1037, 2021.

[226] Y. Liu, C. Gao, L. Dai et al., "The features and progress of electrolyte for potassium ion batteries," *Small*, vol. 16, no. 44, article e2004096, 2020.

[227] Y. Li, F. Wu, Y. Li et al., "Ether-based electrolytes for sodium ion batteries," *Chemical Society Reviews*, vol. 51, no. 11, pp. 4484–4536, 2022.

[228] B. Li, J. Zhao, Z. Zhang et al., "Electrolyte-regulated solid-electrolyte interphase enables long cycle life performance in organic cathodes for potassium-ion batteries," *Advanced Functional Materials*, vol. 29, no. 5, article 1807137, 2018.

[229] Z. W. Seh, J. Sun, Y. Sun, and Y. Cui, "A highly reversible room-temperature sodium metal anode," *ACS Central Science*, vol. 1, no. 8, pp. 449–455, 2015.

[230] S. J. An, J. Li, C. Daniel, D. Mohanty, S. Nagpure, and D. L. Wood, "The state of understanding of the lithium-ion-battery graphite solid electrolyte interphase (SEI) and its relationship to formation cycling," *Carbon*, vol. 105, pp. 52–76, 2016.

[231] J. Zhang, Z. Cao, L. Zhou et al., "Model-based design of stable electrolytes for potassium ion batteries," *ACS Energy Letters*, vol. 5, no. 10, pp. 3124–3131, 2020.

[232] J. Li, Y. Hu, H. Xie et al., "Weak cation-solvent interactions in ether-based electrolytes stabilizing potassium-ion batteries," *Angewandte Chemie International Edition*, vol. 61, no. 33, article e202208291, 2022.

[233] S. Liu, J. Mao, Q. Zhang et al., "An intrinsically non-flammable electrolyte for high-performance potassium batteries," *Angewandte Chemie International Edition*, vol. 59, no. 9, pp. 3638–3644, 2020.

[234] G. Jiang, F. Li, H. Wang et al., "Perspective on high-concentration electrolytes for lithium metal batteries," *Small Structures*, vol. 2, no. 5, article 2000122, 2021.

[235] Y. Yamada, J. H. Wang, S. Ko, E. Watanabe, and A. Yamada, "Advances and issues in developing salt-concentrated battery electrolytes," *Nature Energy*, vol. 4, no. 4, pp. 269–280, 2019.

[236] W. Xu, H. Wang, Y. Gao et al., "A localized high concentration electrolyte for 4 V-class potassium metal batteries," *Energy Advances*, vol. 1, no. 4, pp. 191–196, 2022.

[237] L. Liu, S. Wang, Z. Zhang, J. Fan, W. Qi, and S. Chen, "Fluoroethylene carbonate as an electrolyte additive for improving interfacial stability of high-voltage $LiNi_{0.6}Co_{0.2}Mn_{0.2}O_2$ cathode," *Ionics*, vol. 25, no. 3, pp. 1035–1043, 2018.

[238] K. Kim, H. Ma, S. Park, and N.-S. Choi, "Electrolyte-additive-driven interfacial engineering for high-capacity electrodes in lithium-ion batteries: promise and challenges," *ACS Energy Letters*, vol. 5, no. 5, pp. 1537–1553, 2020.

[239] J. Chen, D. Yu, Q. Zhu et al., "Low-temperature high-areal-capacity rechargeable potassium-metal batteries," *Advanced Materials*, vol. 34, no. 36, article e2205678, 2022.

[240] Z. Lei, B. Chen, Y. M. Koo, and D. R. MacFarlane, "Introduction: ionic liquids," *Chemical Reviews*, vol. 117, no. 10, pp. 6633–6635, 2017.

[241] W. J. Zhou, M. Zhang, X. Y. Kong, W. W. Huang, and Q. C. Zhang, "Recent advance in ionic-liquid-based electrolytes for rechargeable metal-ion batteries," *Advanced Science*, vol. 8, no. 13, article 2004490, 2021.

[242] K. Yoshii, T. Masese, M. Kato, K. Kubota, H. Senoh, and M. Shikano, "Sulfonylamide-based ionic liquids for high-voltage potassium-ion batteries with honeycomb layered cathode oxides," *ChemElectroChem*, vol. 6, no. 15, pp. 3901–3910, 2019.

[243] H. Sun, P. Liang, G. Zhu et al., "A high-performance potassium metal battery using safe ionic liquid electrolyte," *Proceedings of the National Academy of Sciences*, vol. 117, no. 45, pp. 27847–27853, 2020.

[244] W. Xia, Y. Zhao, F. Zhao et al., "Antiperovskite electrolytes for solid-state batteries," *Chemical Reviews*, vol. 122, no. 3, pp. 3763–3819, 2022.

[245] J. F. Wu, W. Zhou, Z. Wang et al., "Building K-C anode with ultrahigh self-diffusion coefficient for solid state potassium metal batteries operating at -20 to 120 degrees C," *Advanced Materiasl*, vol. 35, no. 16, article e2209833, 2023.

[246] A. D. Khudyshkina, P. A. Morozova, A. J. Butzelaar et al., "Poly(ethylene oxide)-based electrolytes for solid-state potassium metal batteries with a Prussian blue positive electrode," *ACS Applied Polymer Materials*, vol. 4, no. 4, pp. 2734–2746, 2022.

[247] Y. Zhang, P. Qiu, J. Zheng et al., "KB(3)H(8)·NH(3)B(3)H(7) complex as a potential solid-state electrolyte with excellent stability against K metal," *ACS Applied Materials & Interfaces*, vol. 14, no. 15, pp. 17378–17387, 2022.

[248] R. Wei, S. Chen, T. Gao, and W. Liu, "Challenges, fabrications and horizons of oxide solid electrolytes for solid-state lithium batteries," *Nano Select*, vol. 2, no. 12, pp. 2256–2274, 2021.

[249] K. J. Kim, M. Balaish, M. Wadaguchi, L. P. Kong, and J. L. M. Rupp, "Solid-state Li-metal batteries: challenges and horizons of oxide and sulfide solid electrolytes and their interfaces," *Advanced Energy Materials*, vol. 11, no. 1, article 2002689, 2021.

[250] L. Ni, G. Xu, C. Li, and G. Cui, "Electrolyte formulation strategies for potassium-based batteries," *Exploration*, vol. 2, no. 2, article 20210239, 2022.

[251] A. Dey, S. Karan, and S. K. De, "Effect of nanofillers on thermal and transport properties of potassium iodide-polyethylene oxide solid polymer electrolyte," *Solid State Communications*, vol. 149, no. 31-32, pp. 1282–1287, 2009.

[252] H. Fei, Y. Liu, Y. An et al., "Stable all-solid-state potassium battery operating at room temperature with a composite polymer electrolyte and a sustainable organic cathode," *Journal of Power Sources*, vol. 399, pp. 294–298, 2018.

[253] H. Fei, Y. Liu, Y. An et al., "Safe all-solid-state potassium batteries with three dimentional, flexible and binder-free metal sulfide array electrode," *Journal of Power Sources*, vol. 433, article 226697, 2019.

[254] M. Hamada, R. Tatara, K. Kubota, S. Kumakura, and S. Komaba, "All-solid-state potassium polymer batteries enabled by the effective pretreatment of potassium metal," *ACS Energy Letters*, vol. 7, no. 7, pp. 2244–2246, 2022.

[255] A. C. Baclig, G. McConohy, A. Poletayev et al., "High-voltage, room-temperature liquid metal flow battery enabled by Na-K|K-β''-alumina stability," *Joule*, vol. 2, no. 7, pp. 1287–1296, 2018.

[256] H. Yuan, H. Li, T. Zhang et al., "A $K_2Fe_4O_7$ superionic conductor for all-solid-state potassium metal batteries," *Journal of Materials Chemistry A*, vol. 6, no. 18, pp. 8413–8418, 2018.

[257] D. Spencer Jolly, J. Perera, S. D. Pu, D. L. R. Melvin, P. Adamson, and P. G. Bruce, "High critical currents for dendrite penetration and voiding in potassium metal anode solid-state batteries," *Journal of Solid State Electrochemistry*, vol. 26, no. 9, pp. 1961–1968, 2022.

[258] J. Zheng, H. Fang, L. Fan, Y. Ren, P. Jena, and Y. Wu, "Antiperovskite K_3OI for K-ion solid state electrolyte," *The Journal of Physical Chemistry Letters*, vol. 12, no. 30, pp. 7120–7126, 2021.

[259] J. B. Grinderslev, K. T. Moller, Y. Yan et al., "Potassium octahydridotriborate: diverse polymorphism in a potential hydrogen storage material and potassium ion conductor," *Dalton Transactions*, vol. 48, no. 24, pp. 8872–8881, 2019.

[260] M. Dimitrievska, H. Wu, V. Stavila et al., "Structural and dynamical properties of potassium dodecahydro-monocarba-closo-dodecaborate: KCB11H12," *The Journal of Physical Chemistry C*, vol. 124, no. 33, pp. 17992–18002, 2020.

[261] U. Oteo, M. Martinez-Ibañez, I. Aldalur et al., "Improvement of the cationic transport in polymer electrolytes with (difluoromethanesulfonyl)(trifluoromethanesulfonyl)imide salts," *ChemElectroChem*, vol. 6, no. 4, pp. 1019–1022, 2019.

[262] Z. Xiao, B. Zhou, J. Wang et al., "PEO-based electrolytes blended with star polymers with precisely imprinted polymeric pseudo-crown ether cavities for alkali metal ion batteries," *Journal of Membrane Science*, vol. 576, pp. 182–189, 2019.

[263] M. Zhang, A. M. Zhang, Y. Chen et al., "Polyoxovanadate-polymer hybrid electrolyte in solid state batteries," *Energy Storage Materials*, vol. 29, pp. 172–181, 2020.

[264] H. Gao, L. Xue, S. Xin, and J. B. Goodenough, "A high-energy-density potassium battery with a polymer-gel electrolyte and a polyaniline cathode," *Angewandte Chemie International Edition*, vol. 57, no. 19, pp. 5449–5453, 2018.

[265] Y. Zhang, A. Bahi, F. Ko, and J. Liu, "Polyacrylonitrile-reinforced composite gel polymer electrolytes for stable potassium metal anodes," *Small*, vol. 18, no. 8, article e2107186, 2022.

[266] J. Mindemark, M. J. Lacey, T. Bowden, and D. Brandell, "Beyond PEO–alternative host materials for Li^+-conducting solid polymer electrolytes," *Progress in Polymer Science*, vol. 81, pp. 114–143, 2018.

[267] X. Lu, G. Xia, J. P. Lemmon, and Z. Yang, "Advanced materials for sodium-beta alumina batteries: status, challenges and perspectives," *Journal of Power Sources*, vol. 195, no. 9, pp. 2431–2442, 2010.

[268] Y.-F. Y. Yao and J. Kummer, "Ion exchange properties of and rates of ionic diffusion in beta-alumina," *Journal of Inorganic and Nuclear Chemistry*, vol. 29, no. 9, pp. 2453–2475, 1967.

[269] X. Feng, H. Fang, N. Wu et al., "Review of modification strategies in emerging inorganic solid-state electrolytes for lithium, sodium, and potassium batteries," *Joule*, vol. 6, no. 3, pp. 543–587, 2022.

[270] X. Lu, M. E. Bowden, V. L. Sprenkle, and J. Liu, "A low cost, high energy density, and long cycle life potassium-sulfur battery for grid-scale energy storage," *Advanced Materials*, vol. 27, no. 39, pp. 5915–5922, 2015.

[271] T. Feng, L. Li, Z. Lv, B. Li, Y. Zhang, and G. Li, "Temperature-dependent electrical transport behavior and structural evolution in hollandite-type titanium-based oxide," *Journal of the American Ceramic Society*, vol. 102, no. 11, pp. 6741–6750, 2019.

[272] Y. Zhao and L. L. Daemen, "Superionic conductivity in lithium-rich anti-perovskites," *Journal of the American Chemical Society*, vol. 134, no. 36, pp. 15042–15047, 2012.

[273] Y. Wang, Q. Wang, Z. Liu et al., "Structural manipulation approaches towards enhanced sodium ionic conductivity in Na-rich antiperovskites," *Journal of Power Sources*, vol. 293, pp. 735–740, 2015.

[274] Y. Pang, Y. Liu, J. Yang, S. Zheng, and C. Wang, "Hydrides for solid-state batteries: a review," *Materials Today Nano*, vol. 18, article 100194, 2022.

[275] T. J. Udovic, M. Matsuo, A. Unemoto et al., "Sodium superionic conduction in $Na_2B_{12}H_{12}$," *Chemical Communications*, vol. 50, no. 28, pp. 3750–3752, 2014.

[276] D. H. P. Souza, K. T. Møller, S. A. Moggach et al., "Hydrated alkali-$B_{11}H_{14}$ salts as potential solid-state electrolytes," *Journal of Materials Chemistry A*, vol. 9, no. 26, pp. 15027–15037, 2021.

[277] J. K. Eckhardt, P. J. Klar, J. Janek, and C. Heiliger, "Interplay of dynamic constriction and interface morphology between reversible metal anode and solid electrolyte in solid state batteries," *ACS Applied Materials & Interfaces*, vol. 14, no. 31, pp. 35545–35554, 2022.

[278] J. Kasemchainan, S. Zekoll, D. Spencer Jolly et al., "Critical stripping current leads to dendrite formation on plating in lithium anode solid electrolyte cells," *Nature Materials*, vol. 18, no. 10, pp. 1105–1111, 2019.

[279] C. Zhang, K. L. Firestein, J. F. S. Fernando, D. Siriwardena, J. E. von Treifeldt, and D. Colberg, "Recent progress of in situ transmission electron microscopy for energy materials," *Advanced Materials*, vol. 32, no. 18, article 1904094, 2020.

[280] Q. Gao, W.-Y. Tsai, and N. Balke, "In situ and operando force-based atomic force microscopy for probing local functionality in energy storage materials," *Electrochemical Science Advances*, vol. 2, no. 1, article E2100038, Article ID 10.1002/elsa.202100038, 2022.

[281] Z. Y. Zhang, S. Said, K. Smith et al., "Characterizing batteries by in situ electrochemical atomic force microscopy: a critical review," *Advanced Energy Materials*, vol. 11, no. 38, article 2101518, 2021.

[282] M. Kitta and H. Sano, "Real-time observation of Li deposition on a Li electrode with operand atomic force microscopy and surface mechanical imaging," *Langmuir*, vol. 33, no. 8, pp. 1861–1866, 2017.

[283] C. Y. Chen, T. Tsuda, Y. Oshima, and S. Kuwabata, "In situ monitoring of lithium metal anodes and their solid electrolyte interphases by transmission electron microscopy," *Small Structures*, vol. 2, no. 6, article 2100018, 2021.

[284] Z. J. Ju, H. D. Yuan, O. W. Sheng et al., "Cryo-electron microscopy for unveiling the sensitive battery materials," *Small Science*, vol. 1, no. 11, article 2100055, 2021.

[285] C. Zhang, M. Chen, Q. Tao, and Z. C. Chi, "Cobalt chloride-stimulated hypoxia promotes the proliferation of cholesteatoma keratinocytes via the PI3K/Akt signaling pathway," *International Journal of Medical Sciences*, vol. 18, no. 15, pp. 3403–3411, 2021.

[286] S. Amara, J. Toulc'Hoat, L. Timperman et al., "Comparative study of alkali-cation-based (Li+, Na+, K+) electrolytes in acetonitrile and alkylcarbonates," *ChemPhysChem*, vol. 20, no. 4, pp. 581–594, 2019.

[287] L. Zhang, X. Li, M. Yang, and W. Chen, "High-safety separators for lithium-ion batteries and sodium-ion batteries: advances and perspective," *Energy Storage Materials*, vol. 41, pp. 522–545, 2021.

[288] D. Zhou, X. Tang, X. Guo et al., "Polyolefin-based Janus separator for rechargeable sodium batteries," *Angewandte*

Chemie International Edition, vol. 59, no. 38, pp. 16725–16734, 2020.

[289] A. L. Michan, B. S. Parirnalam, M. Leskes et al., "Fluoroethylene carbonate and vinylene carbonate reduction: understanding lithium-ion battery electrolyte additives and solid electrolyte interphase formation," *Chemistry of Materials*, vol. 28, no. 22, pp. 8149–8159, 2016.

[290] A. C. Thenuwara, P. P. Shetty, N. Kondekar et al., "Efficient low-temperature cycling of lithium metal anodes by tailoring the solid-electrolyte interphase," *ACS Energy Letters*, vol. 5, no. 7, pp. 2411–2420, 2020.

[291] S. Xie, W. Xie, Q. Zhang, X. Cheng, X. Ouyang, and B. Lu, "Structure-engineered low-cost carbon microbelt hosts for highly robust potassium metal anode," *Advanced Functional Materials*, vol. 33, no. 36, article 2302880, 2023.

[292] H. Shi, Y. Dong, S. Zheng, C. Dong, and Z.-S. Wu, "Three dimensional Ti_3C_2 MXene nanoribbon frameworks with uniform potassiophilic sites for the dendrite-free potassium metal anodes," *Nanoscale Advances*, vol. 2, no. 9, pp. 4212–4219, 2020.

[293] Y. Feng, A. M. Rao, J. Zhou, and B. Lu, "Selective potassium deposition enables dendrite-resistant anodes for ultrastable potassium-metal batteries," *Advanced Materials*, vol. 35, no. 30, article e2300886, 2023.

[294] Q. Shen, Y. He, and J. Wang, "Biomass-derived two-dimensional N,O-doped carbon with embedded binary-metal nanoparticles enables dendrite-free potassium-metal anodes," *Journal of Materials Chemistry A*, vol. 11, no. 18, pp. 9829–9839, 2023.

[295] J. Zhang, D. Cai, L. Zhu, X. Wang, and J. Tu, "Highly stable potassium metal anodes with controllable thickness and area capacity," *Small*, vol. 19, no. 34, article e2301119, 2023.

[296] D. Li, Y. Sun, M. Li et al., "Rational design of an artificial SEI: alloy/solid electrolyte hybrid layer for a highly reversible Na and K metal anode," *ACS Nano*, vol. 16, no. 10, pp. 16966–16975, 2022.

[297] P. Liu, D. Yen, B. S. Vishnugopi et al., "Influence of potassium metal-support interactions on dendrite growth," *Angewandte Chemie*, vol. 62, no. 23, article e202300943, 2023.

[298] H. Ding, J. Wang, J. Zhou, C. Wang, and B. Lu, "Building electrode skins for ultra-stable potassium metal batteries," *Nature Communications*, vol. 14, no. 1, p. 2305, 2023.

[299] A. Haffner, A. K. Hatz, O. E. O. Zeman, C. Hoch, B. V. Lotsch, and D. Johrendt, "Polymorphism and fast potassium-ion conduction in the T5 supertetrahedral phosphidosilicate KSi(2) P(3)," *Angewandte Chemie International Edition*, vol. 60, no. 24, pp. 13641–13646, 2021.